STUDY ON AGRICULTURAL TRACTOR OPERATOR SAFETY IN ROLLOVER ACCIDENTS

A Dissertation Presented for the
Doctor of Philosophy
Degree
The University of Tennessee, Knoxville

Farzaneh Khorsandi Kouhanestani
August 2017

DEDICATION

I dedicate my work to
My Mother
Nahid

and

My Father.
Ali

ACKNOWLEDGEMENTS

I would like to thank my Major advisor Prof. Paul D. Ayers for all of his supports during my Ph.D. program. I learned a lot from him. Also, I would like to thank my committee members, Prof. John B. Wilkerson, Prof. Robert B. Freeland, and Dr. Timothy J. Truster who provided me with great support especially for their valuable suggestions and revision to the papers.

I would like to express my gratitude for my parents, Nahid Khalilian and Ali Khorsandi, my sister, Zohreh Khorsandi, and my brother, Saeid Khorsandi for all their support in whatever I do in my life.

Also, I would like to thank my awesome friends both in Iran, in the U.S. and in other parts of the World who have been part of my journey: Saman Souri, Duncan Mochiki, Casey Sullivan, Isaac Jeldes, and Lilian Wanjiro, for all of their supports.

I also want to thank my fellow students and friends: Dillan Jackson, Jake Dixon, and Guilherme de Moura for helping me in the experimental tests. I would like to thanks all of the faculty members and staff of BESS, especially whom that support me, Dr. William Hart, Mr. Scott Tucker, Artan Xhaferaj, Lesia Rucker, and Sandra Marine.

ABSTRACT

Agriculture is one of the most dangerous industries in the US. Tractor accidents are the major cause of death in agriculture, producing about one half of the fatal accidents. Tractor overturn is the most common cause of death in tractor accidents. Three projects related to tractor operator safety in rollover accident were defined.

The aim of first project is to develop a Finite Element (FE) model to predict the Roll-Over Protective Structure (ROPS) performance under the standard SAE J2194 (SAE, 2009) static test. The developed model was validated by comparing the model results with experimental test results. The developed model can predict the experimental test results with average errors about 9%.

The rigid ROPS are not appropriate for working in low overhead clearance zones. The foldable ROPS (FROPS) was designed to solve the rigid ROPS problem, but lowering and raising the conventional FROPS is time consuming and strenuous. The actuation forces to raise and lower the FROPS were not well known. In the second project a measurement system was designed to measure the actuation force and the angle of the foldable ROPS. Two measurement setups were developed to examine the effect of speed and friction on the actuation torque. Results showed that both friction and speed had significant effect on actuation torque.

In the third project a model was developed to predict the effect of liquid shift on agricultural machineries CG height calculation. The CG location is one of the determinant factors for finding the stability angle. When the tractor tilting angle is higher than the stability angle the tractor will rollover. The new ISO 16231-2 uses lift axle method to determine the CG height and is subject to inaccuracy related to liquid shift. The model was validated by comparing the results with experimental results of a wagon and a full size tractor. The developed model predicted the measured CG height with less than 5% error. The effect of liquid shift on CG height measurement for a vehicle with 16% liquid is 19.5% and for the tractor with 2% of liquid is 0.35%.

TABLE OF CONTENTS

LIST OF TABLES

LIST OF FIGURES

CHAPTER I
INTRODUCTION

Agriculture is one of the most dangerous industries in the US (Bureau of Labor Statistics, 2014). Tractor accidents are the major cause of death in agriculture, producing about one half of the fatal accidents. Tractor overturn is the most common cause of death in tractor accidents. Roughly one third of the fatal tractor accidents are rollover accidents (Reynolds & Groves, 2000). The rollover accident happens when the vehicle tilting angle is higher than the static overturning angle (SOA), which is a function of center of gravity (CG) height. Finding the CG height more accurately could lead to less overturn accidents. The most effective way to prevent overturn deaths during an overturn accident is use of a rollover protective structure (ROPS) in combination with a seat belt. A ROPS is a structure which absorbs a portion of the impact energy generated by the tractor weight in the rollover accident. The ROPS decreases the possibility of severe human injuries by providing a clearance zone to protect the operator inside the ROPS envelope. Three projects related to agricultural tractor operator safety in rollover accidents are defined in this manuscript.

The first project involves developing a Finite Element (FE) model to predict the nonlinear performance for ROPS which are designed with a Computer-based ROPS Design Program (CRDP) (Ayers, Khorsandi, John, & Whitaker, 2016). ROPS must pass a standard ROPS test prior to certification. The experimental standard tests are expensive, time consuming and laborious. The aim of this project is to develop a FE model to predict the ROPS performance under the standard SAE J2194 static test. The developed model was validated by comparing the model results with experimental test results. In the second project a system was designed to measure the actuation force and the angle of the foldable ROPS. The rigid ROPS are not appropriate for working in low overhead clearance zones such as orchards. The foldable ROPS was designed to solve the rigid ROPS problem, but lowering and raising the conventional foldable ROPS is time consuming and strenuous. The actuation forces must meet the allowable force levels based on the OECD Standards (OECD, 2014). A fold assist mechanism would be helpful for raising and lowering the ROPS, but in order to design a fold assist mechanism the actuation force should be measured in advance. Two measurement setups were developed to examine the effect of speed and friction on the actuation torque. In the third project a model was developed to predict the effect of liquid shift on agricultural machineries CG height calculation. The CG location is one of the determinant factors for finding the stability angle. When the tractor tilting angle is higher than the stability angle the tractor will rollover. The new ISO 16231-2 uses lift axle method to determine, the CG height and is subject to inaccuracy related to liquid shift (ISO, 2015). The model was validated by comparing the prediction results with experimental results of a small wagon and a full size tractor.

1.1 DEVELOPING A FINITE ELEMENT MODEL

Tractor accidents are the major cause of death in agriculture. One half of the fatal agricultural accidents are related to tractor accidents. Tractor related fatalities include being run over or be crushed by tractor, engagement in moving parts of the tractor, accidents on road way, and tractor overturn (Reynolds & Groves, 2000). Tractor overturn is the most important cause of death in tractor accidents (Springfeldt, 1996). Tractors overturn are caused by slipping on steep slopes, bumping against obstacles, turning sharp curves, and shearing the soil. Tractor rollover account for up to one third of all tractor related fatalities (Murphy & Yoder, 1998). The most effective way to prevent overturn deaths is the use of ROPS in combination with seat belt.

1.1.1 ROLLOVER PROTECTIVE STRUCTURE (ROPS)

A ROPS is a frame or cab which is installed on the tractor to minimize the possibility and severity of operator injury in rollover accidents. ROPS provides a clearance zone among the envelope of the ROPS to protect the operator in rollover accident. ROPS design is a big challenge for tractor manufacturer and increases the ROPS production expenses. A rigid structure inserts a big shock to the operator body which causes serious operator injuries (Chen, Wang, Zhang, Zhang, & Si, 2012) and inserts a big force and moment to the chassis. Too flexible structure deforms greatly under the load and infringes the clearance zone or leaves the clearance zone unprotected. The ROPS performance criteria must be examined with one of the standard tests.

1.1.2 STANDARD SAE J2194

SAE J2194 (2009) is an official procedure which was developed for testing ROPS performance of wheeled agricultural tractors. SAE J1194 was developed mainly based on three studies which conducted about thirty years ago (Chisholm, a, b, c). The SAE J2194 includes three types of standard tests; field upset, dynamic, and static test. In the field upset test a tractor is driven up a ramp and then overturned. In the impact test the impact forces are inserted by means of a 2000 kg mass that acts as a pendulum. The static test includes sequences of four static forces which are inserted to the ROPS gradually, two vertical forces and two horizontal forces in with an application rate is 5 mm s^{-1}. The field upset is similar to the real rollover accident (Clark, Thambiratnam, & Perera, 2006). The repeatability of field upset test is low, the expenses is high and laborious. The dynamic test is better able to simulate the rollover accident in comparison with the static test, but the deflection measurement during the test is difficult. The repeatability of dynamic test is poor, the test endangers the test staff life and chassis of the tractor might be completely destroyed during the test with a poorly designed ROPS (Rondelli & Guzzomi, 2010).

The static test is less demanding than two other tests, collecting the data is easy, the results are reliable and accurate (Ross & DiMartino, 1982). The majority of manufacturers select the static test (Fabbri & Ward, 2002). SAE J2194 requires either the static or dynamic test or both to certify ROPS performance (Harris, Mucino, Etherton, Snyder, & Means, 2000). Based on SAE J2194 the static test is applicable for tractors heavier than 800 kg. The static test usually consists of sequences of four static tests including, longitudinal, first vertical, transverse load test, second vertical loading test, and in some special cases an over load test. The static test performance requirements would be met if the structural members absorb a predefined level of energy in longitudinal and transverse tests and tolerates a specific force in vertical test without violating the intrusion and exposure criteria. The ROPS should not infringe the clearance zone (intrusion criteria) and ROPS should not leave clearance zone unprotected from the ground plane (exposure criteria). In the next sections the definition of clearance zone and these four static tests based on SAE J2194 standard test for two post ROPS are described.

1.1.2.1 CLEARANCE ZONE

The clearance zone is defined as the safe zone that ROPS provides to protect the operator in rollover accidents (fig. 1.1).

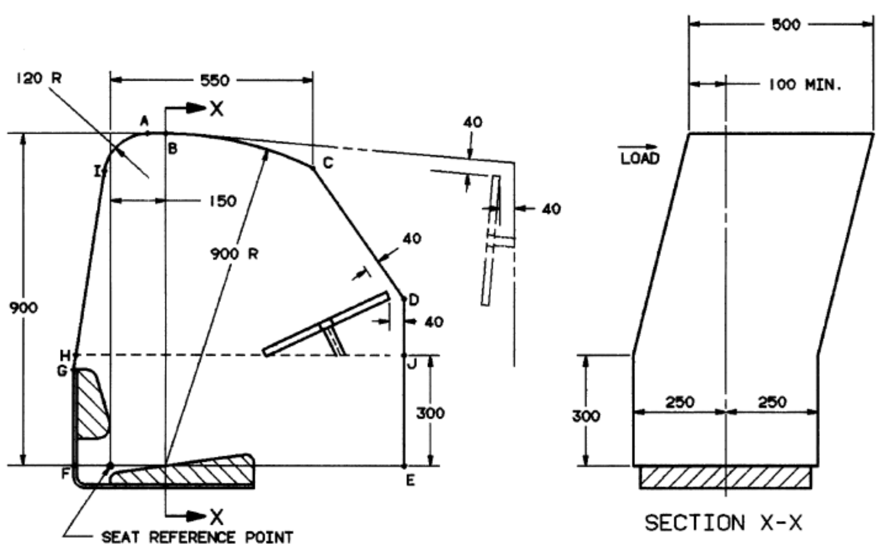

Figure 1.1. Clearance zone from the side (SAE, 2009).

SAE J2194 standard defines the clearance zone based on vertical reference plane and seat reference point. The vertical reference plane passes vertically from the seat reference point (SRP) and the center of steering wheel (fig. 1.1).

1.1.2.2 LONGITUDINAL LOADING TEST

The longitudinal load should be applied horizontally and parallel to the longitudinal tractor median plane with rate less than 5 mm s^{-1}. The load is applied to the uppermost transverse structural member of the ROPS which is most likely to strike the ground first in an overturn accident (fig. 1.2). The first longitudinal test must be inserted from rear of the ROPS until the ROPS absorbed energy (E) is equal to:

$$E= 1.4\ M \qquad (1.1)$$

Where E is absorbed energy (J) and M is tractor reference mass in (kg).

The absorbed energy is the area under force- deflection curve. The tractor reference mass is determined as "A mass, not less than the tractor mass, selected for calculation of the force and energy inputs to be used during test." (Rondelli & Guzzomi, 2010). Commonly, unladen mass of tractor is selected as the reference mass. Unladen mass of tractor is equal to the total mass of vehicle with the ROPS fitted, full liquid tanks (fuel, lubricant, and coolant), and a 75 kg driver (Rondelli & Guzzomi, 2010).

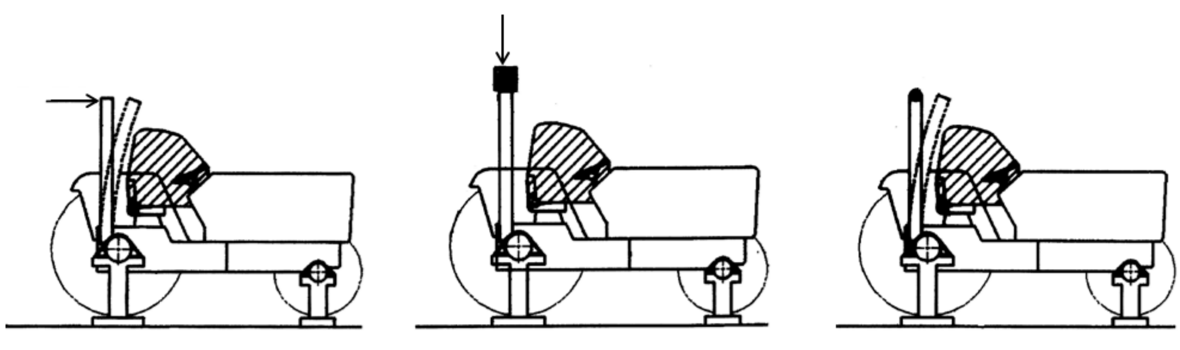

(a) (b) (c)

Figure 1.2. Static tests. (a) Longitudinal load (b) first and second vertical load test (c) transverse loading test (SAE, 2009).

1.1.2.3 FIRST AND SECOND VERTICAL LOADING TEST

The first vertical load is inserted vertically to the uppermost structural member which is called the cross bar (fig. 1.2). The inserted load (F) is equal to:

$$F=20\ M \tag{1.2}$$

Where F is applied force (N). Exerting load should be stopped at least 5 seconds after cessation of any visually detectable movement.

The second vertical test for two post ROPS is exactly the same as the first vertical test (fig. 1.2).

The transverse load, which is also called side load, must be inserted horizontally at 90 degrees to the longitudinal median plane of the tractor. The side load should be applied to the structural member uppermost on the side (fig. 1.2). The test stops when the absorbed energy is equal to:

$$E= 1.75\ M \tag{1.3}$$

1.1.2.4 OVER LOAD TEST

The over load test is required when the applied force decreases by more than 3% over the last 5% of the deflection attained when the absorbed energy by ROPS under side load test reaches 1.75 times of the mass of tractor. The over load test consists of continuing the horizontal loading from 5% of original required energy to 20% additional energy (SAE, 2009).

1.1.3 MODELING

Finite Element (FE) analysis is a numerical approach used to obtain approximate solutions of boundary value problems in engineering. A boundary problem is a mathematical problem in which one or more dependent variables must satisfy a differential equation everywhere within a known domain of independent variables and satisfy specific conditions on the boundary of the field (Hutton & Wu, 2004). Several authors used commercial FE software packages to predict ROPS performance under standard test such as, ANSYS (Alfaro, Arana, Arazuri, & Jarén, 2010) and Abaqus (Clark, 2005; Thambiratnam, Clark, & Perera, 2009).

1.1.4 SUMMARY

The experimental standardized tests are expensive, laborious, time consuming, and destructive. About one third of ROPS fail the standard tests and the test failure postpones ROPS production project and increases the project expenses (Fabbri & Ward, 2002). Using the experimental test alone can't improve ROPS design and performance. Modeling has been introduced as a method that can simulate ROPS performance in rollover accidents, speeds up the design process and reduces the ROPS production expenses. Therefore researchers have used a combination of experimental tests and mathematical models to improve and test ROPS performance. Although computer models are able to predict the force-deflection curve of ROPS, but the experiment test cannot be replaced with computer models. The modeling approach is needed to increase the possibility that the designed ROPS is likely to pass the standard prior to the experimental test.

There is no nonlinear FE model available to predict the behavior of rear mount two post ROPS which was designed with the Computer-based ROPS Design Program (CRDP). The CRDP was developed to quickly generate ROPS designs based on 46 tractor dimensions and the tractor weight (Ayers et al., 2016). The program output is the 2-post, rear-mount ROPS drawings which can be used to construct the ROPS. In the first project a FE model was developed to examine the performance of the rear mount two-post ROPS, designed by the CRDP. The results of the FE model and experimental tests are presented in chapter 2.

1.2 MEASURING THE FORCES TO ACTUATE A FOLDABLE ROPS

Working with ROPS-fitted tractor in places with low overhead clearance zones such as orchards and animal confinement buildings is hard and in some cases impossible. In order to facilitate tractor operation in low overhead clearance zones, foldable ROPS (FROPS) have been developed. The FROPS can be divided to several groups, conventional, the FROPS with manual lift-assist mechanism (Manual), the FROPS with powered lift-assist mechanism (Powered), and automatic FROPS. The conventional FROPS are manually folded, re-erected, and locked. The manual FROPS include lift assist mechanisms that help the operator to fold down and raise the ROPS. The powered FROPS or fold and re-erect upper part of the FROPS by electrical, mechanical, or hydraulic power, but operator controls the ROPS position. The automated FROPS automatically deploy during rollover accident (Robinson, Scarlett, & Seidl, 2012).

1.2.1 CONVENTIONAL FROPS

In conventional FROPS operation when the tractor reaches a point with low overhead clearance zone, the tractor operator turns off the tractor engine, leaves the seat, releases the quick lock, removes the pin, folds down the ROPS, comes back to the seat, turns on the tractor and continues the work. After passing the overhead obstacle the operator repeats all of the previous steps to raise the ROPS. Lowering and raising the ROPS is a time consuming and strenuous process (Panek & Kolli, 1998) therefore, the operator prefers to leave the FROPS in inoperative position (Ayers, 2015). The number of retrofitted tractors with ROPS has increased recently, but the number fatal roll-over accidents of tractors with folded down ROPS has increased.

The national Institute for Occupational Safety and Health (NIOSH) reports no fatalities related to rollover accident with folded down ROPS before 2003, but the percentage of fatal rollover accident with folded down ROPS increased sharply to 25% in 2005 and to 50% at 2012 (FACE, 2014). The survey done by European Commission members showed that 40% of fatalities and serious injuries happened when the ROPS was in inoperative position in rollover accident (Hoy, 2009).

1.2.2 MANUAL SYSTEMS

Several manual mechanisms were developed to minimize the actuation force and help the operator to raise and lower the ROPS with less effort in comparison with conventional FROPS (Finch, Martinez, & Sandoval, 1998; Ludwig, 1990; Panek & Kolli, 1998; Sheehan, 1992).

The manual systems are generally low cost and simple in comparison with powered and automatic systems (Robinson et al., 2012). Ludwig (1990) equipped ROPS with a lever arm and claimed that the operator doesn't need to leave the vehicle seat to raise or re-erect the ROPS. The lever arm slide down with gravity force when the ROPS was in inoperative position (fig. 1.3).

The ROPS could be locked in raised or lowered position by means of pins which were inserted in holes at the pivot point bracket (Ludwig, 1990). This mechanism needed a clearance area rearward of the ROPS as big as the height of the upper part of the FROPS to allow the upper part to fold down. Turning the upper part was awkward and required the operator to leave the seat (Finch et al., 1998).

Sheehan (1992) designed a telescopic rollover protective structure for orchard tractors. The protective member was attached to a compression spring. The compression spring housed within the lower section and facilitated movement of the protective member to the raised position (fig. 1.4). A locking mechanism fixed the movable member to restrict the movement in both lowered and raised positions (Sheehan, 1992). The telescopic FROPS mechanism was expensive and difficult to construct (Finch et al., 1998).

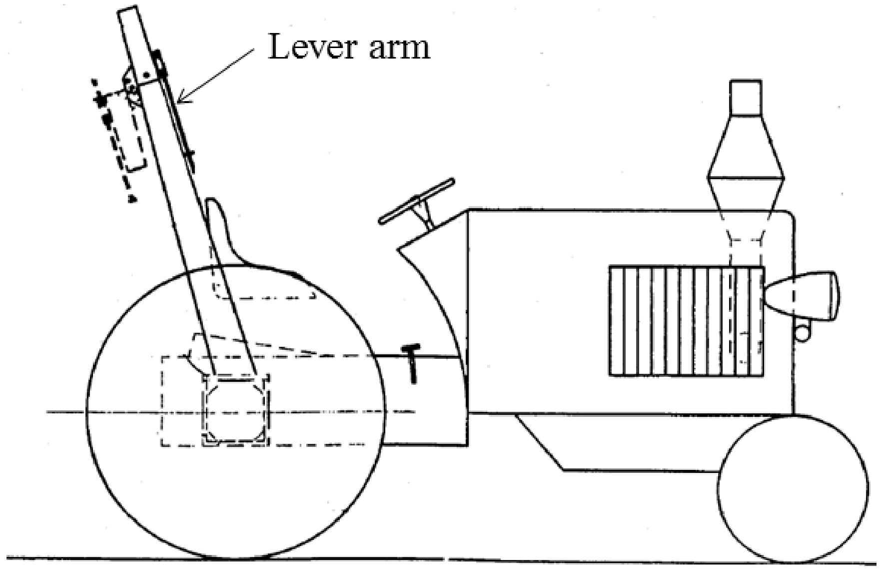

Figure 1.3. FROPS with lever arm, in inoperative position (Ludwig, 1990).

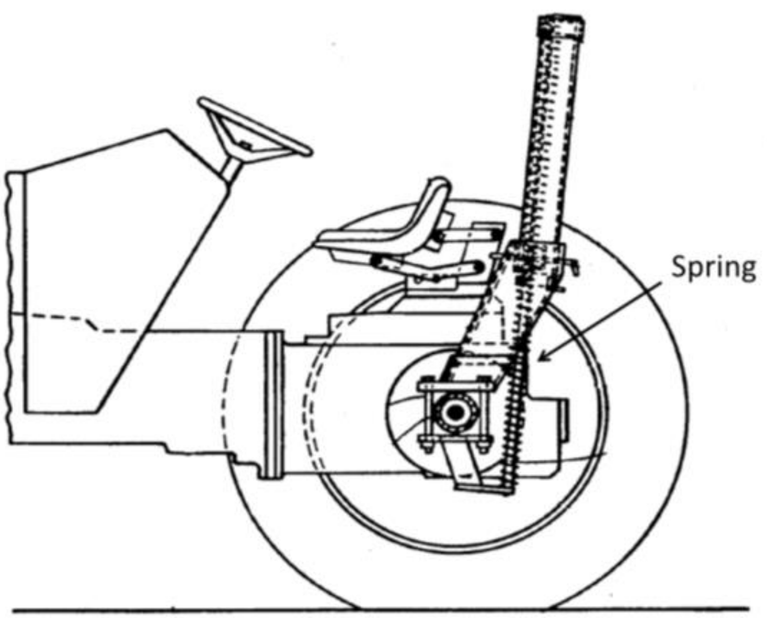

Figure 1.4. The telescopic mechanism in inoperative position (Sheehan, 1992).

Panek and Kolli (1998) developed a manual fold assist mechanism which had a handle and a lift assist spring. The ROPS included a support structure and a cross member which was pivotally coupled to the support structure. The handle was mounted on the cross member and the lift assist was pivotally attached to the support structure and cross member (fig. 1.5). The lift assist mechanism decreased the lifting force by means of a spring and eased the re-erecting process by means of a handle.

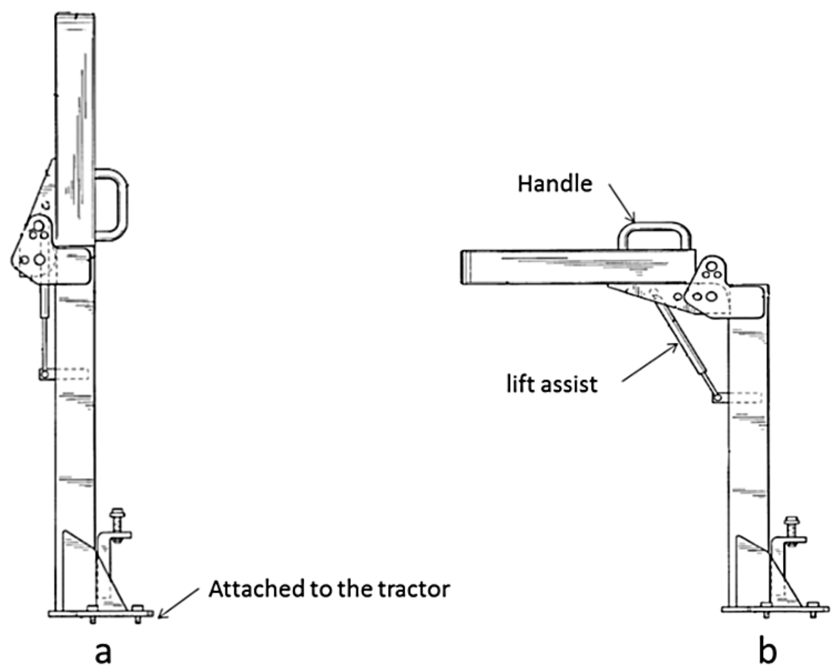

Figure 1.5. Manual lifts assist mechanism with a handle (a) in raised position. (b) In folded down position (Panek & Kolli, 1998).

Finch et al. (1998) developed a collapsible manual FROPS which the upper section was pivotally connected to the fixed lower section by means of a four-bar linkage. The linkage permitted the upper section to turn pivotally rearward and immediately behind of the lower section in the lowered position (fig. 1.6). The engagement surfaces of the lower and upper parts were slanted with respect to the axis of the legs in raised position in order to facilitate the movement of the upper section between the lowered and raised positions. A locking pin fixed the structure in both positions (Finch et al., 1998).

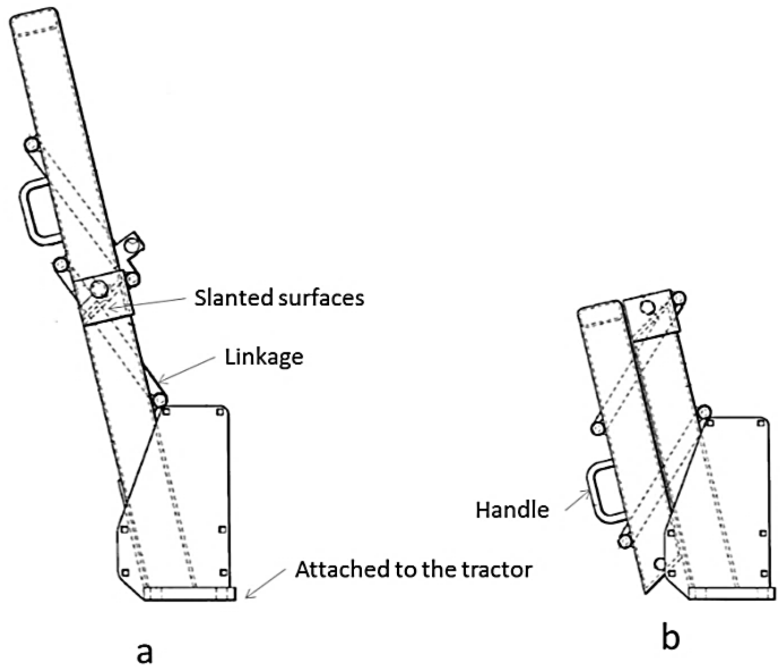

Figure 1.6. Collapsible FROPS in folded down and raised position a) in raised position. (b) In lowered position (Finch et al., 1998).

1.2.3 POWERED SYSTEM

In the powered systems a power system, folds down and re-erects the ROPS, but the process needs an operator's command. Operators do not need to leave the seat and the ROPS may be folded down and raised when the vehicle is in motion (Robinson et al., 2012).

Since the structure of the ROPS changes, the entire required ROPS test should be done again to validate the ROPS performance in upright position. The powered system is more expensive and complex than conventional and manual systems (Robinson et al., 2012).

Ayers et al. (2012) developed a powered system that ROPS was lowered and raised by an electrical motor which the motor shaft was attached to the upper part of the ROPS by means of a fork. An electrical system was used to command the ROPS to fold down and re-erect by pushing a bottom (fig. 1.7). The total time for lowering/unpinning and raising /pinning was 20 seconds.

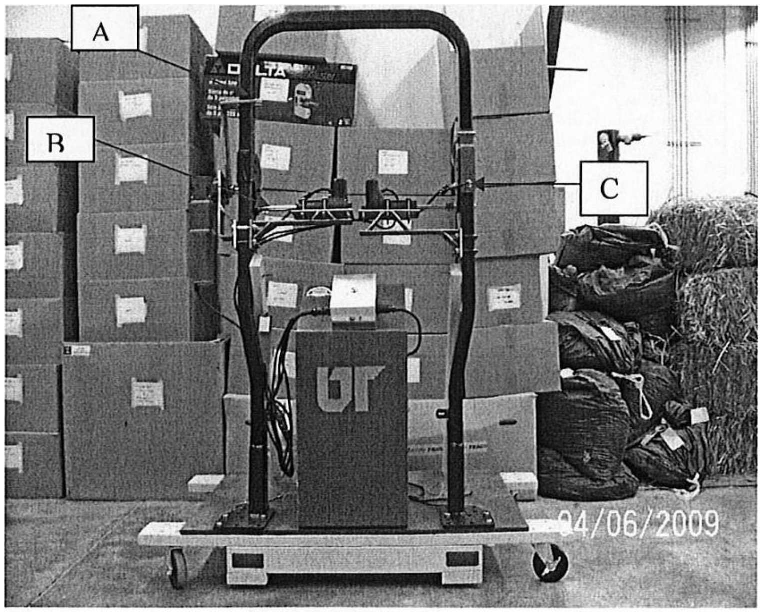

Figure 1.7. Powered ROPS (Ayers et al., 2012).

1.2.4 AUTOMATIC SYSTEM

In the automatic system no operator action is required and the operator does not control the ROPS position. This system is very convenient, but more expensive and complex than the other systems. The performance of the control system must be tested and validated before implementation. All the performance requirements for ROPS must be tested (Robinson et al., 2012). NIOSH developed a low-profile Auto ROPS (AROPS) which automatically and rapidly deploys during rollover event (Powers et al., 2001). AROPS consists of two telescopic tubes which are extended by a spring during rollover accident (fig. 1.8). This ROPS is made of three parts, sensor, control system, and deployment system. The automatic sensor measures the tractor tilting angle and the control system commands the deployment system to releases the upper tube. AROPS normally is in lowered position, but when the vehicle operating angle increased and overturn condition is detected by sensor, the ROPS will be deployed. AROPS can protect the operator in rollover accident even in low clearance zones (Powers et al., 2001). Howard (1998) tested the performance of the second generation of AROPS and results showed that the AROPS deployed in less than 0.3 s and latched securely. The 3rd generation AROPS is the smallest and the most effective AROPS for protecting the operator in rollover accidents (Alkhaledi, Means, McKenzie Jr, & Smith, 2013).

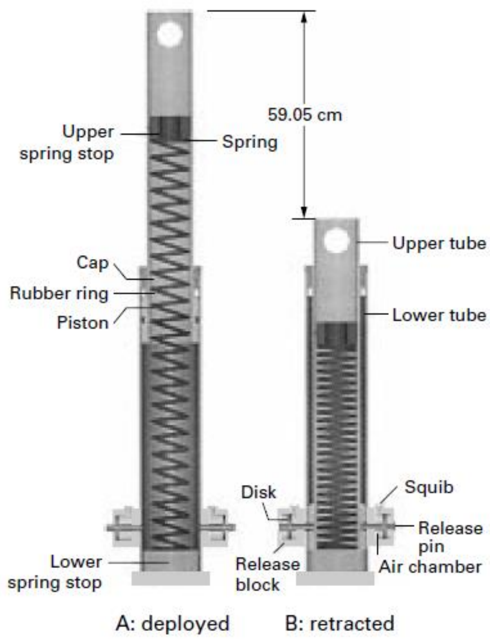

Figure 1.8. Structure and mechanism of auto ROPS (Powers et al., 2001).

1.2.5 OECD CODE

The OECD (2014) standard code is under development for official testing of agricultural tractors FROPS performance. The actuation force is defined as the lifting force inserted tangential to the trajectory of the crossbar to the grasping area (OECD, 2014). The grasping area is the area that the operator exerts the actuation force manually to raise and lower the ROPS. The grasping area includes the cross bar of the ROPS, and the additional handles for lifting the ROPS (fig. 1.9). The actuation force during the folding down process, which starts from +90 degree, must be exerted in downward direction to the crossbar of the ROPS. In some FROPS, at a special angle the actuation force is equal to zero and after this angle the resistive force must be inserted in upward direction to the crossbar to keep the ROPS from falling. This special angle is called breaking point.

The maximum allowable actuation force is defined based on three accessible zones. These zones are accessible for a standing operator while raising and lowering a ROPS manually with no fold assist mechanism (fig. 1.10).

The dimension of accessible zones for folding and raising the ROPS are defined with respect to the horizontal plane of the ground, and vertical planes passing through the outer part of the obstacle that limit the position or displacement of the operator. These three zones are defined based on anthropometric data of small man and medium size woman (OECD, 2014).

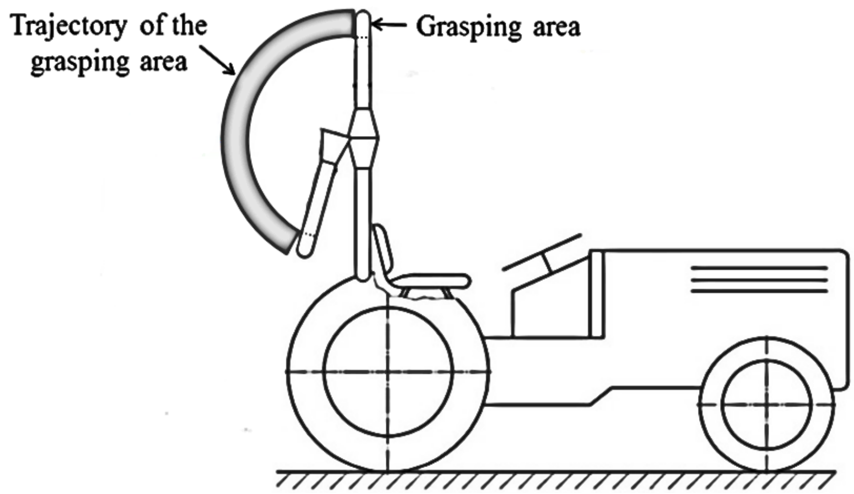

Figure 1.9. Grasping area.

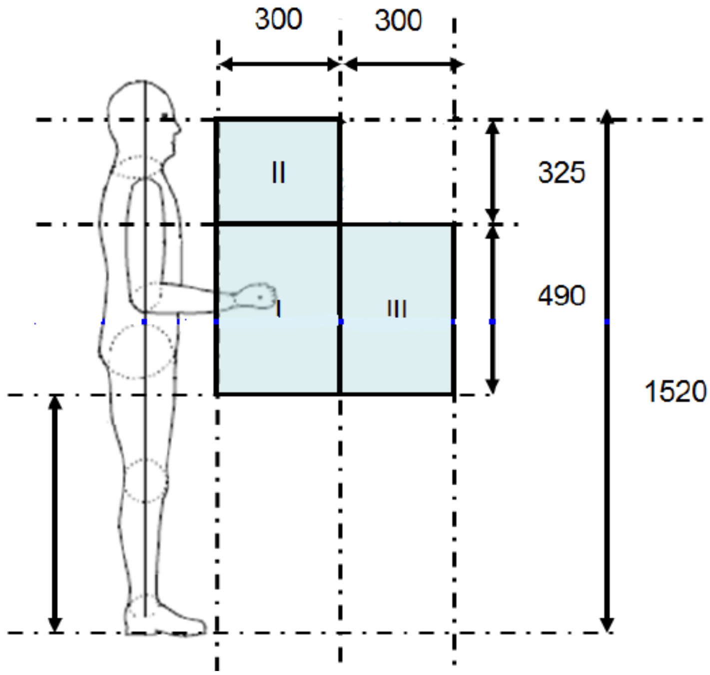

Figure 1.10. Side view of accessible zones zone I: Comfort zone. Zone II: accessible zone without forward leaning of the body. Zone III: Accessible zone with forward leaning of the body (OECD, 2014).

The maximum allowable actuation force depends on the zone that the operator exerts the force (table 1.1). In order to evaluate the OECD code requirements, the actuation force or torque must be measured every 5 degree during raising and lowering the ROPS.

Table 1.1. Maximum allowable forces based on the accessible zones (OECD, 2014).

Zone	I	II	III
Acceptable force (N)	100	75	50

1.2.6 DEVELOPING THE MEASUREMENT SETUP

One of the goals of this study is to measure the angles and the actuation torques of the conventional FROPS. The procedure includes five steps, developing the sensor, sensor calibration, applying the sensor, developing a theoretical model to predict the actuation torques, and comparing experimental test results with theoretical model results. In the first step a torque-angle measurement sensor and an attachment mechanism were developed. The developed system was calibrated before utilizing. The developed system was used to measure the actuation torques-angle of 2 sizes of FROPS in five levels of turning speed. The results are presented in chapter 3.

Another measurement setup was developed to examine the effect of friction on actuation-angle of FROPS. A theoretical curve was developed to predict the actuation torque-angle curve. The results of the developed model were compared with the experimental test results. An angular displacement sensor and a torque measurement sensor were used to develop the actuation torque-angle sensor.

1.2.6.1 ANGULAR DISPLACEMENT SENSOR

The turning angle is the relative angle of the upper part of the FROPS to the horizon. The angle of the raised ROPS is around +90 degree and is equal to zero when the upper part of the ROPS is in horizontal position and the angle is a negative value around -90 when the ROPS is completely folded down. The angle sensor range should be at least 180 degrees to measure the turning angle from -90 to 90 degree. The FROPS upper part angle can be measured with different sensors such as, resistive, optical encoder, magnetic, synchro/resolver displacement sensors, and accelerometer. In the following section the application of displacement sensor for angle measurement will be explained and the sensors are compared to find the best match for the research.

1.2.6.1.1 RESISTIVE DISPLACEMENT SENSOR

The resistive displacement sensors are commonly called potentiometer or Pots. A Pot is an electromechanical device made of an electrical conductive wiper and a fixed resistive element. The wiper is attached to the shaft and moves according to the rotary shaft. The wiper moves against the fixed resistive element and “divided” the fixed resistive element in two parts (fig. 1.11).

The resistance of the resistive element is a function of the length ratio of these two parts. The output is analogue voltage that can be used directly or digitized (Morris & Langari, 2012). The advantages and disadvantages of Pots are listed in table 1.2 (Antonelli et al., 2014).

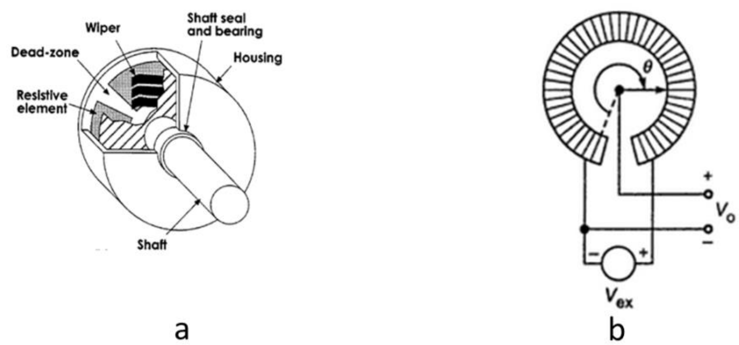

Figure 1.11. Rotary potentiometer a) Schematic b) The circuit (Mathivanan, 2007).

Table 1.2. The advantages and disadvantages of Pots (Mathivanan, 2007; Antonelli et al., 2014).

Advantage	Disadvantage
• Easy to use • Low lost • Non-electronic • High amplitude output • Proven technology	• Limited to the resistive element width • The sensor is affected by inertial loading, frictional load and consequently wear • Large force for moving the contacts

1.2.6.1.2 INDUCTIVE TRANSDUCER DISPLACEMENT SENSOR

Inductive transducers work based on the principles of magnetic circuits and can be divided in two groups, self-generating and manual. The self-generating sensors work based on the principal of the electrical generator. The relative motion between the conductor and magnetic field or a varying magnetic field induces a voltage to the conductor. In some instruments the magnetic field changes as the conductor moves, which finally induces a voltage to the generator.

In the inductive sensors the relative motion between the conductor and the magnetic field is supplied by a measurand motion which usually is mechanical motion. The manual transducer requires an external source of power and the transducer just modulate the excitation signal (Antonelli et al., 2014).

The Rotary Variable Differential Transformer (RVDT) is a manual inductive transducer which has many applications. RVDT has an E-shaped core which the primary winding is wound on the center leg and the two halves of the secondary winding are on the outer leg of the core. The armature is rotated by an externally applied force about the pivot point and above the center legs of the core (fig. 1.12).

When the armature rotates from its reference point, the reluctance through one half of the secondary coil is decreased and increased through the other coil. The electromagnetic fields in the secondary windings are different in the magnitude and the phase as a result of the applied displacement. The output voltage is linear for limited rotation of the armature (-45deg<ɵ<+45deg).The advantages and disadvantages of RVDT are listed in table 1.3.

1.2.6.1.3 OPTICAL ENCODER DISPLACEMENT SENSOR

The angular optical encoders are commonly termed rotary or shaft encoder, since they usually detect the rotation of a shaft. Optical rotary shaft encoders use light to transform the movement in to electrical signals. The devices basically made of two parts, the grating and the detection part. The grating part is made of fixed and moving grating. The moving grating is a disc with radial lines which is attached to the measurand. The fixed grating represents the measurement standard. The measurement is based on the relative position of moving grating respect to the fixed one (fig. 1.13).

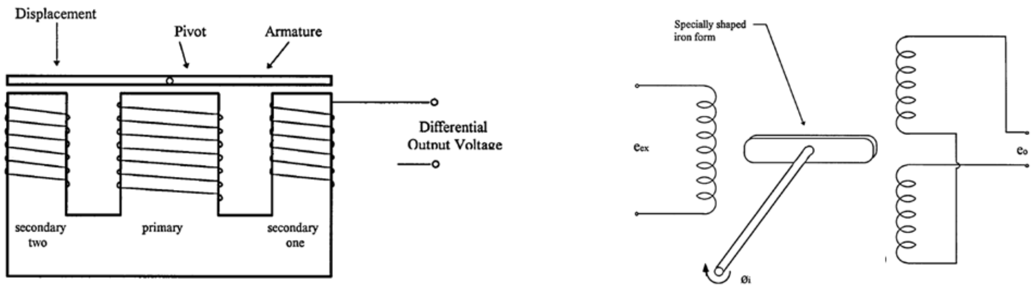

a b

Figure 1.12.The inductive displacement sensor a) schematic of RVDT. b) Electrical circuit (Antonelli et al., 2014).

Table 1.3. The advantages and disadvantages of inductive transducer sensor (Mathivanan, 2007).

Advantages	Disadvantages
• Inherently frictionless • No physical contact between core and coil • Long or infinite mechanical life • High resolution • Very stable • Relatively insensitive to radial motion • Isolation between input and output • Excellent repeatability	• Since the output is proportional to input voltage and frequency, both voltage and frequency excitation should be highly stable • Complicated signal conditioning system is required for phase detection

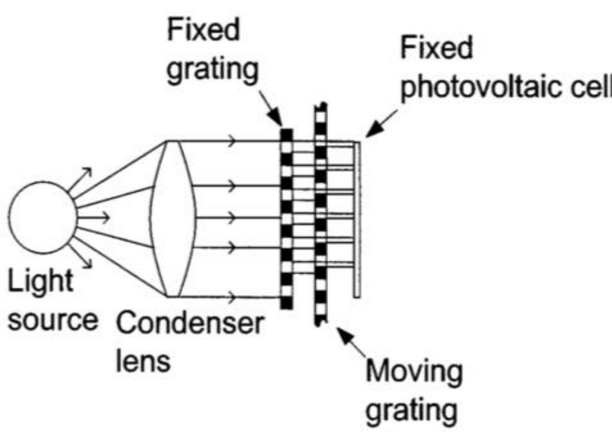

Figure 1.13. Shaft encoder (Antonelli et al., 2014).

1.2.6.1.4 MAGNETIC DISPLACEMENT SENSOR

These sensors rely on the electromagnetic fields and the magnetic properties of the material. Inductive sensors use magnetic field properties, and are based on voltage inducement in a conductor and can measure the displacement in very limited range. There are several types of the magnetic sensors such as, magnetostrictive, magnetoresistive, Hall Effect, and magnetic encoders. The magnetic sensor can measure either increment or absolute displacement (Antonelli et al., 2014).

A magnetostrictive sensor uses a ferromagnetic element to detect the location of a magnet which is displaced along the sensor length. Ferromagnetic materials such as Iron and nickel have a property which was named megnetostriction. The size and shape of ferromagnetic materials under the effect of magnetic field change due to the change in the crystal structure (Antonelli et al., 2014).

The magnetoresistive sensor works based on the change in the electrical resistance of the magnetic material. The electrical resistance of the magnetic material changes when a magnetic field is applied. The electrical resistance of the most magnetic material decrease when a magnetic field applied perpendicular to the current flow (Antonelli et al., 2014).

The Hall Effect is a property exhibited in conductors affected by a magnetic field. A voltage potential appears across the conductor when a magnetic field is applied at right angles to the current flow (Antonelli et al., 2014).

The angular magnetic encoders use a sensing element, read head, and a mechanical enclosure with an input shaft and a brushing. The read head is a disc of magnetic media onto which digital information is stored. The encoded media records the information as magnetized and non-magnetized area. The basic concept of the magnetic encoder is like the shaft encoder (Antonelli et al., 2014).

1.2.6.1.5 INDUCTION POTENTIOMETER (SYNCHRO/RESOLVER DISPLACEMENT SENSOR)

The induction potentiometers are electromagnetic transducers which work based on transformer technology. The sensor is made of three parts, two wound coils and a core. The change in the magnetic flux between two wound coils of a transformer achieved by varying the amount of coupling from the primary winding (excited) to the secondary (coupled) winding. The coupling can be generated by moving one of the windings with respect to the other one or by moving the core element that provides a flux path between the two windings (fig. 1.14).

The difference between the induction potentiometer and the RVDT is that the windings are placed on a stator with two slots (fig. 1.14). The differences between RVDT and inductive potentiometer are shown in table 1.4.

The resolver has multi slot on the stator and two sets of the windings are designed in a concentric coil set and distributed in each quadrant of the laminated stack (fig. 1.15). A close approximation of the sine and cosine wave can be generated on each of the secondary windings. The multi slot rotor lamination and distributing the winding in the rotor, with sine and cosine wave form can improve the accuracy and range even further.

The term "synchro" defines an electromagnetic position transducer that has a set of three phase output windings that are electrically and mechanically spaced by 120 degrees instead of the 90 degrees spacing found in a resolver. In the rotor primary mode, the synchro is excited by a single-phase ac signal on the rotor. As the rotor moves 360 degrees, the three amplitude modulated sine waves on the three phases of the output have a discrete set of amplitudes for each angular position. By interpreting these amplitudes, a table can be established to decode the exact rotary position (Antonelli et al., 2014).

1.2.6.1.6 ACCELEROMETER

The accelerometer can measure both the static due to gravity and dynamic acceleration. The tilting angle of an object can be measured with accelerometer since the static objects are subjected to the gravitational force (g) of the earth and therefore gravity is the acceleration being measured. The accelerometer can be measure the ROPS angle between -90 to +90 degree and the acceleration will change between +1g to -1g. In order to achieve the highest degree of resolution an accelerometer with low *g* and height sensitivity should be used. The relationship between the tilting angle and output voltage is not linear, the sensitivity at 0 degrees where the sensing axis is parallel with horizon) is maximum and by increasing the titling angle the sensitivity will decrease (Clifford & Gomez, 2005).

The relationship between the angle and the acceleration depends on the installation direction (fig. 1.16). If the sensing axis (X) and the direction of gravity are parallel when the object which is in horizontal position, equation 1.4 was used to calculate the tilting angle:

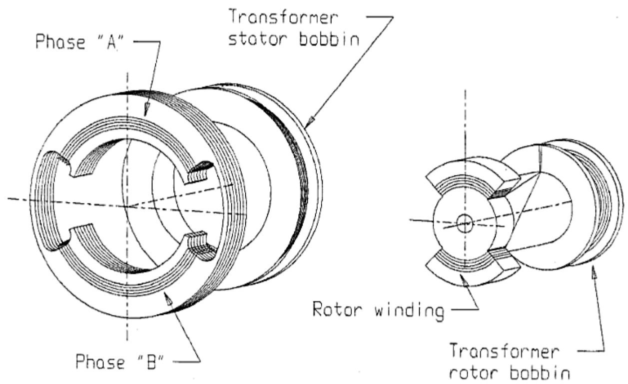

Figure 1.14. The induction potentiometer has windings on the rotor and the stator (Antonelli et al., 2014).

Table 1.4. The advantages and disadvantages of the induction potentiometer in comparison with RVDT (Antonelli et al., 2014).

Advantage	Disadvantage
• The output will have greater sensitivity (more volts per degree) • Better signal to noise ratio • Higher accuracy in most cases	• Additional windings • More physical space is required • Greater variation over temperature • Greater phase shift due to additional winding

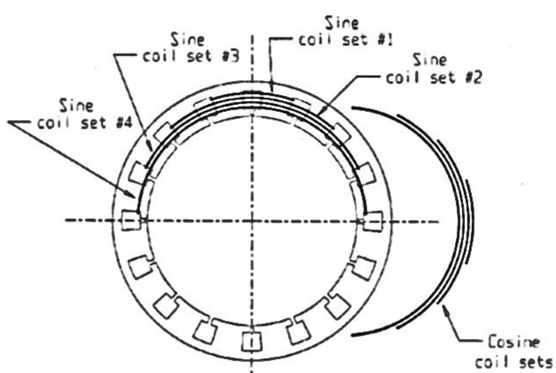

Figure 1.15. The resolver stator has distributed coil windings on a 16- slot lamination to generate sine wave (Antonelli et al., 2014).

$$\theta = \sin^{-1}\left(\frac{V_{Out} - V_0}{\Delta V/\Delta g}\right) \tag{1.4}$$

Where, V_{OUT} is accelerometer output in Volts, V_0 is accelerometer output in Volts in horizontal position, ΔV/Δg is sensitivity, 1g is earth gravity, and θ is tilting angle.

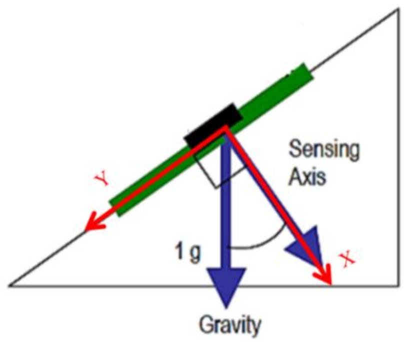

Figure 1.16. Gravity component of the tilted X-axis accelerometer (Clifford & Gomez, 2005).

The accelerometer sensor model Crossbow CXL04LP3 was selected to measure the turning angle. This type of sensor possesses all of the required properties (i.e. range, and resolution, environmental properties) for this study. Some of the other sensors had the required properties, but these sensors should be installed in line with the motor shaft and pivot point. This increases the length of the setup and increases the effect of torsional deflection and consequently the error in torque and angle measurement. The accelerometer was attached to the upper part of FROPS by means of a magnet without disturbing the performance of the torque sensor and motor.

From the Crossbow CXL04LP3 specification sheet the sensitivity and the V_o for X, Y, and Z directions are presented in table 1.5.

Table 1.5. Sensitivity and the Zero-G Voltage (Vo) of Crossbow CXL04LP3

	X axis	Y axis	Z axis
Zero-G Voltage (V_o)	2.545	2.544	2.547
Sensitivity (ΔV/Δg)	0.511	0.511	0.520

In this study the X-axis of the accelerometer is perpendicular to the trajectory of the ROPS, which means that, the accelerometer measures the radial acceleration in X direction. The Y-axis of the accelerometer measures the acceleration tangential to the ROPS trajectory. The gravitational acceleration can be measured both in X and Y direction. For this study, acceleration in X direction was used for angle calculation and acceleration in Y direction was used to improve the calibration.

1.2.6.1.6.1 TEST THE STATIC CALIBRATION

For calibration the angle was measured by the *Fowler Mini-Mag Protractor* model 54-422-450-1 and *Crossbow* CXL04LP3 accelerometer. The measured values by Fowler digital sensor are considered as true measurement and compared with the measured values by accelerometer. The angle was measured from +90 to -90 statically. Results are shown in Fig. 1.17. There is a good agreement between two sensors measurement. The average error is 0.02% and RMSE is 0.15 degree.

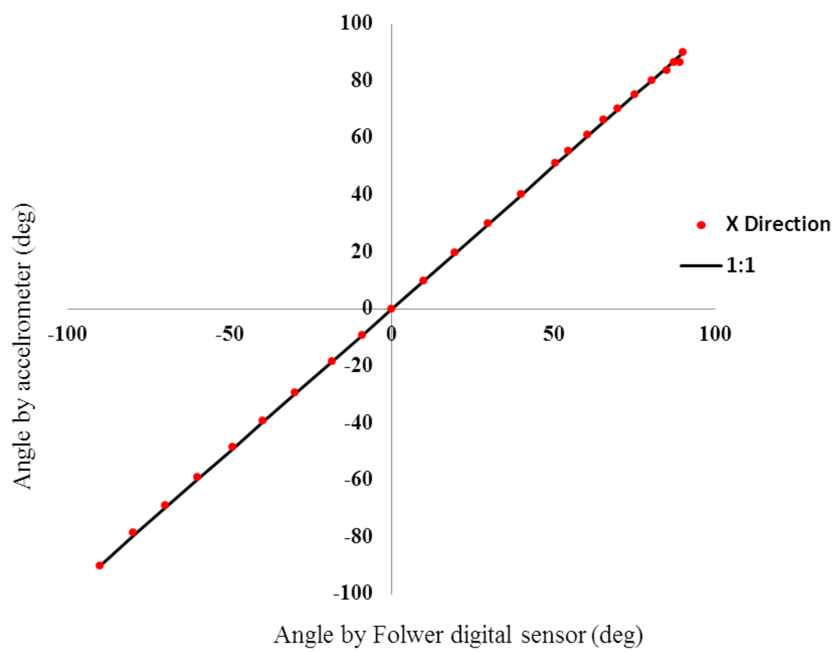

Figure 1.17. The measured angle by Folwer digital sensor and the accelerometer from +90 to -90 in X direction.

The output of the accelerometer sensor was converted to angle by equation 1.4. In order to examine sensitivity and V_0, at least two outputs of the accelerometer are required, the output in +90, or -90, and 0. The maximum output of the sensor in X direction happens when the ROPS angle is +90 and minimum occurs when the ROPS angle is -90. The maximum output of accelerometer in Y direction occurs when the ROPS angle is 0 (fig 1.18). Therefore by finding maximum or minimum of accelerometer in X direction and minimum output in Y direction, The sensitivity and V_0 can be calculate. The V_0 is the accelerometer output in 0 g or 0 angle. The sensitivity was measured by knowing the acceleration in a known point and the sensor output at that point, the static acceleration at +90 degrees is +g and at -90 degrees is –g.

1.2.6.1.6.2 DYNAMIC CALIBRATION TEST WITH FORK

The motor and the fork were used to test the dynamic calibration of the accelerometer (fig. 1.19). The fork was turn by means of a motor and the accelerometer is attached 0.2 m from the pivot point of the motor.

The fork was turned with maximum and minimum possible speeds and the results showed that there is no significant difference between the accelerometer output in the low (1.8 RPM) and high (8.7 RPM) speeds and also in static condition (fig. 1.20), as the maximum values did not change. The angle for two levels of speed is calculated and is shown in figure 1.21. It appears that rotational speed has very little influence on the angle measurement,

The proposed OECD working document describes a maximum rotational speed of 20 deg s^{-1} (3.3 rpm) when testing the automatic locking system. This speed was target speed during the friction field testing of the multiple FROPS. The sensor repeatability is shown in figure 1.22.

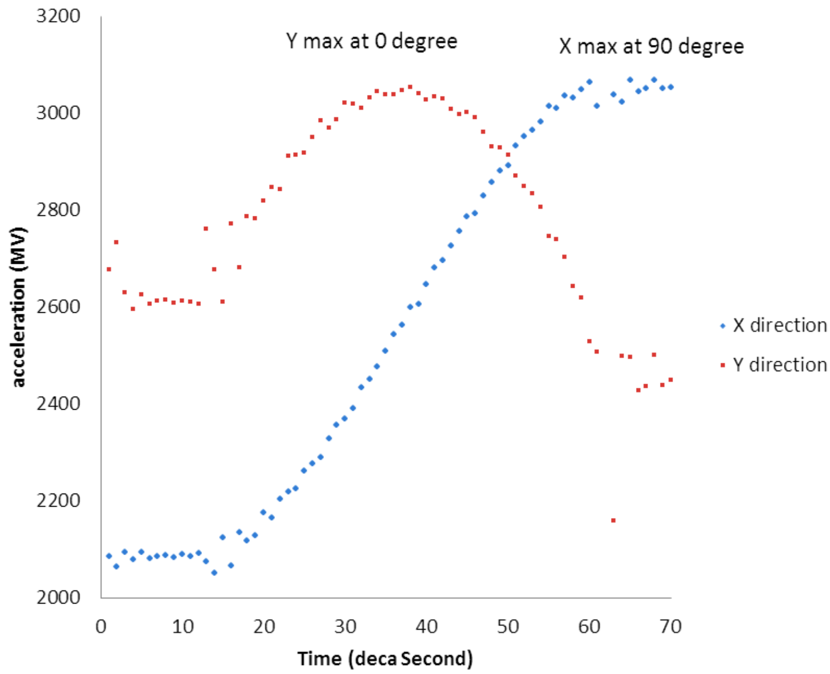

Figure 1.18. The maximum accelerometer output in X direction occurs at +90 and minimum value occurs at -90. The maximum accelerometer output in Y direction occurs at 0 degree.

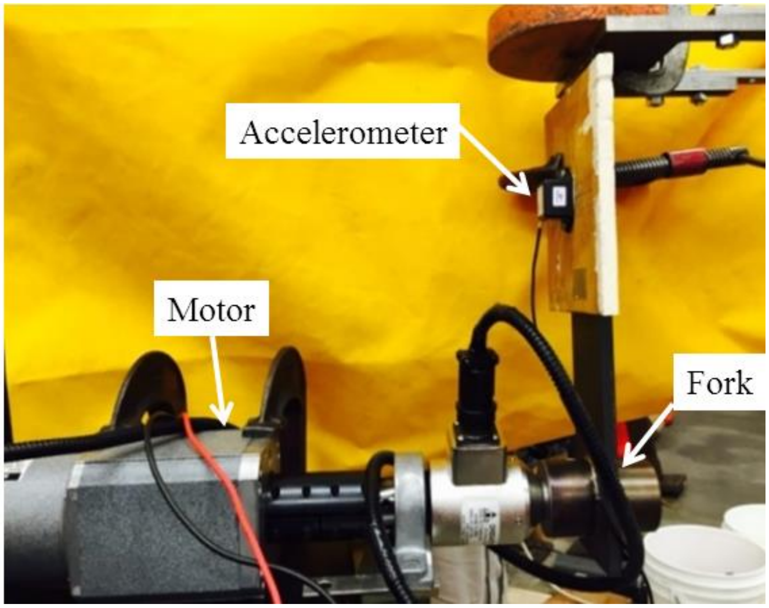

Figure 1.19. Dynamic Calibration of accelerometer.

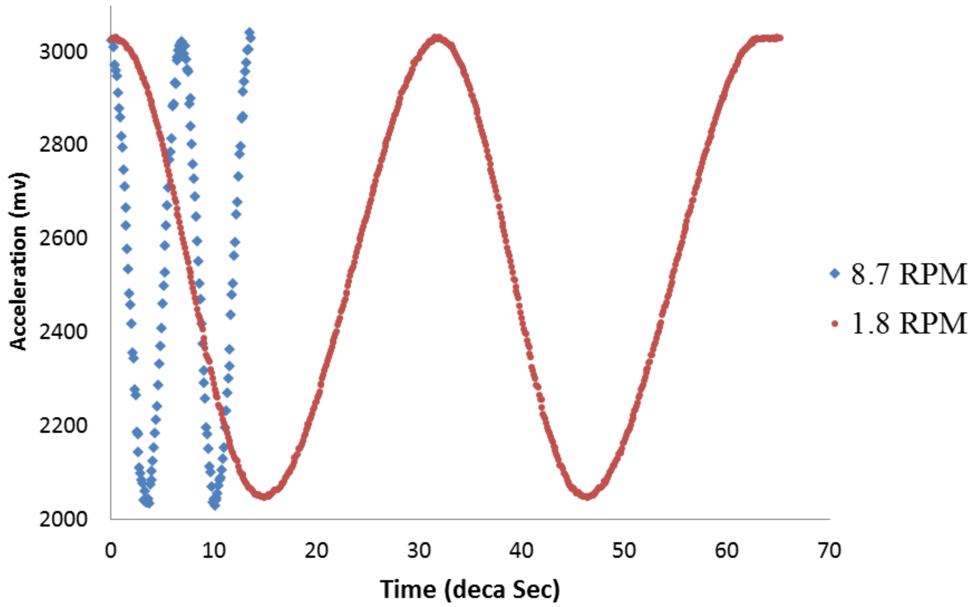

Figure 1.20. The accelerometer output in 720 degree turns (two revolutions).

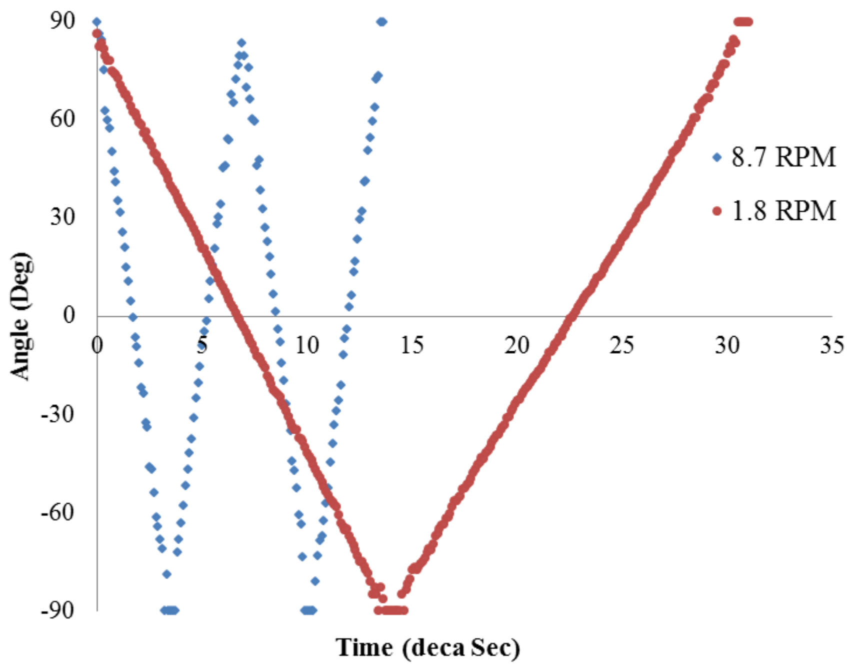

Figure 1.21. Accelerometer output (degree) for low and high turning speed.

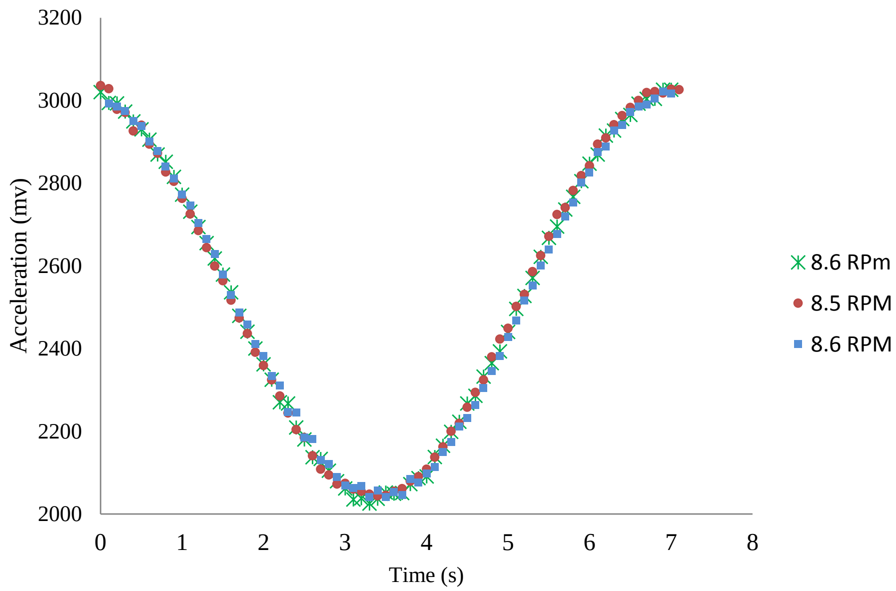

Figure 1.22. Accelerometer repeatability.

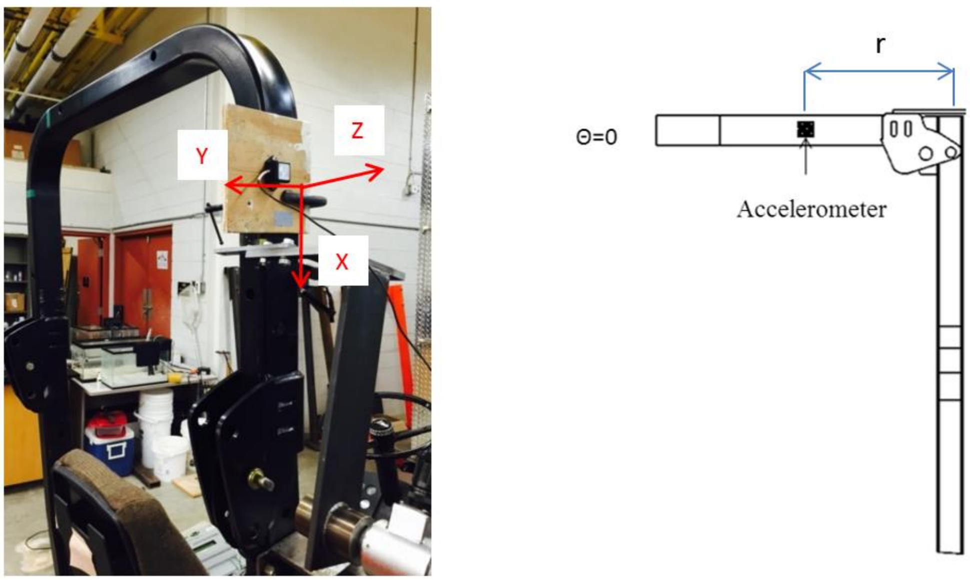

Figure 1.23. The accelerometer attachment to the upper part of the ROPS.

1.2.6.1.6.3 DYNAMIC CALIBRATION TEST WITH ROPS

The performance of accelerometer to measure the ROPS angle was examined. The lever distance (r) of the FROPS is higher than the fork. The X, Y, and Z directions of the accelerometer relative to the ROPS is shown in figure 1.23. The angle based on sensor output in X direction was calculated and shown in figure 1.24.

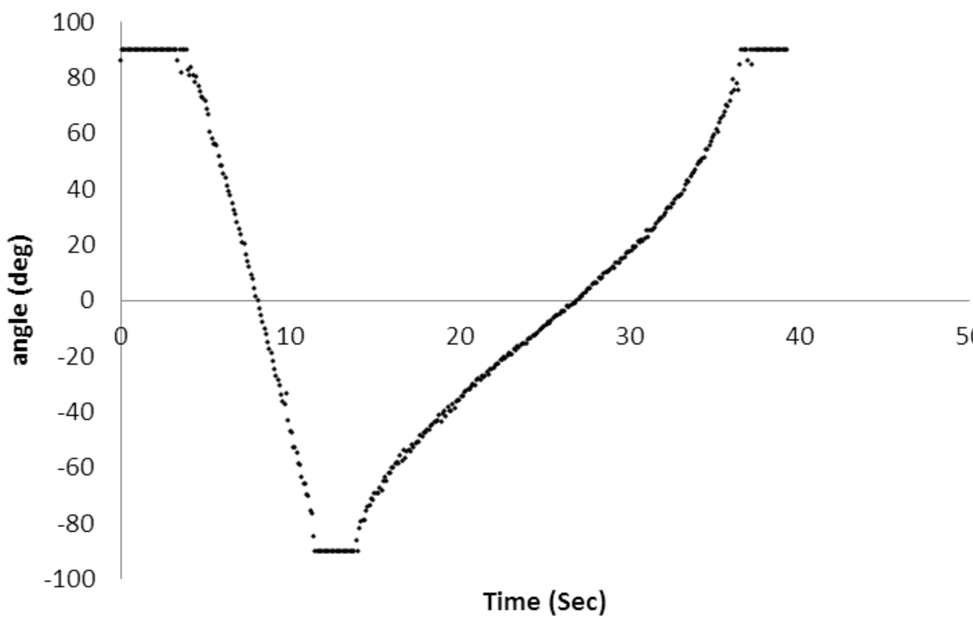

Figure 1.24. The accelerometer output (Degree) in X direction.

1.2.6.1.6.4 TANGENTIAL ACCELERATION (a_θ) AND CENTRIFUGAL ACCELERATION (a_r)

The circular movement of the upper part of the ROPS is non uniform which means that the speed is not constant. The effect of these acceleration on accelerometer output were calculated in this section. The upper part movement includes two parts:

a) The non-uniform speed of the circular motion from 0-0.5 second. The non-uniform circular motion includes the Tangential acceleration (a_θ) and Centrifugal acceleration (a_r) (fig. 1.25).

b) The uniform circular speed of the motion 0.5 sec after the start point to 0.5 sec before the stop point (assumes that the time for motor to reach the selected speed is 0.5 second and the velocity change rate is constant)(fig. 1.25).

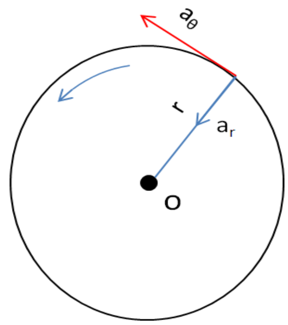

Figure 1.25. Tangential acceleration (a_θ) and Centrifugal acceleration (a_r).

Two accelerations affect the accelerometer measurement, which are:

1) The gravitational acceleration (*g)* which is constant and equal to 9.81 m s^{-2} and changes from (+g to –g)
2) The acceleration due to circular motion of the upper part of the ROPS which evolves:

a) Tangential acceleration (a_θ): Due to change in magnitude of velocity,

$$a_\theta = r\frac{d\omega}{dt} = \frac{d|v|}{dt} \tag{1.5}$$

Where ω is the rotational speed in $s\text{-}^{1}$, t is time in s, a is acceleration in $ms\text{-}^{2}$, and v is speed in $ms\text{-}^{2}$, r is the radius in m.

b) Centrifugal acceleration (a_r): Due to change in in direction of velocity,

$$a_r = -\omega^2 r = -\frac{|v|^2}{r} \tag{1.6}$$

In this study the X-axis of the accelerometer is perpendicular to the trajectory of the ROPS which means that, the accelerometer measures the radial acceleration in X direction. The Y-axis of the accelerometer measures the acceleration tangential to the ROPS trajectory. Therefore the tangential acceleration due to uniform circular speed just affects the acceleration in X direction. The acceleration due to non-uniform motion affects the acceleration measurement both in X and Y direction. The gravitational acceleration can be measured both in X and Y direction.

A. THE FORK

$$a_r = -\omega^2 r = -\frac{|v|^2}{r} = 0.2 \times 0.19^2 = 0.0072 \ (m\, s^{-2}) \ \text{min} \tag{1.7}$$

$$a_r = -\omega^2 r = -\frac{|v|^2}{r} = 0.2 \times 0.91^2 = 0.17 \ (ms^{-2}) \ \text{max} \tag{1.8}$$

The linear velocity is calculated by:

$$V = r\,\omega \ (\text{m s}^{-1}) \tag{1.9}$$

The acceleration is calculated:

$$a = \frac{m(v_{2-}\, v_1)}{ts^2} \tag{1.10}$$

$$a_\theta = r\frac{d\omega}{dt} = \frac{d|v|}{dt} = \frac{0.2*0.19}{0.5} = 0.076 \ (m\, s^{-2}) \ \text{min} \tag{1.11}$$

$$a_\theta = r\frac{d\omega}{dt} = \frac{d|v|}{dt} = \frac{0.2*0.91}{0.5} = 0.36 \ (m\, s^{-2}) \ \text{max} \tag{1.12}$$

When the fork turns for 360 degrees, the accelerometer output changes from 2047 to 3017 (985 mV) and the acceleration changes 19.62 m s^{-2}. The Full Scale Output (FSO) error is 2%. The FSO is the algebraic difference between the output of the minimum input and maximum input.

B. THE ROPS

$$\text{Max: } a_r = -\omega^2 r = -\frac{|v|^2}{r} = 0.4 \times 0.67^2 = 0.18 \ (m\, s^{-2}) \tag{1.13}$$

$$\text{Min: } a_r = -\omega^2 r = -\frac{|v|^2}{r} = 0.4 \times 0.15^2 = 0.009 \ (m\, s^{-2}) \tag{1.14}$$

$$\text{Max: } a_\theta = r\frac{d\omega}{dt} = \frac{d|v|}{dt} = \frac{0.4*0.67}{0.5} = 0.53 \ (m\, s^{-2}) \tag{1.15}$$

$$\text{Min: } a_\theta = r\frac{d\omega}{dt} = \frac{d|v|}{dt} = \frac{0.4*0.15}{0.5} = 0.12 \ (m\, s^{-2}) \tag{1.16}$$

When the ROPS turns for 180 degree, the accelerometer output changes from 2047 to 3017 (985 mV) and the acceleration changes 19.62 m s^{-2}. The error is 2.5%.

1.2.6.2 ACTUATION FORCE

The actuation force can be measured directly as force or can be measured indirectly as torque. In the direct measurement the exerted actuation force can be measured with a force transducer, and the torque can be measured by a torque transducer. The transducers that measure the force and torque are made of elastic members that convert the mechanical quantity to deflection or strain. A deflection sensor such as strain gauge can be used to give electrical signals proportional to the quantity of the measured force or torque. The characteristics of the transducer depend on the size, shape, and material properties of the elastic member and the deflection sensor properties (Dally, Riley, & McConnell, 1993).

1.2.6.2.1 *LOAD CELL SELECTION*

The elastic members that commonly used in the load cells are links, beams, rings, and shear webs. The link type load cell can measure both the tensile and compression. The four strain gages are attached to the elastic member and wired to each other by Wheatstone bridge circuit (Dally et al., 1993). The beam type is usually used for measuring low level loads where the link type load cell is too stiff to measure the force (Dally et al., 1993). This type of load cell seems to be inappropriate for this this research, since the load cell requires measuring the high level of tension and compression loads. The ring type load cell is made of a ring as the elastic member. The deflection is usually measured with a linear variable differential transformer (LVDT). This type of sensor can measure the wide range of loads (Dally et al., 1993). This type of sensor is big and not appropriate for this research. The shear web load cell known as low profile or flat load cell is useful for application where the space is limited along the line of action of load. This load cells is compact and stiff, and appropriate for measuring the dynamic loads with high frequencies (Dally et al., 1993).

1.2.6.2.2 *TORQUE TRANSDUCER SELECTION*

An electromechanical torque transducer is made of a circular shaft as the strain member which the deflection is measured by means of strain gages. The strain gages are mounted on two perpendicular 45 degree helices that are diametrically opposite one another. The strain gages are attached together in a Wheatstone bridge configuration. The applied torque to the sensor causes bending or shearing in the gage area and the torque transducer generates an output voltage signal proportional to the torque. Transducers can be divided in to two categories, rotary (dynamic) and reaction (static). The reaction transducer can measure torque without rotation, while the rotary torque transducer rotates multiple times as a part of the system. Normally, the reaction torque transduce has a cable to supply the excitation voltage to the Wheatstone bridge and for the output signal. Since using a cable for a rotary transducer is not practical, several methods such as slip ring, rotary transformers, rotating electronics, rotating digital electronics and radio telemetry are used to transfer power and signal (Dally et al., 1993). The static transducers are appropriate for this research, since the upper part rotates about 180 degree. A static reaction torque cell (OMEGADYN Inc. model TQ420-2K) was selected to measure the torque.

1.2.6.2.3 TORQUE TRANSDUCER

The torque was measured by a *Reaction Torque Cell* model TQ420-2K. The torque transducer range is 0 to 225 Nm. The torque transducer is attached between the motor and the fork to measure the actuation torques to fold down and raise the fork. The torque transducer performance was tested by adding known weights at a known distance from the axis of the torque transduces. The sensor measured torque with the given calibration had a good agreement with the applied values (fig. 1.26). The expected torque for experiments is up to 135 Nm therefore, the sensor performance was tested between 0 to 135 Nm (fig. 1.26). The average error is 0.38% and RMSE is 0.57 Nm.

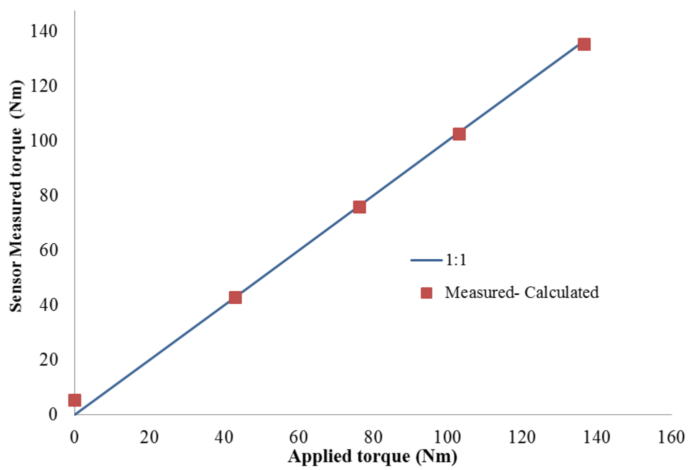

Figure 1.26. Torque transducer performance.

1.2.6.2.4 MEASUREMENT SETUP

Two methods were proposed to measure the actuation force by means of a load cell and one setup was proposed to measure the actuation torque by means of a torque cell. One of the measurement setups was used to measure the actuation force in preliminary tests. In this method, the actuation force and angle were measured by means of a load cell, and accelerometer, respectively. A lever arm was attached to the ROPS and a load cell was attached to the lever arm by means of hook. The operator exerts the force to the load cell to raise the ROPS. The problem with this method is that the operator cannot keep the load cell perpendicular to the lever arm and the force direction must be changed at breaking point (fig. 1.27). Changing the direction of force at the breaking angle makes the measurement inaccurate.

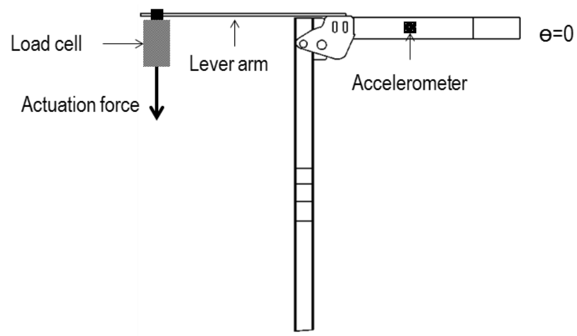

Figure 1.27. Actuation force measurement by adding a lever arm.

The second proposed system includes a load cell, a motor, and a mechanism as shown in figure 1.28. In order to exert the actuation force with specific speed the motor can be used to fold down and raise the ROPS. The load cell can be placed between the lever arm and the ROPS. The load cell should be the only attachment point of the fork to the ROPS. The actuation force (F) is equal to:

$$F = \frac{F_1 l_1}{l} \qquad (1.17)$$

Where F is actuation force (N), l is the distance between the pivot point and the cross bar (m) F_1 is the force which is measured by the load cell (N), and l_l is the length of fork (m). The last proposed measurement setup measures the actuation torque and angle. This setup was selected for this study. Based on OECD code, the actuation force can be measured in form of torque. A motor was attached to the lower part of the FROPS by means of a platform and the motor turned the upper part of the ROPS by means of a fork. The torque transducer was attached between the motor and the fork (fig. 1.29). The force can be calculated by equation 1.18.

$$T = Fl \qquad (1.18)$$

Where T is torque (Nm), F is actuation force (N), l is the distance between the pivot point and the cross bar (m). The developed measurement setup to measure the actuation torque and angle is shown in figure 1.30.

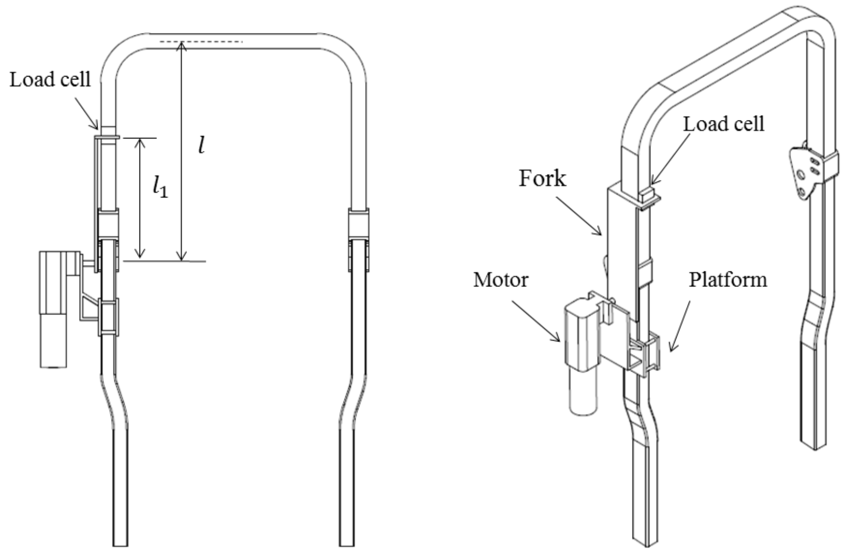

Figure 1.28. Applying a load cell to measure force.

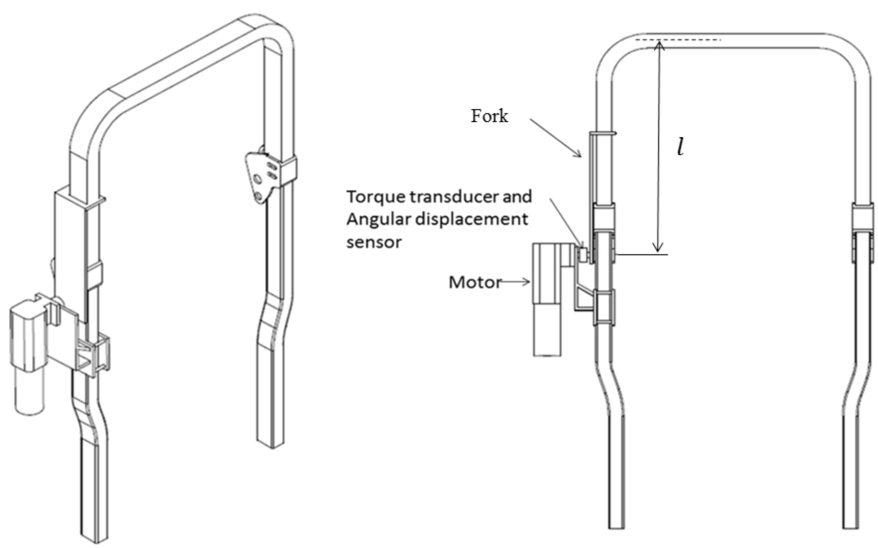

Figure 1.29. The proposed actuation torque-angle measurement setup.

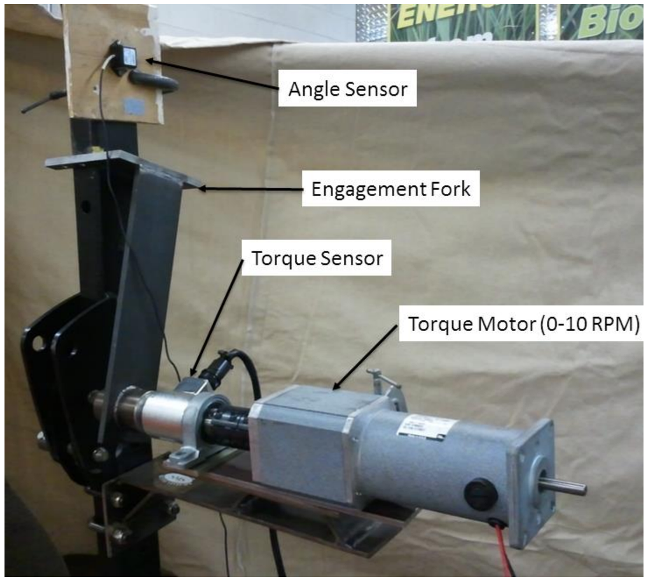

Figure 1.30. The final developed measurement setup to measure actuation torque-angle of FROPS.

1.2.7 SUMMARY

Rigid ROPS are not appropriate for working in low overhead clearance zones. The FROPS was designed to solve the rigid ROPS problem, but folding and raising the conventional FROPS are time consuming and strenuous processes. The manual, powered, and automatic FROPS have been developed to solve the conventional ROPS problem. The powered and automatic FROPS systems are expensive, complex, and in some cases the ROPS must be completely replaced with a new one. Manufacturers have retrofitted tractors with ROPS since 1985 and just 59% of the tractors have been equipped ROPS until 2014 (CDC, 2014). Prediction suggests that only 75% of the tractor in service will be equipped with ROPS at 2024 if no other action is taken (Hoy, 2009). By considering the slow rate of applying ROPS, replacing the available ROPS with automatic systems or adding expensive powered systems seems to be impractical. The manual systems are simple and low cost, but the actuation force is high.

The FROPS actuation forces are not well known and an OECD standard code is developing to regulate actuation forces. Based on OECD standard code the maximum actuation force should not be more than 100 N (OECD, 2014). No turning speed is stated in the standard. The FROPS actuation forces may be influenced by turning speed. Some manual systems employ a lever arm to decrease the actuation force, but the strong and the heavy ROPS require a lift assist mechanism to help the operator (Panek & Kolli, 1998). The actuation force is one of the most important factors that needs to be measured prior to the development of a fold assist mechanism design.

There was no instrumentation available to measure the actuation force as a function of angle of the FROPS. The developed sensing setup was applied to measure the actuation torque of the FROPS to see whether the FROPS meet the standard requirements. Also the effect of turning speed and friction on actuation torque needs to be evaluated. The measured force and angle values can be used to design a fold assist mechanism.

1.3 THE EFFECT OF LIQUID SHIFT ON CG HEIGHT MEASUREMENT

The center of gravity (CG) is the location of a theoretical point representing the total mass of a body. Since off-road vehicles often possess many irregular shapes, it is practically impossible to find the CG location using analytical methods. Various techniques can physically determine the CG of vehicles. These methods are vertical hang, pendulum, lifting axle, and tilt table. The lifting axle method (LAM) is a popular method for determining the CG height of a vehicle. The lateral and longitudinal dimension of CG can be measured when vehicle is in horizontal position, but for measuring the CG height, the vehicle should be tilted. By tilting the vehicle, liquid inside the vehicle moves and changes the load on rear and front axle. The weight distribution on rear and front axle is one of the important factors for determining the CG height based on ISO 16231 (ISO, 2015). But the ISO 16231-2 does not consider the effect of liquid shift on CG height measurement. The effect of liquid shift on CG height needs to be evaluated to consider its influence.

1.3.1 COORDINATE SYSTEM

The coordinate system of the center of gravity (CG) point includes lateral, longitudinal, and vertical distance from origin (fig. 1.31). The longitudinal dimension of the CG (X) is defined as the horizontal distance from transverse reference plane. The transverse reference plane is defined as the vertical plane respect to the ground plane, which passes the center line of the rear axle of the agricultural tractor. The lateral dimension of the CG (Y) is defined as the horizontal distance from the median longitudinal plane. Median longitudinal plane is the vertical plane respect to the ground plane, which passes through the major front and rear axis midway points. The height of CG (Z) is defined as the vertical distance from the horizontal reference plane which is ground surface (fig. 1.31). The intersection of the three planes (transverse reference plane, median longitudinal plane, and horizontal plane) is called origin point (O).

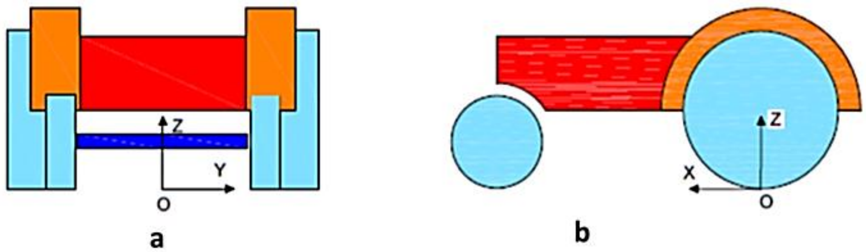

Figure 1.31. Coordinates system and origin point a) Front view. b) Side view.

1.3.2 PENDULUM METHOD

The dynamic pendulum method is the most frequently used method in the testing stations in Europe (Fabbri & Molari, 2004). The CG height calculation in the pendulum method is based on the simple harmonic oscillation equation. The tractor is placed on an oscillating platform. The combination of tractor and platform is called oscillating mass. The oscillation period is a function of suspension length which is the distance between CG height of oscillating mass and the oscillating platform pivot point. The CG height of the platform is known and the CG height of the tractor can be calculated by measuring the oscillation period of the platform and the combination of the tractor and the platform in two different suspension lengths (Fabbri & Molari, 2004). The dynamic pendulum method introduces some uncertainties due to the friction losses in bearings, and air resistance, liquid motion, tire deflection, loose solid part movement, and platform deflection (Fabbri & Molari, 2004).

Fabbri and Molari (2004) measured CG height of narrow track agricultural machinery using the static pendulum method. An inclined platform was used for the CG height measurement. A cable was attached to the platform and the CG height was calculated based on lateral inclination angle, lateral pulling force with tractor, lateral pulling force without tractor, and the distance from the force application point and the median vertical plane of the tractor. Results showed that static pendulum method is more precise than the dynamic pendulum method. They stated that the static method eliminated the problems when using the dynamic method such as, fluid motion, air resistance, the approximation in the simple model of harmonic oscillations and the uncertainties related to the oscillation period measurement (Fabbri & Molari, 2004).

1.3.3 *LIFTING AXLE METHOD*

Measured parameters in the lifting axle method are load on front and rear axle of the vehicle in horizontal position, load on lifted axle, and the some structural geometries of the vehicle (fig. 1.32 and 1.33). The lateral and longitudinal CG measurements are straightforward. The CG height measurement is considerably difficult, since it needs to lift one axle of the vehicle, either the front or rear. The weight of the tractor is equal to the summation of load on the front and rear axles. The CG lateral dimension can be calculated by equation 1.19. All of the symbols in the equations 1.19-1.27 are shown in figures 1.32 and 1.33.

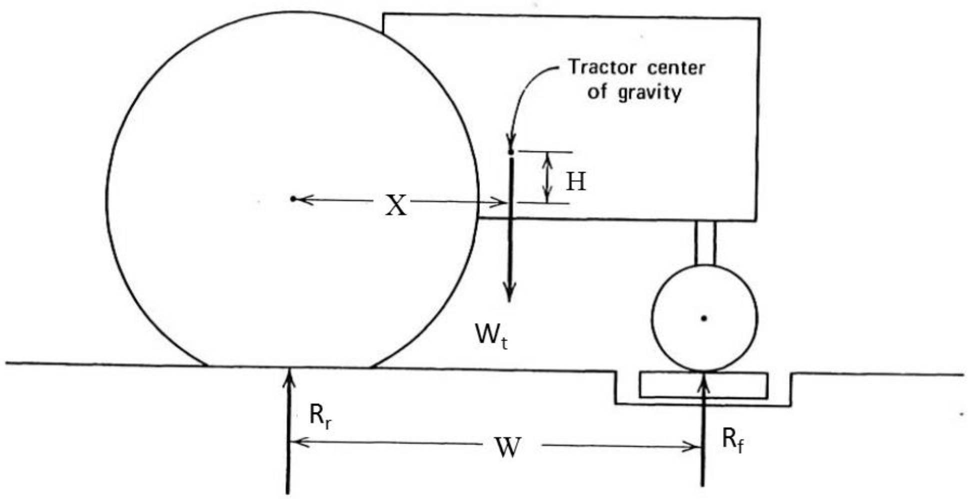

Figure 1.32. Determination of the longitudinal location of the center of gravity using lifting axle method (Liljedahl, Turnquist, Smith, & Hoki, 1996).

$$X = R_f W / W_t \tag{1.19}$$

By lifting the vehicle axle the summation of moments about the rear axle;

$$X'' = \acute{W} \acute{R_f} / W_t \tag{1.20}$$

From the geometry of figure 1.33:

$$X'' = X \cos\lambda - H \sin\lambda \tag{1.21}$$

$$\acute{W} \acute{R_f} / W_t = X \cos\lambda - H \sin\lambda \tag{1.22}$$

$$\acute{W} = (X + \Delta r\ \tan\lambda) \cos\lambda \tag{1.23}$$

Subtituting equation 3.5 in to equation 3.4, dividing by cos λ and solving for H:

$$H = \frac{X\,W_t - \acute{R_f}\,W}{tan\,\lambda\,W_t} - \frac{\acute{R_f}\Delta r}{W_t} \tag{1.24}$$

the angle λ is the only quantity that cannot be directly measured. However,

$$tan\,\lambda_1 = (n - r\,)/\acute{W} \tag{1.25}$$

$$tan\,\lambda_2 = \Delta r/X \tag{1.26}$$

$$\acute{L} = \sqrt{W^2 + (\Delta r)^2 - (n - r)^2} \tag{1.27}$$

Wang, Gao, Ayers, Su, and Yuan (2016) used a test method which was developed based on ISO 16231-2. They used this test method to minimize the effect of springs, fuels, hydraulic oil, lubrication oil, and elastic cells on the CG height measurement of the zero turning radius (ZTR) mower. They lifted the front axle of the vehicle and measured the force on the front axle five times, and repeated the measurements every one degree. They added and subtracted 0.1 kg (deviation of the accuracy of the scale) from the measured weight on the front axle and calculated the CG height for each angle. If the calculated CG heights based on weight on front axle ± 0.1 kg did not exceed ±4% of the CG height, they reported that CG height as the actual CG height of the ZTR mower.

1.3.4 STANDARD ISO 16231-2

ISO 16231 (2015) is a standard for stability assessment of self-propelled agricultural machinery. The CG height affects the vehicle stability (Demšar, Bernik, & Duhovnik, 2012), therefore the first section of ISO 16231-2 is assigned to measuring CG location of un-laden self-propelled agricultural machinery. The static stability angle (SOA) measurement method is explained in the second section. The CG height is measured based on the lifting axle method and by means of scales and support stands. The CG height is calculated based on figure 1.34 and 1.35, and table 1.6. All of the symbols in table 1.6 are shown in figures 1.34 and 1.35.

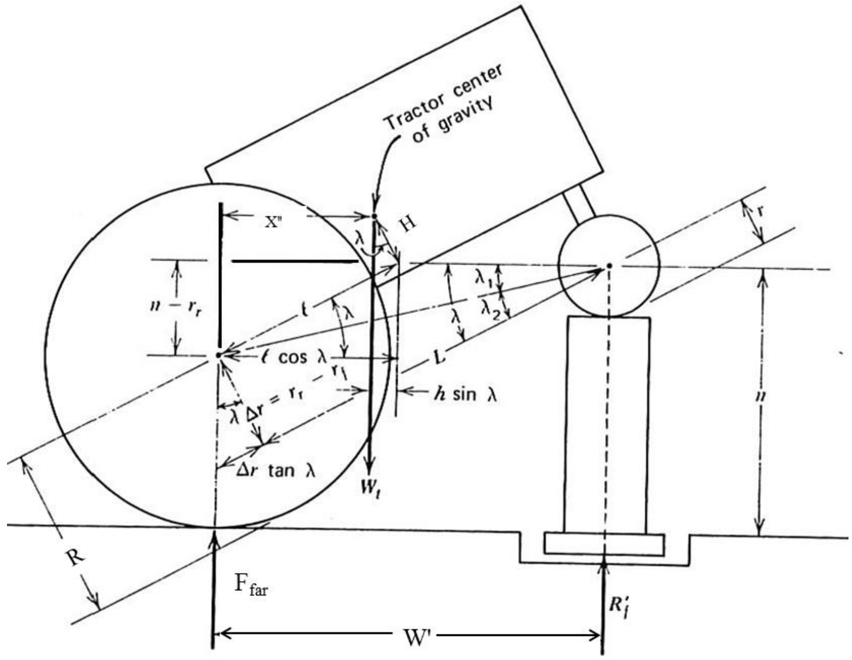

Figure 1.33. Determination of the vehicle location of CG (Liljedahl et al., 1996).

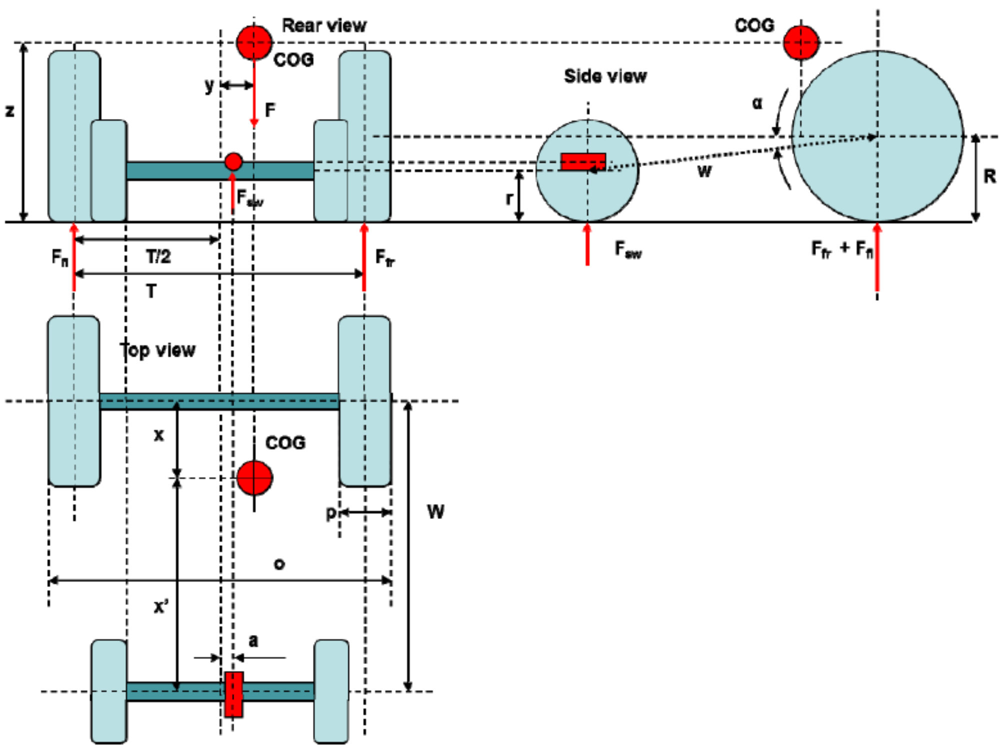

Figure 1.34. Rear, top, and side view of the machine (ISO, 2015).

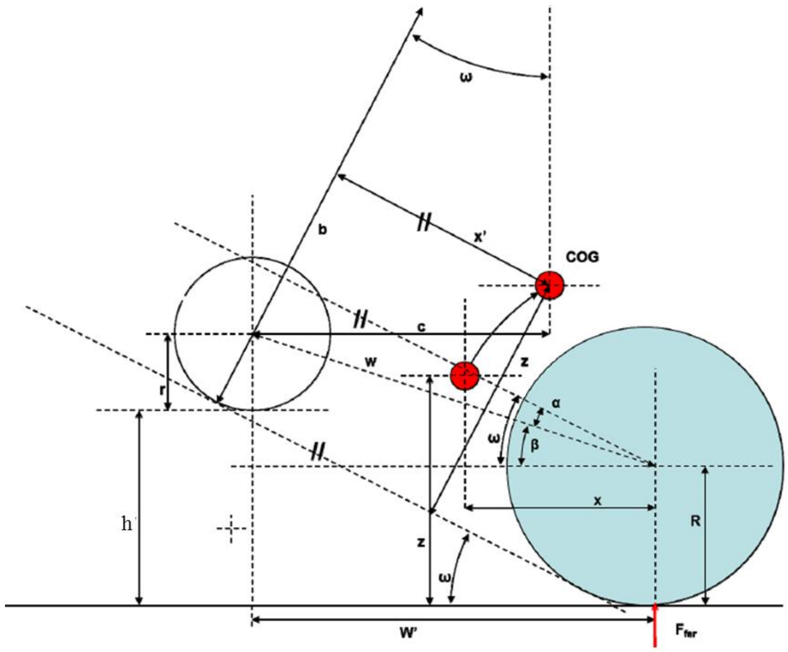

Figure 1.35. Machine in raised position - side view (ISO, 2015).

Table 1.6. CG Calculation (ISO, 2015).

Data description	Symbol	Unit	Calculation
Wheel track of fixed axle	T	M	o-p
Total weight of the machine	Ft	N	$F_{fr}+F_{fl}+F_{sw}$
Lateral position of CG (versus center of fixed axle) (positive number means right from center of fixed axle)	Y		$[(F_{fr}*T)+(T/2+a)*F_{sw}]/F_t-T/2$
Longitudinal position of CG (versus center of swiveling axle)	x'	M	$W(F_{fr}+F_{fi})/Ft$
Longitudinal position of CG (Versus center line of the fixed axle)	X	M	W-x'
Longitudinal distance between wheel centers	W	M	$\sqrt{((R-r)^2+W^2}$
Vertical projection of wheel base in raised position	W'	M	$\sqrt{(w^2-(h+r-R)^2)}$
Angle formed by the line between wheel centers and horizontal through the center of the fixed axle wheels	A	Deg	$\cos^{-1}(W/w)$
Angle formed by the line between wheel centers and horizontal through the center of the fixed axle wheels in raised position	B	Deg	$\tan^{-1}((h+r-R/\acute{W})$
Lifting angle	Ω	Deg	α+β
Vertical projection of longitudinal distance between CG and the swiveling axle in raised position	C	M	$F_{far}\times\acute{W}/F_t$
Auxiliary line for calculation	B	M	$r+(c/\sin\omega)$
Height of CG	Z	M	$b-(\acute{x}/\tan\omega)$

Standards usually provide some remarks to decrease the error caused by unexpected factors such as, liquid shift and tire deflection. ISO 16231-2 provides several remarks in order to improve the test procedure (ISO, 2015):

1. Steel wheels should be used in order to avoid error caused by the tire deflection under different loads in different tilting angles.
2. Suspension systems shall be locked.
3. If the steel wheels are not used, the tire should be inflated to the maximum permissible pressure specified by the tire manufacturer.
4. The change in the tire radius in horizontal and tilted position should not be greater than 1.5% of the wheel radius.
5. The plane of the scale should be horizontal and parallel to the ground plane.
6. The wheels on the scale must be free to rotate and be in the position for towing the vehicle. Therefore the parking brakes shall not be applied and the transmission system must be in the position for towing the vehicle.
7. It is recommended to lift the axle with the smaller wheel diameter.
8. Reading the weight on scale shall be done after complete rest of the lifted axle on the scale.
9. It is recommended to lock the swiveling axle with wedges, when lifting the vehicle.
10. The values of weighing during 5 consecutive measurements must fall within a range of 1.0% of the maximum measured load from the fixed axle in raised position.
11. "Calculate the CG, using the deviation of the accuracy of the scale (+ and -) and determine the percentage of deviation of the height of the CG (+/-). This number shall not exceed +/- 4%. In case it exceeds +/- 4%, the height of the wheel stands shall be increased in order to decrease the deviation."

The lateral and longitudinal dimension of CG can be measured when vehicle is in horizontal position, but for measuring the CG height, the vehicle should be tilted. By tilting the vehicle, liquid inside the vehicle moves and changes the load on rear and front axle. The weight distribution on rear and front axle is one of the important factors for determining the CG height based on ISO 16231-2. Based on the ISO 16231-2 the significant effect of liquid shift should be considered on CG height calculation, but the standard does not quantify this effect.

1.3.5 SUMMARY

Agricultural machineries are prone to rollover because of off road application, and variable and high location of CG. In order to minimize the risk of rollover accidents, the stability of agricultural machinery should be assessed. The CG height should be measured for the stability assessment. The vehicle CG height can be measured by several methods such as, vertical hang, tilt table, static and dynamic pendulum method, and lifting axle method. The pendulum method and lifting axle method are the most common methods. The lifting axle method is less demanding, less expensive and easier method than the pendulum method, but the accuracy of the lifting axle method is less than the stable pendulum method.

In all of these CG measurement methods the vehicle is tilted for measuring the CG height. By tilting the vehicle the liquids inside the vehicle moves. The newly developed ISO 16231-2 does not consider the effect of liquid shift on CG height measurement in lifting axle method. Although many authors admit fluid affects measurement of CG, no studies have investigated that effect. The significant effect of liquid shift needs to be considered in the CG height calculation.

1.4 OBJECTIVES

Three projects related to operator safety are described in this manuscript. The specific goals of each project are presented in this section. The aim of first project is to develop a Finite Element (FE) model with no calibration to predict the performance of agricultural tractors ROPS designed by CRDP, under static SAE J2194 standard. The specific objectives comprise of:

1. Simulating the SAE J2194 static side and rear loading tests for ROPS with FE,
2. Predicting the force-deflection results of the ROPS under simulated standard tests,
3. Comparing the ROPS performance deflection (RPD) for the simulated and experimental tests, and
4. Evaluating the influence of elastic-plastic material properties of the ROPS on simulation results.

The aim of second project is to evaluate the effect of speed and friction on rear mount foldable ROPS actuation torques. It is hypothesized that raising and lowering speed and friction may affect the actuation torque. In the first section, the effect of turning speed on the actuation torque was investigated by actuating the FROPS at five-speed levels that include two static actuation torques measurement. A theoretical model was developed to predict the actuation torque based on the geometry and the material density of the FROPS. The aim of the second section of this project is to evaluate the effect of friction on actuation torque. The specific objectives are to measure and compare:

1. The actuation torque with and without greasing.
2. The dynamic and static actuation torques.
3. The actuation torque for several models of the FROPS.
4. The actuation torque of several FROPS of the same model.

The aim of the third project is to model the effect of liquid movement on the center of gravity location of off-road vehicles. Although many experts acknowledge that liquid shift in a tilted vehicle affects the measurement of its CG, few studies have investigated the extent of the effect. Currently, there is no recommendation to adjust the CG height calculation due to liquid movement. Therefore, the overall goals of our research are to:

1. Develop, demonstrate, and validate a theoretical model to predict the effect of liquid repositioning on the CG location, and
2. Validate the model using a prototype and an agricultural utility tractor.

1.5 REFERENCES

Alfaro, J. R., Arana, I., Arazuri, S., & Jarén, C. (2010). Assessing the safety provided by SAE J2194 Standard and Code 4 Standard code for testing ROPS, using finite element analysis. *Biosystems engineering, 105*(2), 189-197. doi:http://dx.doi.org/10.1016/j.biosystemseng.2009.10.007

Alkhaledi, K., Means, K., McKenzie Jr, E., & Smith, J. (2013). Reducing occupational fatalities by using NIOSH 3rd generation automatically deployable rollover protective structure. *Safety science*, *51*(1), 427-431.

Antonelli, K., Astakhov, V., Bandyopadhyay, A., Bhatia, V., Claus, R., Dayton, D., . . . BG, Z. (2014). *Measurement, Instrumentation, and Sensors Handbook: Spatial, Mechanical, Thermal, and Radiation Measurement. Part III: Displacement Measurement*, *Linear and Angular* (J. Webster & H. Eren Eds. 3 ed.). FL, USA: CRC. Press.

Ayers, P. D., Khorsandi, F., John, Y., & Whitaker, G. (2016). Development and evaluation of a computer-based ROPS design program. *Journal of agricultural safety and healt*h. 22(4): 285-295.

Ayers, P. D., Groothuis, M., Kruckeberg, J., Nichols, W., Samba, A., Shaver, C., & Bradley, C. (2012). *Design of a powered foldable ROPS*. Paper presented at the ASABE, Dallas, TX.

Ayers, P. D. (2015). *Engineering controls for foldable ROPS actuation assistance*. Center for agricultural health & safety of Colorado State University.

Bureau of Labor Statistics. (2014). Census of fatal occupational injuries summary, 2013. Retrieved 5 October 2015, from Bureau of Labor Statistics www.bls.gov/news.release/cfoi.nr0.htm

CDC. (2014). Workplace safety and health topic: 25 June 2014. Retrieved Accessed 5 November 2014, from Center for disease control and prevention www.cdc.gov/niosh/topics/aginjury/

Chen, C., Wang, G., Zhang, Y., Zhang, Y., & Si, J. (2012). Effect of lateral stiffness coefficient of loader ROPS on human injury in a lateral rollover incident. *Biosystems engineering, 113*(2), 207-219. doi:http://dx.doi.org/10.1016/j.biosystemseng.2012.08.003

Chisholm, C. (1979a). A mathematical model of tractor overturning and impact behaviour. *Journal of agricultural engineering research*, *24*(4), 375-394.

Chisholm, C. (1979b). Experimental validation of a tractor overturning simulation. *Journal of agricultural engineering research, 24*(4), 395-415.

Chisholm, C. (1979c). The effect of parameter variation on tractor overturning and impact behaviour. *Journal of agricultural engineering research*, *24*(4), 417-440.

Clark, B. J. (2005). The behaviour of rollover protective structures subjected to static and dynamic loading conditions.

Clark, B. J., Thambiratnam, D. P., & Perera, N. J. (2006). Analytical and experimental investigation of the behaviour of a rollover protective structure. *The Structural Engineer*, *84*(1), 29-34.

Clifford, M., & Gomez, L. (2005). Measuring tilt with low-g accelerometers. *Freescale Semiconductor*.

Dally, J. W., Riley, W., & McConnell, K. (1993). Instrumentation for engineering measurements: New York, John Wiley and Sons Inc.

Demšar, I., Bernik, R., & Duhovnik, J. (2012). A mathematical model and numerical simulation of the static stability of a Tractor. *Agriculturae Conspectus Scientificus (ACS), 77*(3), 143-150.

Fabbri, A., & Molari, G. (2004). Static measurement of the centre of gravity height on narrow-track agricultural tractors. *Biosystems engineering, 87*(3), 299-304.

Fabbri, A., & Ward, S. (2002). Power and machinery: validation of a finite element program for the design of Roll-over Protective Framed Structures (ROPS) for agricultural tractors. *Biosystems engineering, 81*(3), 287-296. doi:http://dx.doi.org/10.1006/bioe.2001.0012

FACE. (2014). Workplace Safety & Health Topics, Fatality Assessment and Control Evaluation (FACE) Program. Retrieved 30 March 2015, from Centers for Disease Control and Prevention http://wwwn.cdc.gov/NIOSH-FACE/Default.cshtml?state=ALL&Incident_Year=ALL&Category2=0001&Submit=Submit.

Finch, E. O., Martinez, F. A., & Sandoval, J. A. (1998). Roll-over protective system for tractors: Google Patents.

Harris, J., Mucino, V., Etherton, J., Snyder, K., & Means, K. (2000). Finite element modeling of ROPS in static testing and rear overturns. *Journal of agricultural safety and health, 6*(3), 215-225.

Howard, S. (1998). *A Study of Impact Using 80-dermometer Rubber.* (M.S.), West Virginia University.

Hoy, R. M. (2009). Farm tractor rollover protection: Why simply getting rollover protective structures installed on all tractors is not sufficient.

Hutton, D. V., & Wu, J. (2004). *Fundamentals of finite element analysis* (Vol. 1): McGraw-Hill New York.

ISO. (2015). ISO /DIS 16231-2:Self-propelled agricultural machinery-Assessment of stability-Part 2: Determination of static stability and test procedures. geneva switzerland: International Standard Organization.

Liljedahl, J. B., Turnquist, P. K., Smith, D. W., & Hoki, M. (1996). *Tractors and their power units*: American Society of Agricultural Engineers (ASAE).

Ludwig, D. (1990). Rollover protection system for vehicles: Google Patents.

Mathivanan, N. (2007). *PC-based instrumentation: concepts and practice*: PHI Learning Pvt. Ltd.

Morris, A. S., & Langari, R. (2012). *Measurement and instrumentation: theory and application*: Academic Press.

Murphy, D. J., & Yoder, A. (1998). Census of fatal occupational injury in the agriculture, forestry, and fishing industry. *Journal of agricultural safety and health, 4*(5), 55.

OECD. (2014). Standard codes for the official testing of agriculture and forestry tractors, Sub-Working Group (SWG) On Rear Foldable ROPS.

Panek, B. J., & Kolli, S. (1998). For a construction or agricultural vehicle: Google Patents.

Powers, J., Harris, J., Etherton, J., Ronaghi, M., Snyder, K., Lutz, T., & Newbraugh, B. H. (2001). Preventing tractor rollover fatalities: performance of the NIOSH AutoROPS. *Injury Prevention, 7*(suppl 1), i54-i58.

Reynolds, S. J., & Groves, W. (2000). Effectiveness of roll-over protective structures in reducing farm tractor fatalities. *American Journal of Preventive Medicine, 18*(4), 63-69.

Robinson, B. J., Scarlett, A. J., & Seidl, M. (2012). Development of technical requirements, performance specifications for functional and occupational safety topics of agricultural and forestry vehicles - Final Report. *Transport research laboratory creating the future of transport, client project report CPR1642. European Commission, DG Enterprise & Industry*.

Rondelli, V., & Guzzomi, A. L. (2010). Selecting ROPS safety margins for wheeled agricultural tractors based on tractor mass. *Biosystems engineering, 105*(3), 402-410. doi:http://dx.doi.org/10.1016/j.biosystemseng.2009.12.013

Ross, B., & DiMartino, M. (1982). Rollover protective structures. Their history and development. Prof. *Safety*, *May*, 15-23.

SAE. (2009). SAE J 2194 Rollover Protective Structures (ROPS) for wheeled agricultural tractors. *Society of Automotive Engineers: USA*.

Sheehan, R. T. (1992). Counterbalanced telescopic rollbar for tractors: Google Patents.

Springfeldt, B. (1996). Rollover of tractors—international experiences. *Safety Science*, *24*(2), 95-110.

Thambiratnam, D. P., Clark, B. J., & Perera, N. (2009). Performance of a rollover protective structure for a bulldozer. *Journal of engineering mechanics, 135*(1), 31-40.

Wang, X., L. Gao, P. Ayers, S. Su, and C. Yuan. 2016. The influence of lift angle on center of gravity measurements for zero turn radius mowers. *Applied Engineering in Agriculture* 32(2): 189-199.

CHAPTER II
DEVELOPING AND EVALUATING A FINITE ELEMENT MODEL FOR PREDICTING THE ROLLOVER PROTECTIVE STRUCTURE NONLINEAR BEHAVIOR UNDER SAE J2194 STATIC TEST

This chapter is a reformatted version of a paper, by the same name published in the journal of Biosystems Engineering, 156: 96–107, by Farzaneh Khorsandi, Paul. D. Ayers, Timothy. J. Truster.

2.1 ABSTRACT

This research focuses on applying Non-linear Finite Element (FE) techniques to predict ROPS force-deflection curves under the simulated standardized static tests. The Society of Automotive Engineers (SAE) J2194 ROPS static standard test was selected for this study. According to the SAE J2194 standard, ROPS must be capable of absorbing predefined levels of energy under longitudinal (rear) and transverse (side) load tests before collapsing as well as avoiding large deformations that infringe upon the driver's clearance zone or leave the clearance zone unprotected. A nonlinear finite element approach was developed in Abaqus and applied to predict the response of two rear-mount two-post ROPS under simulated side and rear test conditions: Allis Chalmers 5040 and Long 460. The ROPS were designed with Computer-based ROPS Design Program using a bolted corner bracket assembly to simplify the ROPS design process. The FE model was found to predict the ROPS performance deflection (RPD) with less than 25% error compared to experimental test measurements. The FE model predicted the ROPS behavior under rear loads more accurately than under side loads. Also, the developed FE model based on measured stress-strain curves from test specimens was found to predict the ROPS behavior more accurately than the FE models developed based on the Ramberg-Osgood material model.

Keywords: Finite element analysis, ROPS, Standard, Virtual test.

2.2 INTRODUCTION AND LITERATURE REVIEW

The agriculture industry has been ranked among the most dangerous industries in the United States. The Bureau of Labor reported that approximately 123 farmers and farm workers died from work-related injuries in the US in 2013 (Bureau of Labor Statistics, 2014). Tractor accidents are the leading cause of mortality in agriculture, accounting for one-half of all fatal agricultural accidents (Hoy, 2009). Tractor overturning is the main cause of mortality in tractor accidents (Springfeldt, 1996), which includes tipping the tractor sideways or backward (Ayers, Dickson, & Warner, 1994). Tractor rollover accounts for up to one-third of all tractor-related fatalities (Murphy

& Yoder, 1998). The use of a Rollover Protective Structure (ROPS) in a combination with a seat belt has proven to be the most effective method to prevent fatalities from tractor overturning. A ROPS is a frame or cab which is installed on the tractor to protect the operator by absorbing a portion of the impact energy generated by the tractor weight in a rollover accident. The ROPS provides a safe zone, called the clearance zone, between the envelope of the ROPS and tractor seat. Of the several types of ROPS such as two-post ROPS, four-post ROPS, and cab, the most common is the two-post ROPS (Murphy and Buckmaster, 2014), which consists of a reversed U-shaped crossbar located above the head of the operator on posts which are bolted to the vehicle frame or axle housing.

2.2.1 ROPS PERFORMANCES AND REGULATIONS

The first standard for evaluating ROPS performance was developed in Sweden the 1950s (OEEC, 1959). The use of standard ROPS on tractors in Sweden was a significant factor in decreasing the number of fatal rollover accidents from 15 in 1957 to only one fatality in 1990 (Thelin, 1998). In the United States (US), the Occupational Safety and Health Administration (OSHA) required almost all tractors produced after 1976 and operated by nonfamily employees on US farms to be equipped with ROPS. Only 10% of the farm tractors in the US fall under the OSHA jurisdiction (Reynolds & Groves, 2000). Increasingly since 1985, about 59% of the tractors produced by manufacturers in the US are equipped with ROPS (Ayers et al., 1994); CDC, 2014). However, tractor rollover is still a common type of fatal accident in the US, and a significant amount of tractors are still not equipped with standardized ROPS.

The ROPS performance must be determined through applicable standard tests. The SAE J2194 (2009) static test is a low demanding test in which the data collection is straightforward and the results are reliable and accurate (Ross & DiMartino, 1982). Most manufacturers select the static test for ROPS evaluation (Fabbri & Ward, 2002). The static test for rigid two-post ROPS includes a sequence of four static loads: (1) horizontal rear (longitudinal), (2) first vertical, (3) horizontal side (transverse), and (4) second vertical loadings. The displacement rate in the horizontal static test must be less than 5 mm s-1. The ROPS passes the static test if it absorbs a predefined level of energy in longitudinal and transverse tests and tolerates a particular force in the vertical test without structural member rupture. Also, the ROPS should not infringe the clearance zone (intrusion criteria), and the ROPS should not leave clearance zone unprotected from the ground plane (exposure criteria). The ROPS rupture is indicated by incapability to tolerate additional loading.

Designing ROPS to pass the appropriate standard is a challenge for manufacturers, which increases the ROPS production expenses. ROPS design requires a balance of 1) ROPS material strength and allowable deflection to meet energy criteria, 2) elastoplastic material properties to decrease peak moments at the mounting brackets, and 3) ROPS positioning and alignment to provide a safe zone for the operator. Excessively rigidity transmits a significant shock to the mounting and exerts a considerable force and moment to the chassis. Overly flexible structures deform substantially under the load and infringe on the safe zone or leave the clearance zone unprotected.

2.2.2 MODELING

While the static test is less demanding than the alternative dynamic or field-upset test, it is still costly and time-consuming. Fabbri and Ward (2002) reported that about one-third of ROPS standard tests failed at the Bologna test stations in Italy. The test failure prolongs the ROPS production and increases the project expenses. Using the experimental performance test alone does not provide an efficient ROPS design process. Therefore, researchers have used a combination of experimental tests and mathematical models to improve and evaluate ROPS performance (Chen et al., 2012; Karliński, Rusiński, & Smolnicki, 2008). The ROPS experimental tests have not been replaced with mathematical models, since SAE J2194 does not allow theoretical model results to satisfy the ROPS performance test. Nonetheless, modeling increases the understanding of the ROPS behavior under the standardized test and can be used as a tool to evaluate minor structural modifications and also decrease the possibility of test failure.

Several authors developed analytical models for predicting the behavior of ROPS in simulated standardized tests (Clark, 2005; Kim & Reid, 2001; Swan, 1988; Thambiratnam et al., 2009; Yeh, Huang, & Johnson, 1976). Subsequently, numerical approaches such as the finite element (FE) method have been applied to simulate ROPS deflection under the standard tests.

Fabbri and Ward (2002) developed an FE-based program to predict common ROPS behavior under the Organization for the Economic Co-operation and Development (OECD, 2008) and the Economic European Community (EEC, 1987) standardized tests. The developed FE model employed several different material models such as elastic-perfectly plastic, bi-linear, tri-linear or the Ramberg-Osgood model. The FE model results were compared with the results of the experimental test, analytical and numerical models developed with commercial software packages. The developed FE model was accurate for predicting force-deflection to within 30% of the actual test values of a two-post ROPS with stiff fixing points to the tractor. In the case of weak fixing points, the FE model results were within 50% of the actual test values. The developed program was able to predict the behavior of cabs and four-post ROPS with errors less than 20%. The accuracy of the program was directly related to the accuracy of the geometry creation, the description of the material properties, and the boundary conditions.

Alfaro et al. (2010) simulated the standardized static test based on the OECD code 4 and SAE J2194 using Abaqus. The FE model predictions for a four-post ROPS and a cab indicated close agreement with experimental test data. They estimate the maximum allowable tractor mass based on the ROPS force-deflection curves under the simulated standardized test. Harris et al. (2011) developed an FE model utilizing a bi-linear stress-strain relationship in ANSYS to predict cost-effective ROPS performance under the SAE J2194 and OSHA 29 CFR 1928.52 standard tests. After calibration, the FE model could predict the force for rear load and side load with an accuracy of 10% and 5%, respectively, at the point when the ROPS met the energy criterion. The authors conclude that the SAE J2194 static test provides a more conservative design test than the OSHA static test. A FE model with LS-DYNA was developed to simulate the behavior of the ROPS and FOPS of agricultural tractors based on OECD standard code 4 and 10. The simulator predicted the absorbed energy for the rear, side, and two crushing tests for ROPS successfully. The simulator predicted the performance of the FOPS under first, second, and third impact and showed the weak points of the ROPS and FOPS under the tests (Hailoua Blanco, Martin, & Ortalda, 2016).

2.3 JUSTIFICATION

The experimental standardized ROPS tests are expensive, laborious, time-consuming, and destructive. About one-third of ROPS fail the standard tests, and the test failure postpones ROPS production project and increases the project expenses. Using the experimental test alone is inefficient in improving the ROPS design and performance. Modeling has been introduced as a method that can simulate the ROPS performance in standard tests, speeds up the design process, evaluates ROPS modifications, and reduces the ROPS production expenses. Although computer models can predict the force-deflection curve of ROPS, the experiment test cannot be replaced with computer models. The modeling approach is needed to increase the possibility that the designed ROPS is likely to pass the standard before the experimental test. Therefore researchers have used a combination of experimental tests and mathematical models to improve and test ROPS performance.

There is no FE model available to predict the behavior of rear-mount two-post ROPS designed by newly developed computer-based ROPS design program (CRDP). The designed ROPS using the CRDP are assembled mainly using bolts. The bolted corner bracket attachment at the corners may rotate and absorb some of the energy during the loading test, especially side load test. There is also some adjustment at bolts holes which affects the ROPS deflection.

In some of the previous FE models, the model needed to be calibrated to predict the ROPS behavior (Alfaro et al., 2010; Thambiratnam et al., 2009). The material properties and stress-strain behavior are critical inputs of the FE model. None of the published FE models to date have reported using experimentally measured constitutive relations in the plastic region for ROPS. In the previous studies constitutive laws such as Ramberg-Osgood, elastic-perfectly plastic, bi-linear, and tri-linear were used (Fabbri & Ward, 2002; Harris, Winn, Ayers, & McKenzie Jr, 2011; Thambiratnam et al., 2009).

2.4 OBJECTIVE

In this work, an FE model with no calibration, was developed to predict the performance of agricultural tractors ROPS designed by CRDP, under static SAE J2194 standard. The specific objectives comprise of 1) simulating the SAE J2194 static side and rear loading tests for ROPS, 2) predicting the force-deflection results of the ROPS under simulated standard tests, 3) comparing the ROPS performance deflection (RPD) for the simulated and experimental tests, and 4) evaluating the influence of elastic plastic material properties of the ROPS on simulation results.

2.5 MATERIAL AND METHODS

The FE model was developed in three steps: 1) design and manufacture the ROPS, 2) examine the ROPS performance under the experimental test, and 3) develop and validate the FE model. Two ROPS for Allis Chalmers 5040 and Long 460 tractors were designed using CRDP. The behavior of the designed ROPS were evaluated experimentally based on SAE J2194 standard test. The FE model was developed using the commercial FE commercial package Abaqus and validated by comparing the predicted and experimental test results.

2.5.1 DESIGN THE ROPS WITH CRDP

CRDP was developed to generate quickly ROPS designs based on 46 tractor dimensions and the tractor weight (Ayers, Khorsandi, John, and Whitaker, 2016). The program output is the 2-post, rear-mount ROPS drawings which can be used to construct the ROPS (fig. 2.1). The drawing includes the posts, crossbeam, baseplate, corner brackets, and strappings. All of the ROPS dimensions were presented in the CAD drawing within a Microsoft Excel file. The parts were assembled using bolts to secure the corner brackets and welding for the strapping and baseplate attachment. The final drawing is presented in figure 2.1. The constructed ROPS using the CRPD needs to be tested based on standardized experimental tests (Ayers et al., 2016).

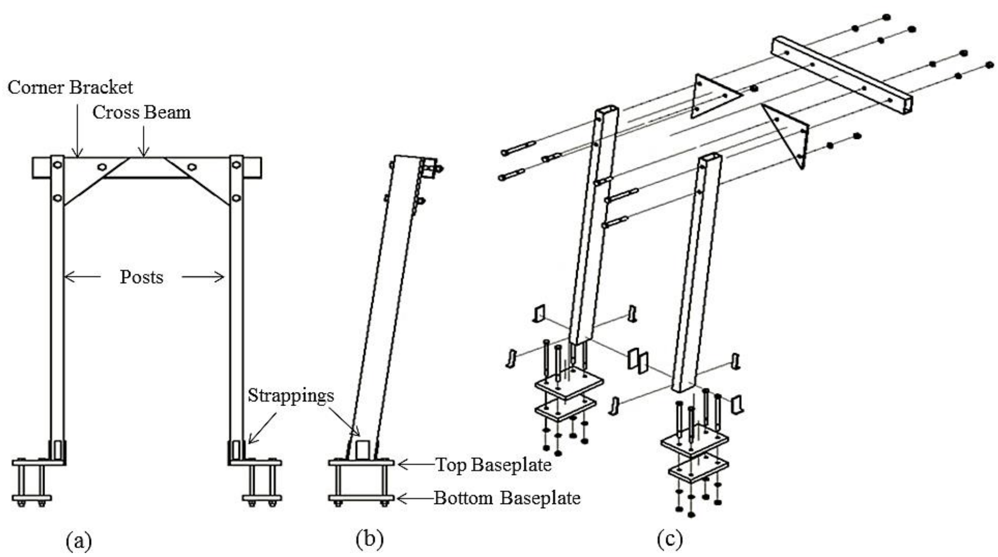

Figure 2.1. Drawing of the designed ROPS using CRDP (a) Front view. (b) Side view. (c) Exploded view (Ayers et al., 2016).

The summaries of Allis Chalmers and Long 460 ROPS dimensions are presented in table 2.1 and 2.2. These two models of tractors were selected since they were among the most frequently requested ROPS from New York Center for Agricultural Medicine and Health ROPS retrofit program, and there is no ROPS commercially available for them (Ayers et al., 2016).

Table 2.1. The output of CRDP, Summery of material and dimensions for Allis Chalmers 5040 ROPS all dimensions in In. (Ayers et al., 2016), (D: Diameter, G: Grade, L: Length, T: Thickness, W: Width,)

Part	Quantity	Dimensions			
Posts Tubing	2	T = 0.1875	W = 2	D = 3	L = 69.8
Crossbeam Tubing	1	T = 0.1875	W = 3	D = 2	L = 38.8
Top Baseplate	2	T = 0.75	L = 8.875	W = 6.28125	
Bottom Baseplate	2	T = 0.75	L = 8.875	W = 5.8125	
Corner Braces	2	T = 0.375	L = 12	W = 12	
Baseplate Strapping	1	T = 0.25	L = 20	W = 1	
Baseplate Strapping	3	T = 0.25	L = 4	W = 1	
Baseplate Bolts	8	D = 0.5	G = 8	L = 10	

Table 2.2. The output of CRDP, Summery of material and dimensions for Long 460 ROPS all dimension in In. (Ayers et al., 2016), (D: Diameter, G: Grade, L: Length, T: Thickness, W: Width).

Part	Quantity	Dimensions			
Posts Tubing	2	T = 0.1875	W = 2	D = 4	L = 63.4
Crossbeam Tubing	1	T = 0.1875	W = 4	D = 2	L = 25.3
Top Baseplate	2	T = 1	L = 9.75	W = 7.8125	
Bottom Baseplate	2	T = 1	L = 9.75	W = 5.8125	
Corner Braces	2	T = 0.375	L = 12	W = 12	
Baseplate Strapping	3	T = 0.25	L = 4	W = 1	
Baseplate Strapping	1	T = 0.25	L = 5	W = 2	
Baseplate Bolts	8	D = 0.625	G = 8	L = 10	

2.5.2 EXPERIMENTAL TEST

The constructed ROPS were sent to FEMCO Inc. in McPherson, KS, for experimental static standard tests. The applied loads were regulated based on SAE J2194 standard tests. The test included sequences of rear and side tests. The test was conducted using a ROPS test stand, hydraulic cylinders, a data acquisition system, a force transducer, and a displacement potentiometer. The static tests were stopped when the energy criteria were met, and the ROPS deflections were recorded (Ayers et al., 2016).

2.5.2.1 LONGITUDINAL (REAR) LOAD TEST

The rear load was applied horizontally and parallel to the longitudinal tractor median plane. Since more than half of the tractors weight was on the rear wheels, the longitudinal loads were applied from the rear. The load was applied to the cross beam that is typically the first component that contacts the ground in a rear rollover accident (fig. 2.2). The load was exerted to the cross beam and to the point which is located one-sixth of the cross bar width from one end of the cross beam. The rear load was applied until the ROPS absorbed energy (E_n) reaches the required energy based on equation (2.1):

$$E_n = 1.4\ M \tag{2.1}$$

Where E_n is the absorbed energy (J), and M is the tractor reference mass in (kg). The absorbed energy is the area under the force-deflection curve.

Figure 2.2. Rear load test Long 460 ROPS.

2.5.2.2 TRANSVERSE (SIDE) LOADING

The side load was inserted horizontally and perpendicular to the median longitudinal plane of the tractor. The side load pushed the one side of the cross beam at which the rear load had not been applied. The test stops when the absorbed energy is equal to:

$$E_n = 1.75\ M \tag{2.2}$$

2.5.2.3 PARAMETERS OF PERFORMANCE

The reference mass and the required absorbed energies and loads for the Allis Chalmers 5040 and Long 460 tractors are presented in table 2.3. The ROPS Allowable Deflection (RAD) is defined as the maximum allowable deflection of the ROPS without violating the intrusion or exposure criteria. The ROPS Performance Deflection (RPD) is defined as the ROPS deflection during the four static tests. The RPD is the ROPS deflection to the point that the ROPS absorbs the predefined levels of energy in horizontal tests and the ROPS deflection under the vertical tests. During all of the tests, the RPD must be smaller or equal to the RAD to satisfy SAE J2194 requirements.

A mathematical model was developed, validated, and implemented to evaluate the ROPS exposure criteria of ROPS under the standard SAE J2194 static test (Ayers et al., 1994). The model calculated RAD utilizing tractor dimensions, ROPS mounting points, and ROPS dimensions. The RAD for Allis Chalmers 5040 and Long 460 ROPS were computed using a Matlab code which was based on Ayers et al. (1994) research (table 2.3). The intrusion criteria were defined based on the ROPS dimensions and the location of ROPS mounting and clearance zone.

Table 2.3. Calculated applied force and required energy as a function of tractor mass based on SAE J2194 standard.

	Allis Chalmers 5040	Long 460
Tractor mass (kg)	2032	1842
Rear load test, required absorbed energy (J)	2844.8	2578.8
Rear load test, RPD (mm)	229	176
Rear load test, RAD (mm)	420	400
Rear load test, permanent deflection (mm)	96	70
Side load test, required absorbed energy (J)	3556.0	3224.0
Side load test, RPD (mm)	221	168
Side load test, RAD (mm)	295	30
Side load test, permanent deflection (mm)	108	87

2.5.3 FINITE ELEMENT MODEL

The ROPS behavior under standard tests were simulated by developing 24 FE models in Abaqus. Abaqus (2011) was selected for this study which is one of the most robust commercial software packages for nonlinear analysis (Yu & Li, 2012). The overall modeling procedure in FE software packages includes six steps to investigate engineering problems such as predicting the nonlinear behavior of ROPS: geometry creation, defining material properties, mesh generation, determining boundary conditions, simulation execution, and post-processing.

The developed models include two types of ROPS (Long 460 and Allis Chalmers 5040), two finite element mesh resolutions and element types (C3D4 with global size 0.08, and C3D10M with global size 0.01), two tests (side and rear load test), and three material models (1: Experimental test based on ASTM test, 2: Ramberg-Osgood model based on ASTM test, and 3: Ramberg-Osgood model based on available online data).

The designed ROPS for this study were made of tubular elements with a rectangular cross section which are reinforced with two bolted corner plates and welded strappings at the baseplates. The 3D CAD geometry model was drawn in 3D SolidWorks and was imported into Abaqus (fig. 2.3).

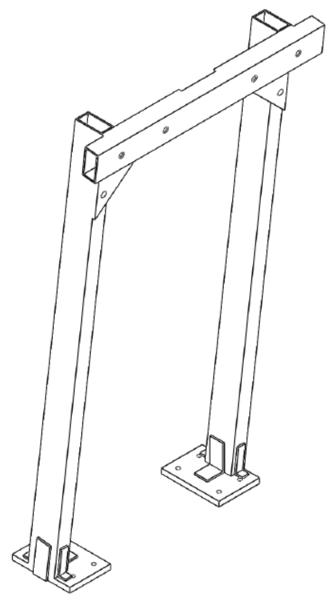

Figure 2.3. Creation of the ROPS geometry in SolidWorks.

2.5.3.1 MATERIAL PROPERTIES

The material properties can have a significant influence on the FE results, and need to be evaluated. Typically, static ROPS testing produces a significant elastic-plastic deflection under SAE J2194 standard test; therefore material properties in both elastic and plastic ranges are required in the FE model. The tubular ROPS parts in this study were made of steel ASTM 500 grade B and the plates were made of steel ASTM A 513. Mechanical properties in the elastic range include modulus of elasticity (E) and Poison ratio (υ). The material property in the plastic range includes the stress-strain relationship which can be measured directly or predicted by applying material models. Three different constitutive relations for material in the plastic range were developed, including a stress-strain relationship developed based on the experimental test, and two constitutive relations developed based on Ramberg-Osgood law.

The tensile testing of ASTM steel 500 grade B was performed in accordance with ASTM E8. The results include yield stress (σ_y), ultimate stress (σ_u), and the stress-strain relationship of steel (fig. 2.4 and table 2.4). The experimental tensile test is more expensive and time-consuming compared to constitutive laws. Thus the developed constitutive relations based on Ramberg-Osgood was used to predict the force-deflection curves (Equation 2.3 and 2.4). This model can predict stress-strain relationship based on E, σ_u, and σ_y which are usually available on-line for different steels. Several researches have proved the accuracy of the Ramberg-Osgood model for predicting the elastic constitutive relations of steel alloys (Rasmussen, 2003; Wei & Elgindi, 2013).

$$\varepsilon(x) = \frac{1}{E}\sigma(x) + 0.002\left(\frac{1}{\sigma_y}\right)^{q-2} |\sigma(x)|^{q-2}\sigma(x) \tag{2.3}$$

$$q = 1 + \frac{\ln 20}{\ln(\sigma_u/\sigma_y)} \tag{2.4}$$

Both predicted and measured constitutive relations was used to develop different FE models and the final results were compared.

2.5.3.2 MESH GENERATION

Two types of tetrahedral elements with two different element sizes were selected for meshing the ROPS, taking advantage of automatic mesh generator. The ROPS were meshed using either four-node linear tetrahedral elements (C3D4) with global size 0.08 or ten-node quadratic tetrahedral elements (C3D10M) with global size 0.01 (fig. 2.5). The tetrahedral elements provide a comprehensive description of geometrical details of problems which include both circular and rectangular parts. The second-order modified tetrahedral elements (C3D10M) are an effective alternative to the linear elements (C3D4), for complex geometries and are robust for large deformation. First order tetrahedral elements (C3D4) are overly stiff (Ellobody, 2014), which resulted in under-prediction of deflection.

Table 2.4. The measured material properties based on ASTM E8 standard.

Material Properties	Source	
	(O'neal Steel, 2015)	ASTM results
Modulus of Elasticity (MPa):	200	200
Poison ratio	0.33	0.33
Yield Stress (MPa):	317.159	384.451
Ultimate Stress (MPa)	399.896	494.285
Q	13.92	12.92

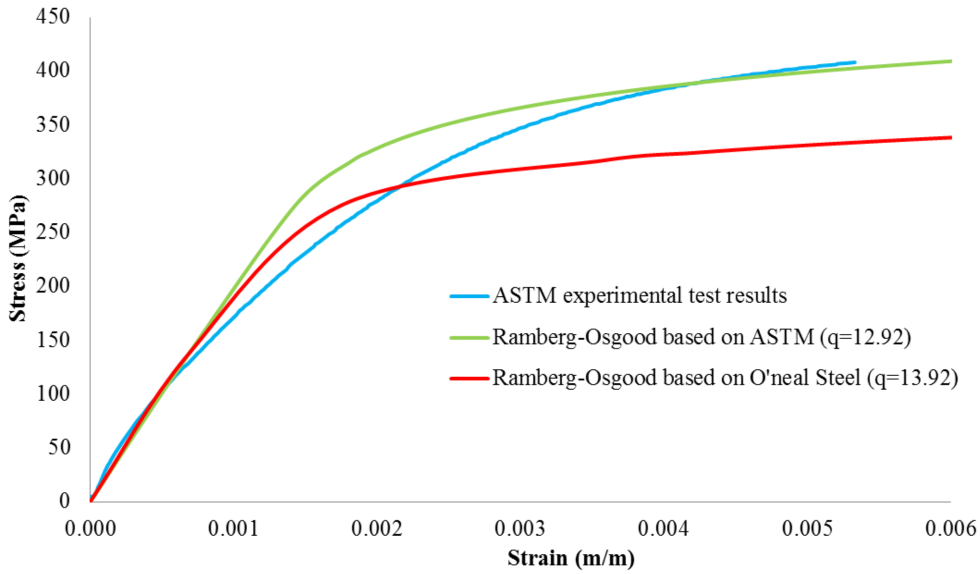

Figure 2.4. The ASTM 500 steel grade B Stress-Strain relationship, the experimental ASTM E8 tests, the Ramberg-Osgood model developed based on O'neal steel, and the developed Ramberg-Osgood model based on Experimental ASTM E8data.

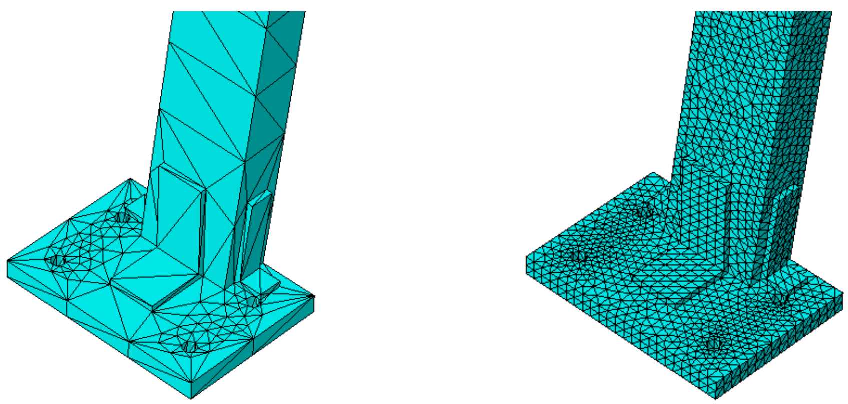

(a) (b)

Figure 2.5. Basement plate of the Long 460 Meshed ROPS (a) C3D4 with global size 0.08 (b) C3D10M with global size 0.01.

2.5.3.3 *DETERMINING THE BOUNDARY CONDITION*

Typically the ROPS are attached to the tractor chassis using bolts at baseplates. In this research, the fasteners between the ROPS and tractor was not modeled since NOISH reported that the deflection at this point is negligible (Harris et al., 2000). Since the ROPS in the experimental tests were attached to a stiff fixed platform, the attachment points at the bottom of the baseplates were restrained in all six degrees of freedom within the FE model.

The forces were inserted based on the SAE J2194 standard which were presented in table 2.3. The side and rear loads were applied as pressure loads on a specific area and were increased at a constant rate from zero up to the point when the ROPS absorbs the predefined level of energy based on equations 2.1 and 2.2. The loads were applied at intervals of one-tenth of the expected maximum required load. During each step, the deflections were calculated to develop the force-deflection curve.

2.6 RESULTS AND DISCUSSION

The results include the ROPS behavior under the experimental and the simulated standard tests. The experimental test results for rear and side load test include the deflection, force, and absorbed energy. The experimental test results and FE model outputs were presented in two types of graphs, force-deflection and energy-deflection curves. The force-deflection curves were used to compute the energy-deflection curves. The ROPS deflection under the applied load is calculated and used to develop the force-deflection curves. In Figure 2.6, the deflection of Long 460 ROPS under the simulated side load (16000 N) is shown. The deflection is equal to 0.0796 m at the measurement point which is the point that ROPS deflection was measured in the experimental test. Considering that the rear load was applied to one-sixth of the cross beam from the left side. The experimental and predicted force-deflection curves for rear and side load tests of the Allis Chalmers ROPS are presented in Figures 2.7 and 2.8, respectively. Figures 2.9 and 2.10 show the force-deflection curves of the Long 460 ROPS under the experimental and simulated rear and side tests. The ultimate stress was checked based on Von Mises criterion and showed that there is no rupture in the structure during the tests (fig 2.7-2.10). The effect of the steel properties on predicted force-deflection curves was examined. Three force-deflection curves were developed with Abaqus for each test by applying three levels of material properties including, one measured stress-strain relationship based on ASTM E8 and two predicted stress-strain curves based on Ramberg-Osgood model (fig. 2.4).

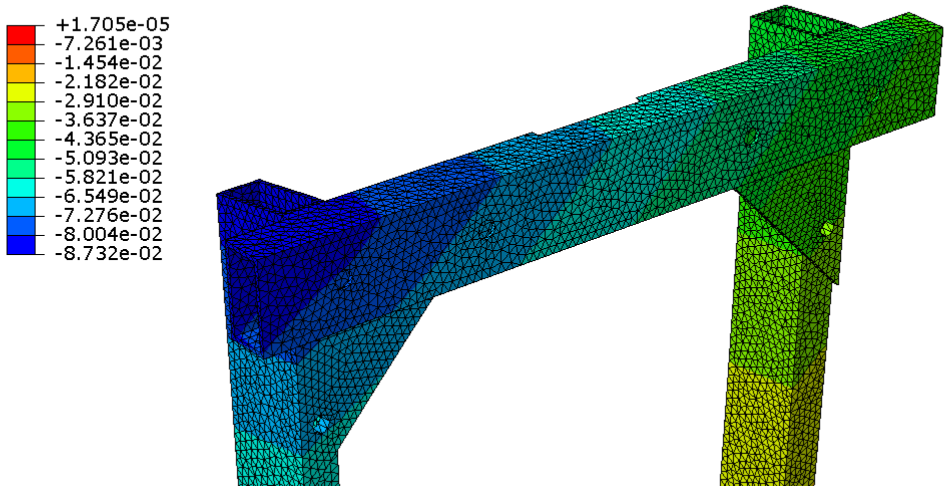

Figure 2.6. Rearward deflection of the Long 460 ROPS under the rear load , applied force is equal to 16000 N, material properties based on constitutive relation based on the experimental test (ASTM E8), mesh C3D10 M, mesh size 0.01 (deflection in m).

Results showed that the Ramberg-Osgood model with lower q factor predicts stiffer material and consequently stiffer structure compared to the Ramberg-Osgood model with high q. Which means under the same load the stiffer structure deflects less than the more flexible structure. Comparing the stress-strain relationship in figure 2.4 with the force-deflection curves in figures 2.7 and 2.8, the predicted force-deflection curves of ROPS follow the same trend as the strain-stress curves of material (figs. 2.7-2.10). The differences between the experimental and predicted force-deflection curves can possibly be due to the bolt adjustments at the holes in experimental tests. The simulated structure in the FE model is a single part, which couldn't predict adjustments at bolt holes. Results showed that the FE model can predict the force-deflection curves under the rear load more accurately than the side load test (figs. 2.7-2.10). In the experimental side load test, the force was applied in a plane perpendicular to the bolt pivot joints. There may be some movement between the ROPS parts and rotation around the pins pivot point, as the ROPS was an assembled structure. The bolt adjustment and lock up in the hole may be another reason which apparently occurred at 40 mm deflection in the side load test of Allis Chalmers ROPS (fig. 2.10). The FE model geometry consists of one part and could not predict any movement between parts and rotations around the pivot point. The FE model results can be improved by using an assembled structure rather than a fixed structure. The assembled structures may predict the movement between parts, pin adjustments at holes, and rotations at pivot points.

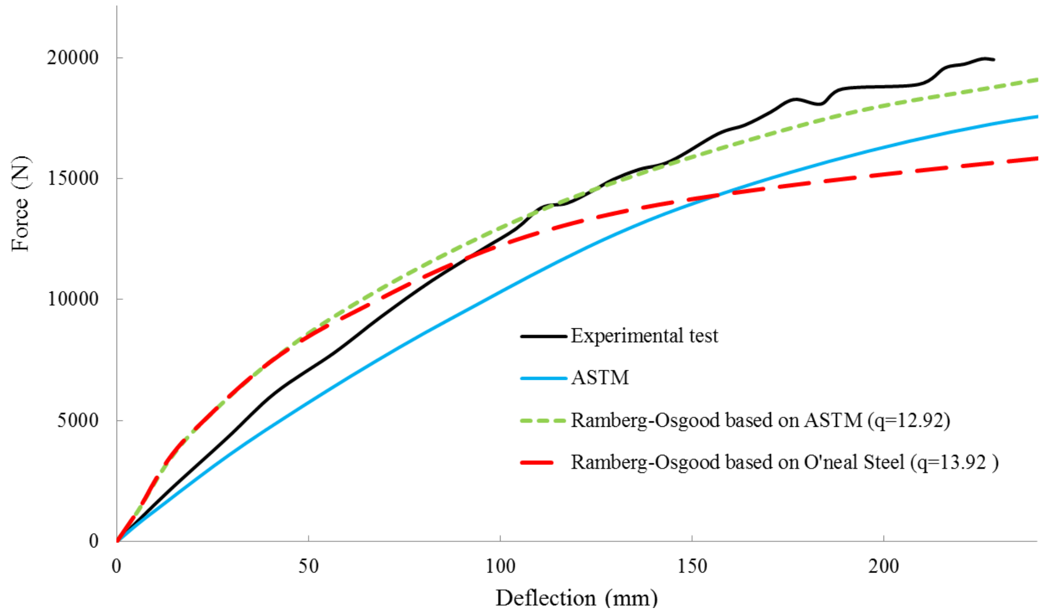

Figure 2.7. ROPS deflection under rear loading for Allis Chalmers 5040 ROPS (C3D10M, 0.01).

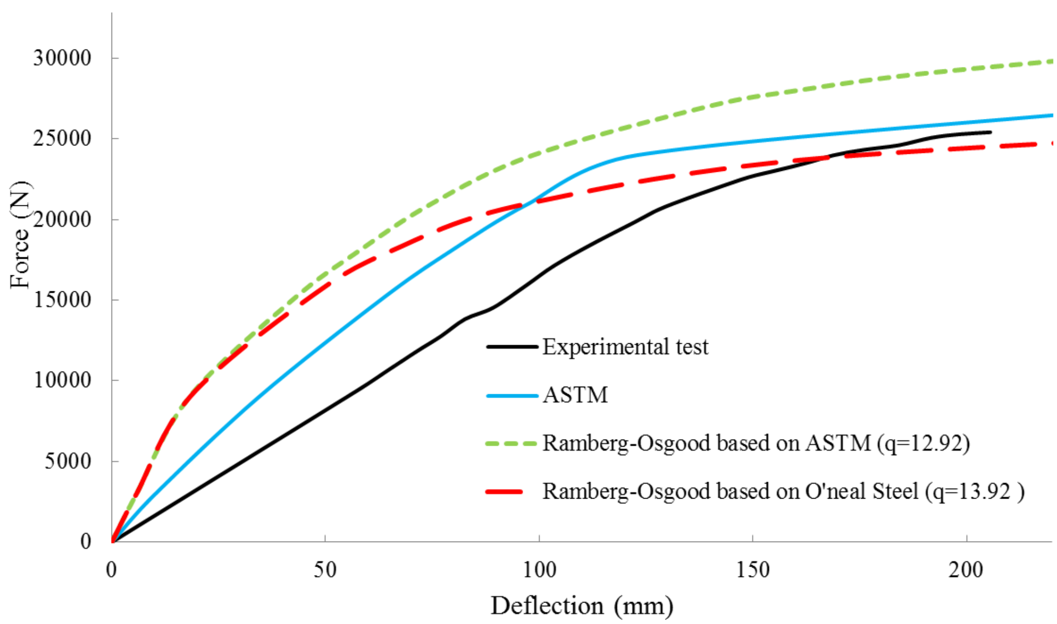

Figure 2.8. ROPS deflection under side loading Allis Chalmers 5040 ROPS (C3D10M, 0.01).

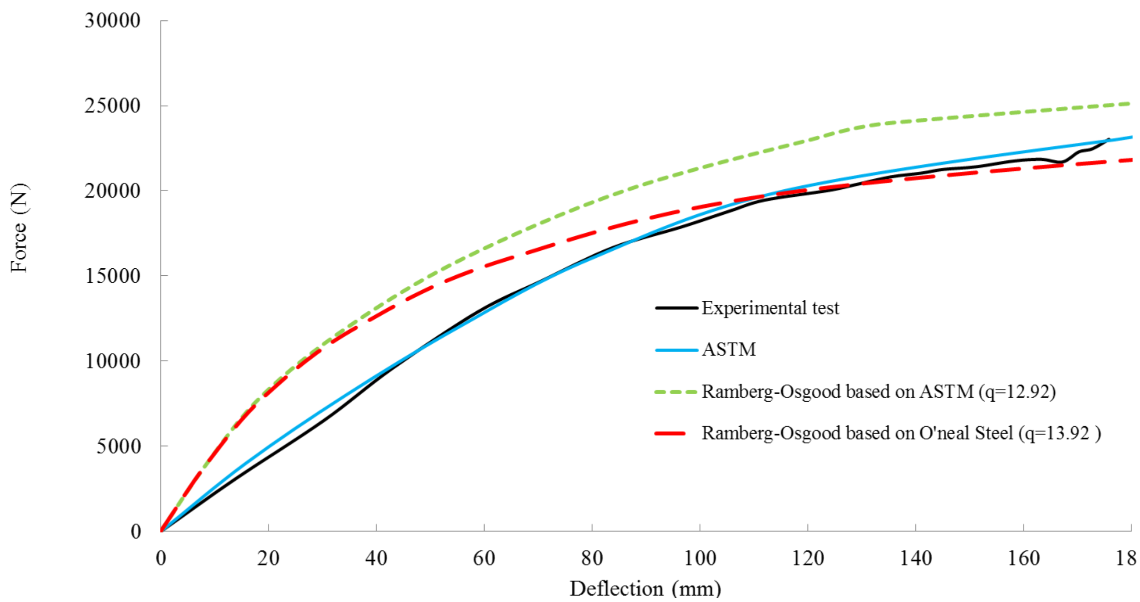

Figure 2.9. ROPS deflection under rear loading for Long 460 ROPS (C3D10M, 0.01).

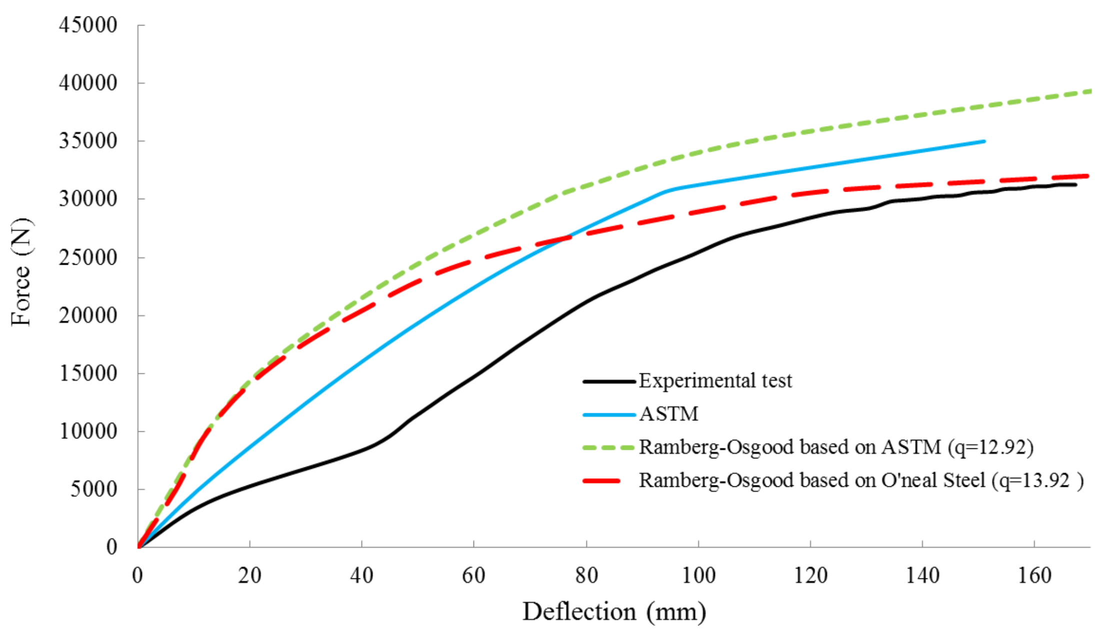

Figure 2.10. ROPS deflection under side loading Long 460 ROPS (C3D10M, 0.01).

The energy-deflection curve for each test was developed, calculating the area under the force-deflection curve. The energy-deflection curve for rear and side loading tests of Allis Chalmers ROPS are presented in figures 2.12 and 2.13. Figures 2.14 and 2.15 demonstrate the energy-deflection curves of Long 460 ROPS. The energy-deflection curves were used to calculate the RPD. In the simulated tests, the RPD is the vertical projection of the intersection point of the energy-deflection curve with the predefined level of absorbed energy. For example, the RPD for the Allis Chalmers ROPS in rear loading test with material properties based on ASTM constitutive relation (blue line) with the predefined level of energy (2844.8 J) (black dashed line), is 255.5 mm (fig. 2.11). For ROPS to pass the standard tests, the RPD should be smaller than RAD. In all of the experimental and simulated tests RPD is much lower than the RAD (table 2.5 and 2.6).

While the test outcome (passing or failing) is an important output of these tests, it is also important that the developed force-deflection curves be close to the experimental test results. The accurate FE model can be used as a design tool to predict the effect of minor structural modifications on ROPS behavior under the test.

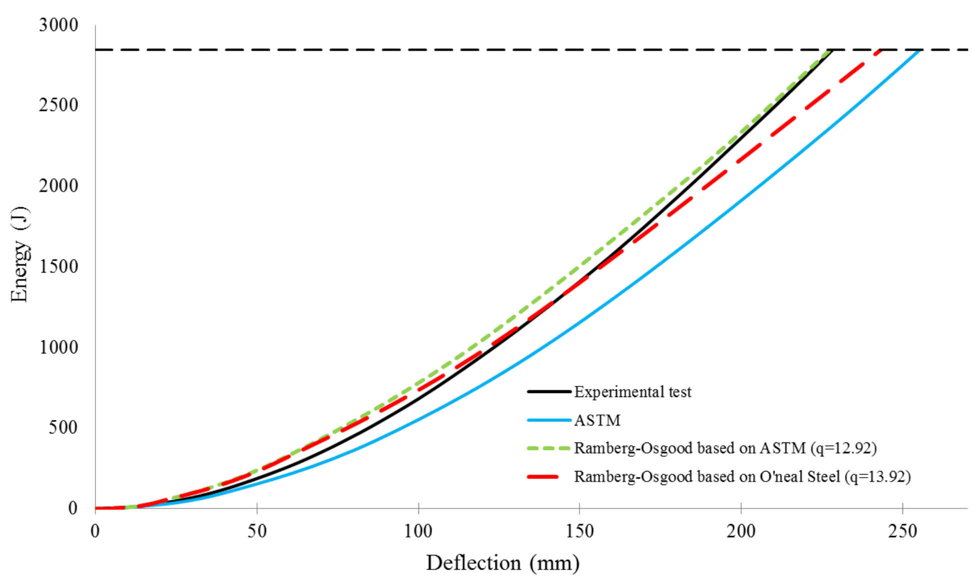

Figure 2.11. ROPS absorbed energy under rear loading for Allis Chalmers 5040 ROPS (C3D10M).

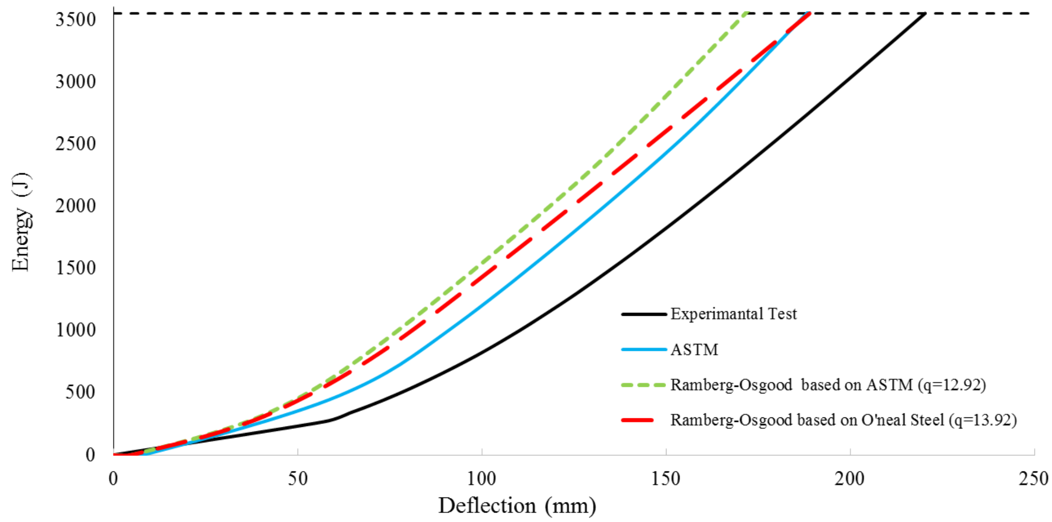

Figure 2.12. ROPS absorbed energy under side loading for Allis Chalmers 5040 ROPS (C3D10M).

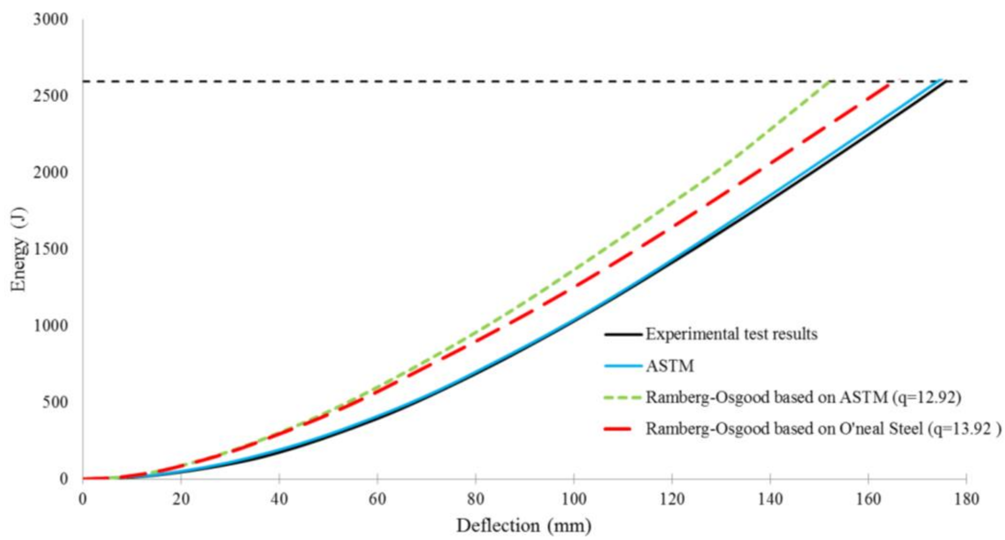

Figure 2.13. ROPS absorbed energy under rear loading for Long 460 ROPS (C3D10M).

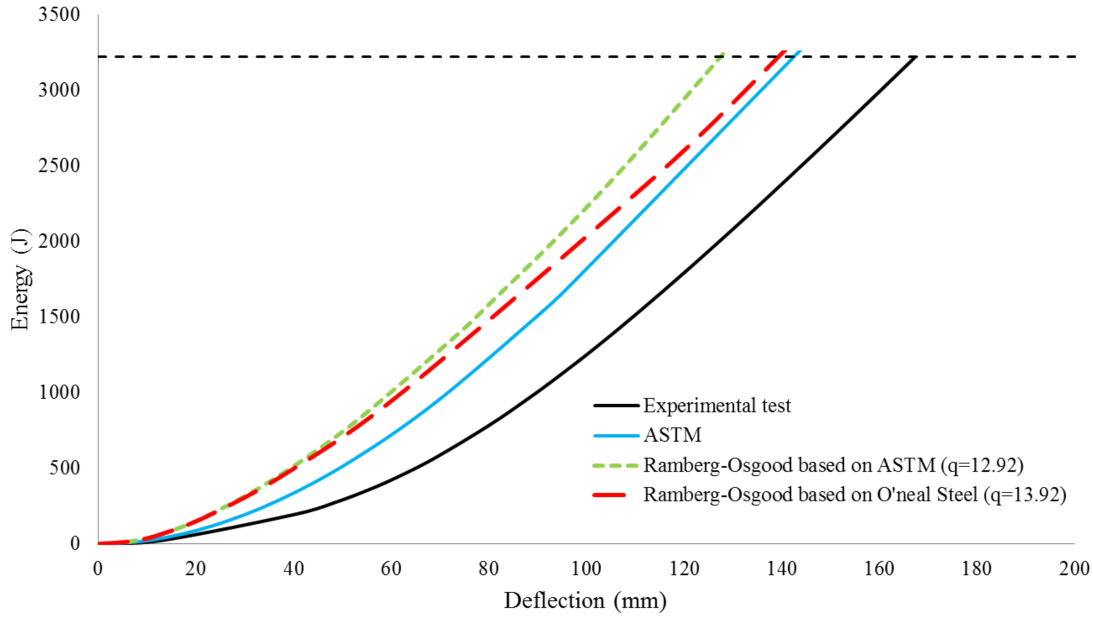

Figure 2.14. ROPS absorbed energy under side loading for Long 460 (C3D10M).

Table 2.5. ROPS Displacement at maximum absorbed energy (C3D10M)

	Allis Chalmers 5040 ROPS				Long 460 ROPS			
	Rear (mm)	Error (%)	Side (mm)	Error (%)	Rear (mm)	Error (%)	Side (mm)	Error (%)
RAD	426	-	295	-	400	-	360	-
Experimental	229	0.0%	221	0.0%	176	0.0%	168	0.0%
ASTM RPD	255.5	11.6%	196.0	-11.3%	174.0	-1.1%	144.0	-14.3%
RO O’neal steel RPD	244.0	6.1%	193.0	-12.7%	166.0	-5.7%	128.0	-23.8%
RO ASTM RPD	228.5	-0.2%	176.0	-20.4%	148.0	-15.9%	140.0	-16.7%

Table 2.6. ROPS Displacement at maximum absorbed energy (C3D4)

	Allis Chalmers 5040 ROPS				Long 460 ROPS			
	Rear (mm)	Error (%)	Side (mm)	Error (%)	Rear (mm)	Error (%)	Side (mm)	Error (%)
Experimental RPD	229	0.0%	221	0.0%	176	0.0%	168	0.0%
ASTM RPD	245.0	7.0%	189.0	-14.5%	161.0	-8.5%	132.0	-21.4%
RO O’neal steel RPD	244.0	6.6%	189.0	-14.5%	157.0	-10.8%	127.0	-24.4%
RO ASTM RPD	221.0	-3.5%	172.0	-22.2%	143.0	-18.8%	118.0	-29.8%

Both ROPS passed all of the simulated tests. Errors for three out of four virtual tests based on ASTM material properties were smaller than the Ramberg-Osgood models. Also, the developed FE models based on ASTM, predicted the shape of the experimental force-deflection curves better than the FE models developed based on Ramberg-Osgood material model (figs. 2.7-2.10).

The error was calculated comparing the experimental RPD with the predicted RPD (tables 2.5 and 2.6). Equation 2.5 was used to calculate the error:

$$\text{Error}\% = \frac{\text{RPD}_\text{P} - \text{RPD}_\text{E}}{\text{RPD}_\text{E}} \times 100 \tag{2.5}$$

Where RPD_P is predicted RPD and RPD_E is experimental RPD.

Comparing the virtual test results for the meshed ROPS with C3D4 node (element size 0.08) and C3D10M node (element size 0.01), showed that the coarse linear elements were stiffer than the fine quadratic elements (fig. 2.15 and 2.16). Both the node order and global size were effective to increase the structure flexibility. Therefore the ROPS with C3D4 elements deflects less than the ROPS with C3D10M elements. The developed FE models applying C3D10M elements predict the ROPS behavior under virtual tests better than developed FE models with C3D4 elements. The RPD percent errors for ROPS with C3D4 elements were higher than C3D10M elements for all of the tests except for the rear test of Allis Chalmers 5040 ROPS (tables 2.5 and 2.6). The CPU time of the coarse C3D4 elements was much lower than the fine C3D10M elements.

2.7 CONCLUSION

The aim of this study is to develop an FE model to predict the ROPS behavior under SAE J2194 standard test. For two types of ROPS (Allis Chalmers 5040 and Long 460), 24 FE models for rear and side load tests with variation in element type and size as well as material properties were developed. The developed FE models were validated by comparing virtual test results with the experimental test results. The ROPS should not infringe the clearance zone or leave the clearance zone unprotected to pass the test, practically; the RPD should be smaller than allowable ROPS deflection (RAD). Both ROPS pass all of the experimental and virtual tests, as RPD were much smaller than the RAD for all of the tests.

Results showed that the developed FE models can predict the rear test results more accurately than the side load test results. In most of the side tests the FE models were stiffer than

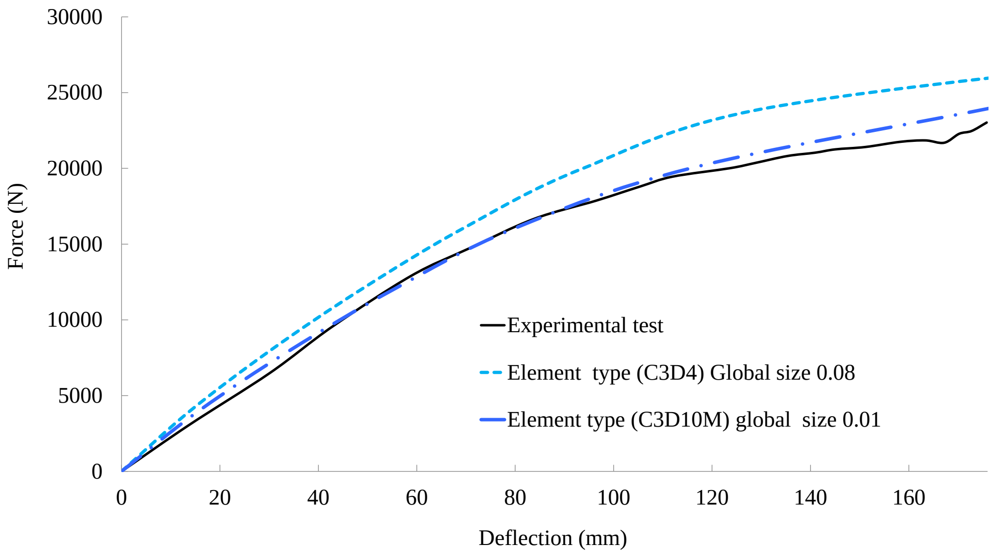

Figure 2.15. Long 460 ROPS experimental and virtual rear load test with two element types and element sizes.

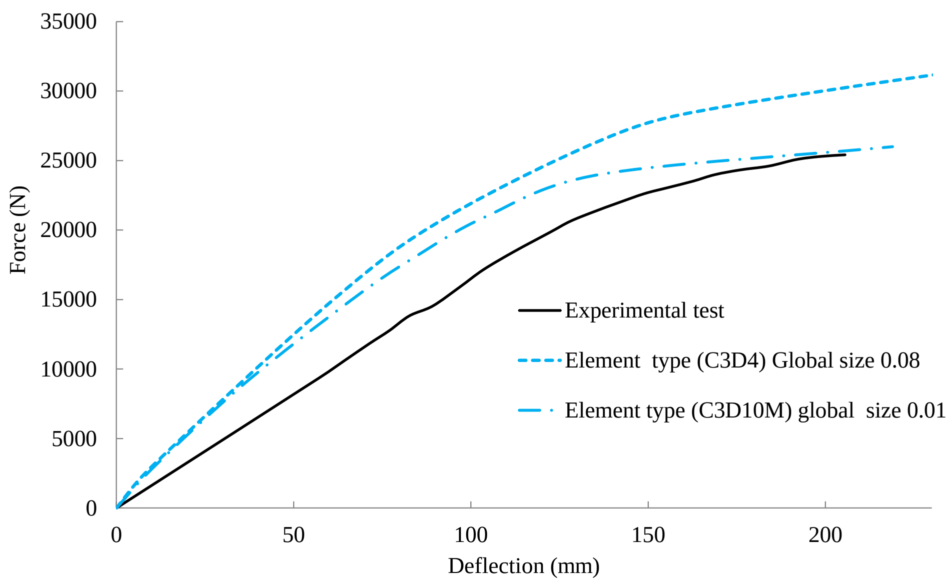

Figure 2.16. Allis Chalmers 5040 ROPS experimental and virtual side load test with two element types and element sizes.

The experimental tests, as the developed geometries were a single part and did not consider the adjustments at holes, rotations, and movements between parts. The FE model results could be improved by using an assembled structure which may predict the movement and rotations between parts. The developed FE model by applying experimentally measured material properties, resulted in the most accurate RPD prediction in 75% of the tests (three out of four tests). The meshed ROPS with fine quadratic mesh (C3D10M node, 0.01), resulted in the more accurate FE model compared to the linear coarse mesh (C3D4 node, 0.08).

Two ROPS passed all of the virtual tests as the experimental tests based on calculated RPD. Therefore all of the finite element results appears to be acceptable. But for a ROPS with close RPD value to RAD value, the less conservative FE models may not result (pass or fail) as the experimental test. The other criterion that should be considered for evaluating the FE tests reliability is the similarity of force-deflection curves of the virtual tests with the experimental tests.

The developed FE models using the ASTM material properties and meshed ROPS with C3D10M elements with global size 0.01 are recommended for future test FE models. Also these FE models appear to be more conservative, and the predicted force-deflection curve matched the experimental force-deflection curves. Since the model results for two model of ROPS designed by CRDP are accurate, it can be used for other two-post ROPS designed by CRDP. The recommended FE model may be used to evaluate the effect of the small structural modification on ROPS behavior under SAE J2194 standard test without retesting the ROPS.

2.8 REFERENCES

Abaqus. (2011). ABAQUS Version 6.11-1. Providence, R.I.: ABAQUS, Inc.

Alfaro, J. R., Arana, I., Arazuri, S., & Jarén, C. (2010). Assessing the safety provided by SAE J2194 Standard and Code 4 Standard code for testing ROPS, using finite element analysis. *Biosystems Engineering, 105*(2), 189-197. doi: http://dx.doi.org/10.1016/j.biosystemseng.2009.10.007

Ayers, P. D., Dickson, M., & Warner, S. (1994). Model to evaluate exposure criteria during roll-over protective structures (ROPS) testing. *Transactions of the ASAE, 37*(6), 1763-1768.

Ayers, P. D., Khorsandi, F., John, Y., Whitaker, G. (2016). Development and evaluation of a computer-based ROPS design program. Journal of Agricultural safety and health. 22(4): 285-295.

Bureau of Labor Statistics. 2014. Census of fatal occupational injuries summary, 2013. Washington D.C.: Bureau of Labor Statistics. Available at:www.bls.gov/news.release/cfoi.nr0.htm. Accessed 5 October 2015.

CDC. (2014). Workplace Safety and Health Topic: 25 June 2014. Atlanta, Ga.: Center for Disease Control and Prevention. Available at:www.cdc.gov/niosh/topics/aginjury/. Accessed 5 November 2014.

Chen, C., Wang, G., Zhang, Y., Zhang, Y., & Si, J. (2012). Effect of lateral stiffness coefficient of loader ROPS on human injury in a lateral rollover incident. *Biosystems Engineering, 113*(2), 207-219.

Clark, B. J. (2005). The behaviour of rollover protective structures subjected to static and dynamic loading conditions.

EEC. (1987). European Economic Community, Directive 87/402/EEC: Roll-over protection structures mounted in front of the driver's seat on narrow-track wheeled agricultural and forestry tractors. Strasbourg.

Ellobody, E. (2014). *Finite Element Analysis and Design of Steel and Steel–Concrete Composite Bridges*: Butterworth-Heinemann.

Fabbri, A., & Ward, S. (2002). PM—Power and Machinery: validation of a finite element program for the design of Roll-over Protective Framed Structures (ROPS) for agricultural tractors. *Biosystems Engineering, 81*(3), 287-296. doi: http://dx.doi.org/10.1006/bioe.2001.0012

Hailoua Blanco, D., Martin C., & Ortalda A. (2016). Virtual ROPS and FOPS testing on agricultural tractors according to OECD standard code 4 and 10. 14 th international LS-DYNA Users conference.

Harris, J., Mucino, V., Etherton, J., Snyder, K., & Means, K. (2000). Finite element modeling of ROPS in static testing and rear overturns. *Journal of agricultural safety and health, 6*(3), 215-225.

Harris, J. R., Winn, G. L., Ayers, P. D., & McKenzie Jr, E. A. (2011). Predicting the performance of cost-effective rollover protective structure designs. *Safety science, 49*(8), 1252-1261.

Hoy, R. M. (2009). Farm tractor rollover protection: Why simply getting rollover protective structures installed on all tractors is not sufficient. *Journal of agricultural safety and health, 15*(1), 3-4.

Karliński, J., Rusiński, E., & Smolnicki, T. (2008). Protective structures for construction and mining machine operators. *Automation in Construction, 17*(3), 232-244.

Kim, T., & Reid, S. (2001). Multiaxial softening hinge model for tubular vehicle roll-over protective structures. *International journal of mechanical sciences, 43*(9), 2147-2170.

Murphy, D. J., and Buckmaster, D. R. (2014). Rollover protection for farm tractor operators. State College, Pa. Available at:http://extension.psu.edu/business/ag-safety/vehicles-and-machinery/tractor-safety/e42. Accessed 9 March 2015.

Murphy, D. J., & Yoder, A. (1998). Census of fatal occupational injury in the agriculture, forestry, and fishing industry. *Journal of agricultural safety and health, 4*(5), 55.

OECD. (2008). OECD standard code for the official testing of rollover protective structures on agricultural and forestry tractors. Organization for the Economic Co-operation and Development: Paris, France.

OEEC. (1959). OEEC standard code for the official testing of agricultural and forestry tractors. Organization for the European Economic Co-operation: Paris, France.

O'neal Steel. (2015). ASTM A500 Tubing. O'neal Steel: Birmingham, AL. Available at: http://www.onealsteel.com/carbon-steel-hollow-tube-a500.html. Accessed 13 April 2015.

Rasmussen, K. J. (2003). Full-range stress–strain curves for stainless steel alloys. *Journal of constructional steel research, 59*(1), 47-61.

Reynolds, S. J., & Groves, W. (2000). Effectiveness of roll-over protective structures in reducing farm tractor fatalities. *American journal of preventive medicine, 18*(4), 63-69.

Ross, B., & DiMartino, M. (1982). Rollover protective structures. Their history and development. Prof. *Safety, May*, 15-23.

Springfeldt, B. (1996). Rollover of tractors—international experiences. *Safety Science, 24*(2), 95-110.

Swan, S. A. (1988). Rollover protective structure (ROPS) performance criteria for large mobile mining equipment. Information Circular/1988: Bureau of Mines, Washington, DC (USA).

Thambiratnam, D. P., Clark, B. J., & Perera, N. (2009). Performance of a rollover protective structure for a bulldozer. *Journal of engineering mechanics, 135*(1), 31-40.

Thelin, A. (1998). Rollover fatalities—Nordic perspectives. *Journal of agricultural safety and health, 4*(3), 157.

Wei, D., & Elgindi, M. B. (2013). Finite Element Analysis of the Ramberg-Osgood Bar. *American Journal of Computational Mathematics, 3*(03), 211.

Yeh, R. E., Huang, Y., & Johnson, E. L. (1976). An Analytical Procedure for the Support of ROPS Design: SAE Technical Paper.

Yu, M.-H., & Li, J.-C. (2012). *Computational plasticity: With emphasis on the application of the unified strength theory*: Springer Science & Business Media.

CHAPTER III
MEASURING THE FORCES TO ACTUATE A FOLDABLE ROPS

This chapter is a reformatted version of a paper, the effect of speed on foldable ROPS actuation forces, submitted to the Journal of Agricultural Safety and Health by Farzaneh Khorsandi, Paul. D. Ayers, Dillan Jackson, John. B. Wilkerson (2016). The chapter also include the results of the effect of friction on foldable ROPS actuation forces.

3.1 ABSTRACT

The number of fatalities caused by tractor rollovers has decreased in recent years, but the number of fatal tractor rollover accidents with folded down Roll-Over Protective Structure (ROPS) has increased. Operating a ROPS-equipped tractor in low overhead clearance zones is difficult and sometimes impossible. The Foldable ROPS (FROPS) was designed to solve the rigid ROPS problem, but lowering and raising the conventional FROPS is a time consuming and strenuous process. When the operators fold down FROPS to pass low overhead clearance zones, some prefer to leave it in the folded down or inoperative position increasing the risk of a rollover fatality. The actuation forces to raise and lower a FROPS are not well known, and may be influenced by actuation speed. A completely randomized block design with two blocks, five levels of speed, and multiple replications was conducted to investigate the effect of speed on actuation torque. The blocks were the two sizes of tractor FROPS. The test included five levels of speed containing two levels of static measurement and three levels of dynamic measurements. A variable speed motor system was used to control the speed to raise and lower the FROPS. The actuation torque is a function of FROPS upper part shape, dimensions, material density, turning acceleration and, friction. A theoretical model was developed to predict the actuation torque based on the FROPS shape, dimensions, and material density. For one ROPS, due to friction, the dynamic actuation torque for rising was higher and for lowering was lower than the theoretical torque. Indicator variable regression technique was used to analyze the effect of speed on the actuation torque. Results showed that speed had a significant ($P>0.05$) effect on actuation torque. Although statistically there were significant differences between the dynamic actuation torques, these differences were relatively small and negligible compared to the differences with the static torques.

Keywords.

Actuating Force, Foldable Roll-Over Protective Structure, Tractor, Safety, Standards.

3.2 INTRODUCTION

The tractor rollover accident is the major cause of occupational death in US agriculture (NIOSH, 2014). The most effective way to prevent overturn deaths during rollover accidents is the combined use of a rollover protective structure (ROPS) with a seat belt (NIOSH, 2013). A ROPS is a structure which absorbs a portion of the impact energy generated by the tractor weight in the rollover accident. The ROPS decreases the possibility of severe human injuries by protecting the operator's clearance zone. The number of fatalities caused by tractor rollovers has decreased in recent years, partially due to retrofitting more tractors with ROPS. The Swedish government has required ROPS on all tractors built after 1957. Consequently, the number of fatal rollover accidents reduced from 15 to 1 from 1957 to 1990 (Thelin, 1998). Since 1985 tractor manufacturers in the US have equipped tractors with standardized ROPS (Ayers et al., 1994). The number of fatal rollovers has decreased using ROPS. The National Institute for Occupational Safety and Health (NIOSH, 2013) estimated that if ROPS were placed on all of the US tractors, the number of fatal rollover accidents could be decreased by 71%. But only 59% of the agricultural tractors in 2012 were equipped with ROPS (NIOSH, 2014).

The overhead obstacle was reported as the most important reason for the operator not to install a ROPS (Spielholz et al., 2006). Working with ROPS-equipped tractors in low overhead clearance zones such as orchards and animal confinement buildings is difficult and in some cases impossible. In order to facilitate tractor operation in low overhead clearance areas, foldable ROPS (FROPS) have been developed. The FROPS usually is made of two parts, the upper part or the turning frame and the lower part which is fixed to the tractor (fig. 3.1). The height of the conventional FROPS can be decreased by turning the upper frame downward. The upper part of the FROPS is attached using a pin at the pivot point to the lower section of the FROPS (fig. 3.1).

However the FROPS only partially solved the problem of low clearance applications, recent surveys reveal a new issue. The number of fatal accidents and severe injuries in tractor rollover accidents with folded-down FROPS has increased in the last few years (NIOSH FACE, 2015; Hoy, 2009; Pessina et al., 2015). In a March 2015 review of NIOSH Fatality Assessment and Control Evaluation reports, there were no rollover fatalities with tractors with the FROPS folded down prior to 2003 (NIOSH FACE, 2015).

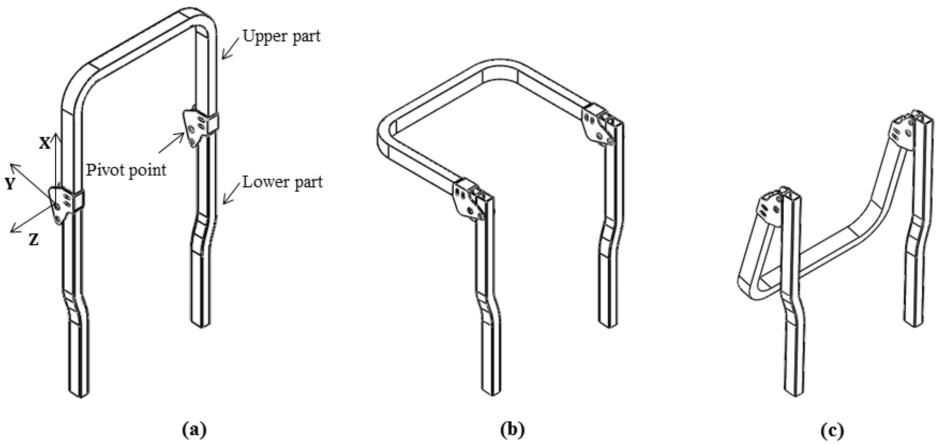

Figure 3.1. FROPS positions a) FROPS in raised or protective position, b) FROPS in the horizontal position. c) FROPS in folded down or inoperative position.

Since 2005, 25% of the rollover fatalities occurred with FROPS folded down. And since 2010, 50% of reported fatal tractor rollover accidents occurred with the FROPS folded down. Although this is a small sample size, the trend is disturbing. The survey conducted by European Commission members showed that in tractor rollover accidents, 40% of fatalities and serious injuries occurred when the FROPS was in the inoperative position (Hoy, 2009). Pessina et al. (2015) reported that 30% of the tractor rollover fatalities in Italy from 2008-2014 resulted from the FROPS in the folded-down position.

One possible explanation for leaving the FROPS in folded down position is that raising and lowering the FROPS is a time consuming and strenuous process. After lowering the FROPS to pass an obstacle, some operators prefer to leave the FROPS in the folded-down position.

An OECD working draft is being considered to regulate rear-mount foldable ROPS actuation force (forces to raise and lower the FROPS). Based on the OECD working draft, the maximum actuation force should be less than 100 N, but this criterion could increase up to 50% for some points and lowering the FROPS (OECD, 2014). The actuation force is measured at the grasping area on the upper section of the FROPS. An option exists to measure the torque to actuate the FROPS in 5-degree increments and then calculate the actuation force, knowing the upper part length. Although no recommendation is made in the working draft on the rotational speed of the foldable ROPS actuation, a maximum angular speed of 20 deg s-1 (3.3 RPM) is recommended for testing an automatic locking system (OECD, 2014).

Current FROPS actuation forces are not well known. Pessina et al. (2015) measured the actuation forces to raise front-mount foldable ROPS. They measured the static actuation force for 17 tractors and five angles (0, 30, 45, 60, and 90) utilizing a force gauge and a digital inclinometer. The results showed that the actuation forces for nearly all of the FROPS are greater than the 100 N criteria based on the OECD working draft. The influence of the rotational speed on actuation force was not investigated.

The aim of this study was to evaluate the effect of rotational speed on rear mount foldable ROPS actuation torque. It is hypothesized that raising and lowering speed may affect the actuation torque. The effect of turning speed on the actuation torque was investigated by actuating the FROPS at five-speed levels that include two static actuation torques measurement. A theoretical model was developed to predict the actuation torque based on the geometry and the material density of the FROPS.

3.3 MATERIAL AND METHODS

The initial goal of this study is to measure the actuation torque as a function of the FROPS turning angle. The torques were measured at five-speed levels that include two static torques levels. The procedure for the test includes two steps, 1) developing the measurement setup, and 2) conducting the experimental tests to evaluate the influence of rotational speed on the actuation torque.

3.3.1 MEASUREMENT SETUP

In the first step, a measurement system was developed to measure the actuation torque and the angle. Based on the OECD working draft, the actuation force can be determined by measuring the actuation torque and then calculating the force at the grasping area (OECD, 2014). The OECD working draft determined the posts of FROPS as the grasping area. Since specific grasping points have not been explored accurately, and the torque can easily be used to calculate the force at each grasping point; the actuation torque was the preferred measurement rather than the actuation force. The measurement system includes a power setup and a sensing setup (fig. 3.2).

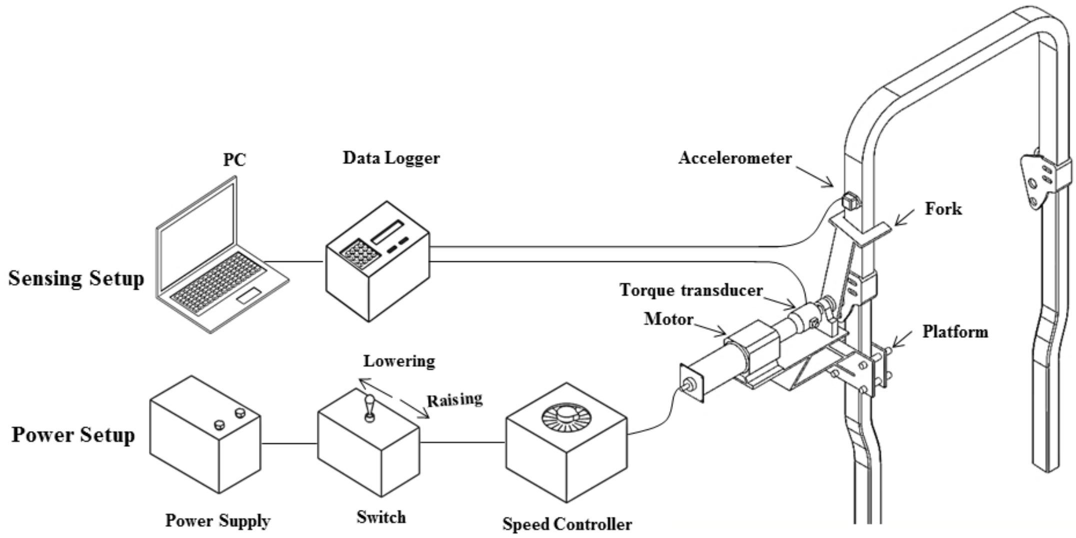

Figure 3.2. Measurement setup.

3.3.1.1 POWER SETUP

The actuation system composed of a motor, platform, fork, speed controller, switch, and a battery. A reversible gear motor (Groschopp, model PM801-PL73) was used to turn the upper part of the FROPS. The motor was mounted on a platform that was attached to the fixed section of the FROPS. The motor applied torque utilizing a fork, gripping the upper part of the FROPS. The gear motor shaft was collinear with the pivot point of the FROPS (fig. 3.1).

The speed controller (IRONHORSE TM model GSD1) was used to change the motor speed. The turning direction of the motor was controlled employing a switch that was attached between the speed controller and the battery. The switch also controlled the start or stop of the turning process. A 12 volt DC battery was used to supply the motor power (fig. 3.2).

3.3.1.2 SENSING SETUP

The measuring system includes an angular displacement and a torque measurement sensor. The turning angle is the relative angle of the upper part of the FROPS to the horizon which is the Y direction in figure 3.1(a). The top frame turning range is roughly 180 degrees (fig. 3.1). The angle of the raised locked FROPS is usually lower than +90 degrees, since the FROPS is often tilted rearward for better protection of the operator (fig. 3.1 a). The turning angle is equal to zero when the upper part of the FROPS is in the horizontal position (fig. 3.1 b). The angle for the completely folded down ROPS is near -90 degrees (fig. 3.1 c). Usually, the FROPS is pinned in the lowered position before reaching -90 degrees which is called the lowered locking position. The FROPS upper part angle was measured with an accelerometer (Crossbow CXL04LP3).

The tilting angle of an object can be measured using an accelerometer since the objects are subjected to the gravitational force (g) of Earth. At the low rotational speeds evaluated, the effects of tangential acceleration and centrifugal acceleration on the accelerometer output due to the circular motion of the upper part of the FROPS were negligible. The relationship between the angle and the acceleration depends on the installation direction. If the sensing axis (X) is parallel to the upper part of the FROPS, equation 3.1 can be used to calculate the tilting angle:

$$\theta = \sin^{-1}\left(\frac{V_{out} - V_o}{\Delta V/g}\right) \tag{3.1}$$

Where

θ = tilting angle (degree)

V_{OUT} = the accelerometer output (V),

V_0 = accelerometer output when the sensing axis is horizontal (V),

$\Delta V/g$= is sensitivity (V s^2 m^{-1}), and g is Earth gravity (9.81 m s^{-2}).

The sensitivity of the sensing axis (X direction) was 0.489 (V s2 m-1) and V0 is 2.527 V. The sensor was attached to the top of the FROPS utilizing a magnet. The magnet does not affect the sensor output.

A reaction torque cell (OMEGADYN Inc. model TQ420-2K) was used to measure the torque. The torque transducer had a maximum limit of 225 Nm. The torque transducer was attached between the motor and the fork. A Campbell Scientific (CR23X micro logger) data logger read and saved the accelerometer and torque transducer outputs at a 20 Hz sampling frequency.

3.3.2 EXPERIMENTAL TEST DESIGN

The experimental tests were conducted based on a completely randomized blocks design. The test includes two blocks with five levels of speed and multiple replications within each block. The blocks were two different FROPS models. The first FROPS was a Deere & Company (model SE1 00995), which was designed for Deere tractors (models 4120, 4320, 4520, and 4720). The second FROPS was a FEMCO, Inc. (model 3011013466), for use on Deere tractors (models 2210 and 2305). The weight of the upper part of Deere and FEMCO FROPS are 219.8 N and 109.8 N, respectively. The FROPS were selected from two different weight categories of agricultural tractors.

The five-speed levels include three dynamic and two static levels. The speed levels are defined based on the motion condition of the ROPS. For the dynamic levels, the actuation forces were measured while the FROPS was continuously raised or lowered. For the static levels, the actuation forces were measured when the FROPS was stopped at a point or started moving from a static position.

The selected dynamic speed levels for each FROPS are listed in table 3.1. Torque and angle measurements were made while both raising and lowering each FROPS. Three replications were conducted for each dynamic test, except the high speed Deere FROPS. For safety concerns, only 2 high speed dynamic tests were conducted with the heavier Deere FROPS.

Table 3.1. Three levels of actuation speed (RPM), average and standard deviation, for raising and lowering the Deere and FEMCO FROPS.

	Raising			Lowering		
	Low	Medium	High	Low	Medium	High
Deere	2.6 (0.4)	4.7 (0.1)	6.7 (0.7)	2.5 (0.2)	4.4 (0.1)	6.1 (0.9)
FEMCO	0.9 (0.3)	7.1 (0.7)	9.3 (0.3)	0.7 (0.3)	4.6 (0.1)	7.3 (0.3)

Two concepts of static actuation torques were defined; the holding and initiation static torques. The holding torque was measured while the upper part of the FROPS was held at certain angles for at least 3 s. As the FROPS starts its transition from static to dynamic movement, initially a sharp change of the torque values around the measured holding torque values was apparent. The initial value of the torque in the transient step was recorded as the static initiation torque, as the upper part of the ROPS raised or lowered from static position to 3.3 RPM (20 degree s^{-1}).

3.3.3 DEVELOPING A THEORETICAL MODEL

A mathematical model was developed to determine the theoretical actuation torque for both the Deere and FEMCO FROPS. The FROPS actuation torque is a function of weight, the center of gravity (COG) location, turning acceleration of the upper part, and the friction.

The weight and COG of the upper part can be calculated knowing the shape, dimensions, and the density of the upper part of the FROPS. The acceleration affects the inertial force and consequently the actuation torque. The friction force depends on the coefficient of friction and the normal force. The coefficient of friction is not a constant value and depends on several factors such as the movement condition (static, dynamic) and contact surface properties. The model was developed only based on the shape, dimensions, and the material density of upper part of the FROPS.

3.4 RESULTS AND DISCUSSION

The measured actuation torque-angle results to raise and lower the Deere FROPS are shown in figure 3.3. The figure includes three replications of the lowest speed test and the theoretical torque. The measured torques tend to be higher than the theoretical torques values for raising, and tend to be smaller for lowering the FROPS.

Friction caused the differences between the theoretical model and the experimental test results. The direction of the vertical (about the horizon) component of the friction force and weight were in the same direction and toward the ground for the raising process. But the vertical component of the friction force and weight were in reverse directions in the lowering process. Thus, the actuation torques to raise the FROPS were greater than the measured resistive torques when the FROPS was lowered. Roughly, the theoretical torque plus the torque due to friction was equal to the raising torque values. Conversely, the theoretical torques minus the torque due to friction produced the measured lowering torques.

The upper part of the Deere FROPS leaned 12 degrees rearward from the vertical in the upright locked position. Therefore, the lowering process started around the upper lock point which was 78 degrees and moved down to the lower locked position at -71 degrees. The raising process started at -71 degrees and rotated with a constant rotational speed up to 78 degrees. When lowering, the actuation torque for the Deere FROPS was negative from 78 degrees to 67 degrees, and then the torque was positive.

The point at which the actuation torque was equal to zero (about 67 degrees) was called the breaking point. Before this point, the fork pushed the FROPS to overcome the friction and folded down. After the breaking point, the fork held the FROPS from folding down.

The peak point was defined as the angle at which the maximum torque occurred. The peak point for the Deere FROPS was approximately -13 degrees. That point occurred at the FROPS angle when the COG of the upper FROPS section was horizontal with the pivot point, as determined by the theoretical model.

The theoretical and experimental test results of the FEMCO FROPS actuated at low dynamics rotational speed are shown in figure 3.4. The difference between the raising, lowering, and theoretical torques were small, which means that the dynamic friction resistance was low. There was a gap between pivot point plates of the FEMCO FROPS; therefore the normal force and consequently the friction were low. The FEMCO FROPS leaned 19 degrees rearwards from the vertical in the upright locked position.

Therefore, the lowering graph started around 71 degrees and was rotated down to -71 degrees. The actuation torques were positive for both raising and lowering process. There was no breaking point for the FEMCO FROPS because there was minimal friction and no need to push the FROPS for lowering. The maximum torque occurred at -8 degrees which coincided with theoretical model results. Figures 3.3 and 3.4 shows good repeatability of the measurement setup, based on the similar results for three replications.

Figures 3.5 and 3.6 show the results of raising and lowering the FROPS in three levels of dynamic speeds. The graphs show that the measured torques of the three dynamic speed levels were similar. Analysis of variance (ANOVA) was conducted with SAS to examine the effect of speed on torque at three dynamic levels. The maximum torque which occurred at peak point was selected for the statistical analysis.

The peak angle of the Deere FROPS was -13 degrees and for the FEMCO FROPS was -8 degrees. For the Deere FROPS the average of torques values between -12 and -14 degrees from each treatment were calculated and used as the peak torque values. The average torques values between -7 and -9 degrees were used for FEMCO ROPS.

The means were compared with Fisher's LSD at the 5% significance level. ANOVA test results showed that speed affects peak values of the dynamic torques ($P>0.05$), but there was no obvious trend in the mean peak values. The differences in the peak values were less than 5% (table 3.2).

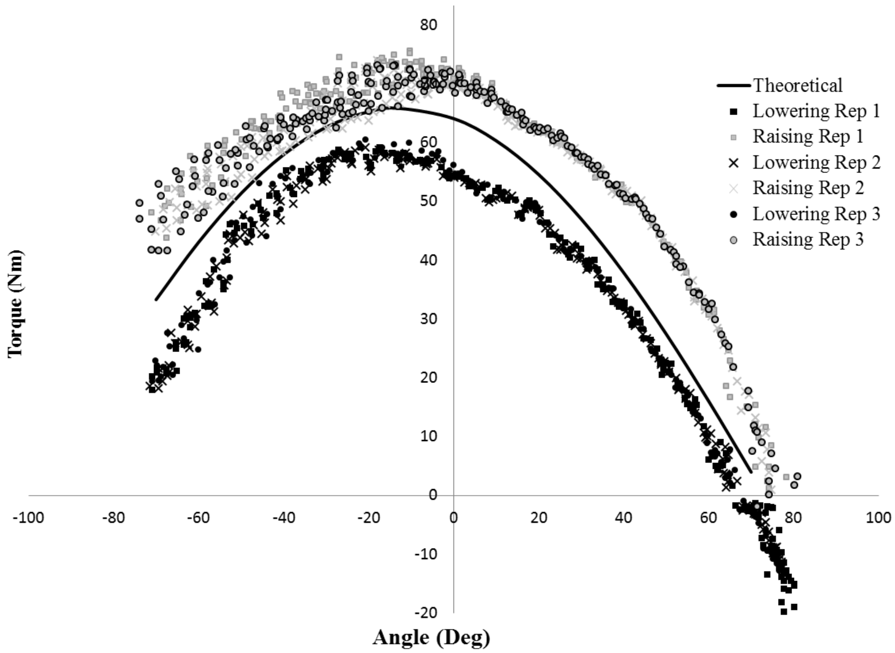

Figure 3.3. Actuation torques for raising (speed 2.6 RPM) and lowering (speed 2.5 RPM) for three replications for Deere FROPS, and theoretical torque for raising and lowering.

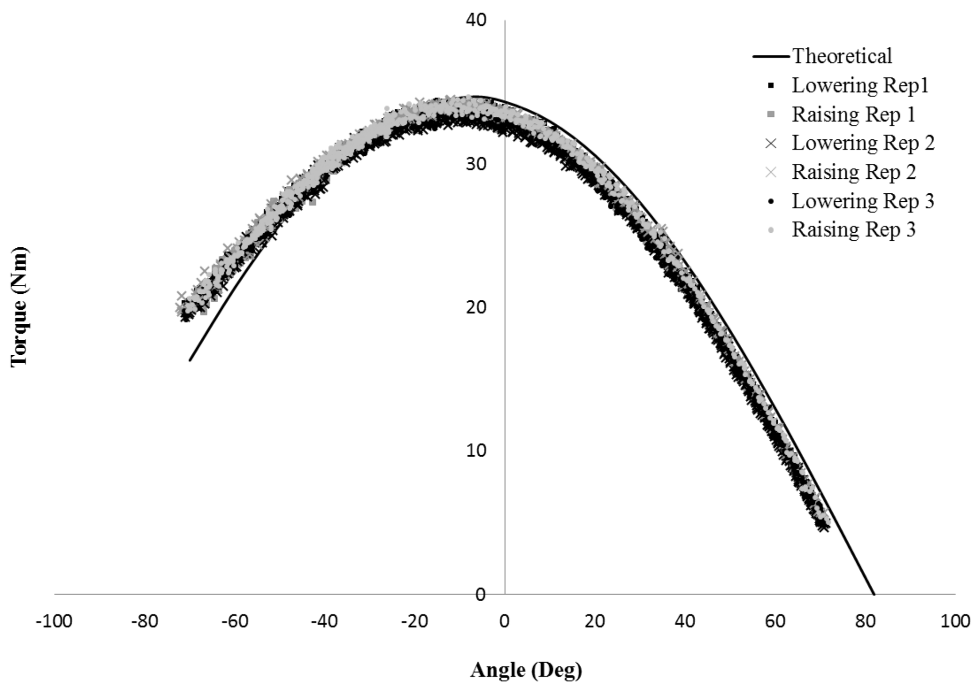

Figure 3.4. The actuation torques for raising (speed 0.9 RPM) and lowering (speed 0.7 RPM) for three replications for the FEMCO FROPS, and theoretical torque for raising and lowering.

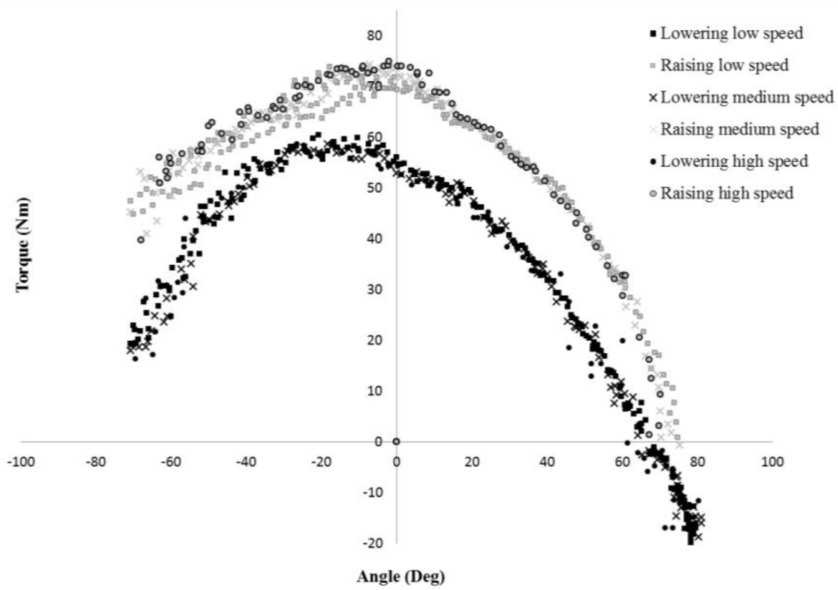

Figure 3.5. The actuation torques for raising and lowering at three different levels of speed of the Deere FROPS.

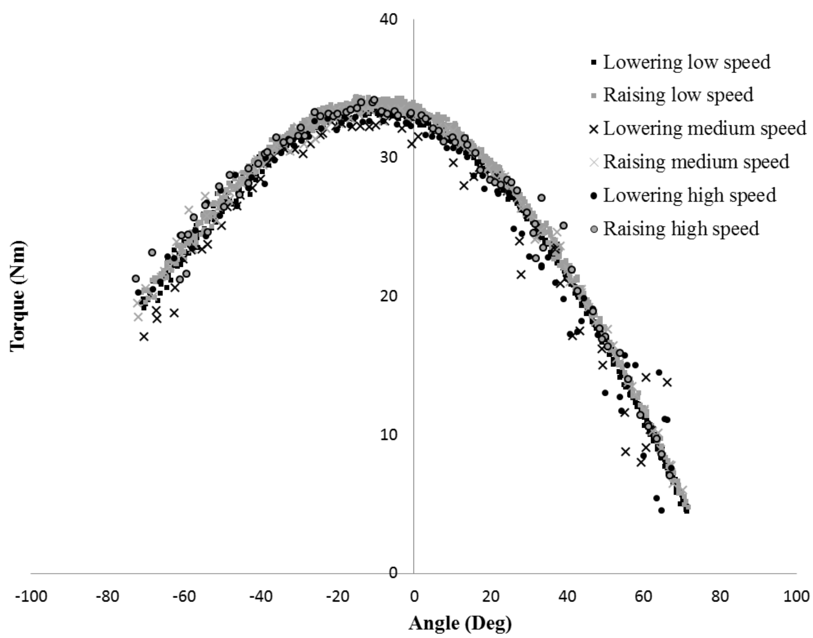

Figure 3.6. The actuation torques (Nm) for raising and lowering at three different levels of speed of the FEMCO FROPS.

During the raising of the FROPS from a static position, a peak of initial torque above the holding torque was apparent as the FROPS starts its transition from static to dynamic movement. As the FROPS was lowered from its holding position, a substantial lowering of the torque was seen as the FROPS was released from its holding position (fig. 3.7). The initial value of the torque in the transient step was recorded as the static initiation torque, as the upper part of the ROPS raised or lowered from static condition to turning speed equal to 3.3 RPM (20 degree s^{-1}).

The results of the holding and static initiation torques measurement for raising and lowering of the Deere and FEMCO were shown in figures 3.7 and 3.8. The raising initiation torques at the peak point were 30 and 19% above the holding torques for the Deere and FEMCO FROPS, respectively. The lowering initiation torques dropped by 33 and 25% from the holding torques for the Deere and FEMCO FROPS (figs. 3.7 and 3.8). These percentage values for Deere FROPS were higher than the FEMCO FROPS, since the friction and the weight of the Deere ROPS were greater than the FEMCO FROPS. The inertial force for a heaver FROPS is higher than the lighter one, with the same acceleration. The static holding torque includes the moment of static friction and weight of FROPS upper part around the pivot point. The holding torques had good agreements with the theoretical curves, considering the effect of friction (figs. 3.7 and 3.8). The initiation torque was comprised of the weight, dynamic friction, and inertial force effects. The inertial force, dynamic friction, and weight vectors were in the same direction for the transient raising. The inertial and frictional force vectors were in the opposite directions with the weight for the transient lowering.

An indicator variable regression technique was used to analyze the effect of speed on the actuation torque (T) as a function of angle (θ). Quadratic regression lines were separately fit to the five-speed levels (figs. 3.9, 3.10, 3.11, and 3.12). The models explained more than 95% of the variations in the measured torques for almost all of the treatments (tables 3.3, 3.4, 3.5 and 3.6). Statistical analysis results showed that intercepts ($P>0.05$), linear slopes ($P>0.05$), and quadratic slopes ($P>0.05$) were significantly different between the speed treatments (tables 3.3, 3.4, 3.5 and 3.6). Therefore speed has a statistically significant, but small effect on the actuation torque.

Although there were statistically significant differences between the dynamic actuation torques, these differences are relatively small compared to the differences among the parameters of static torques especially for the initiation treatments (figs. 3.9, 3.10, 3.11, and 3.12). The difference between the holding torque and the dynamic torque for Deere FROPS was greater than the FEMCO FROPS due to the higher frictional force in the Deere FROPS. The difference between the holding and transient static torque was due to the effect of dissimilar friction forces and the inertial force.

Table 3.2. Mean comparison of peak torques values.

Treatments	Deere Lowering	Deere Raising	FEMCO Lowering	FEMCO Raising
Low	57.4[a]	70.7[b]	33.3[a]	33.9[a]
Medium	56.7[a]	72.4[a]	32.5[b]	33.2[b]
High	57.3[a]	73.0[a]	31. 9[c]	33.4[b]

Values followed by the same letter are not significantly different (P>0.05).

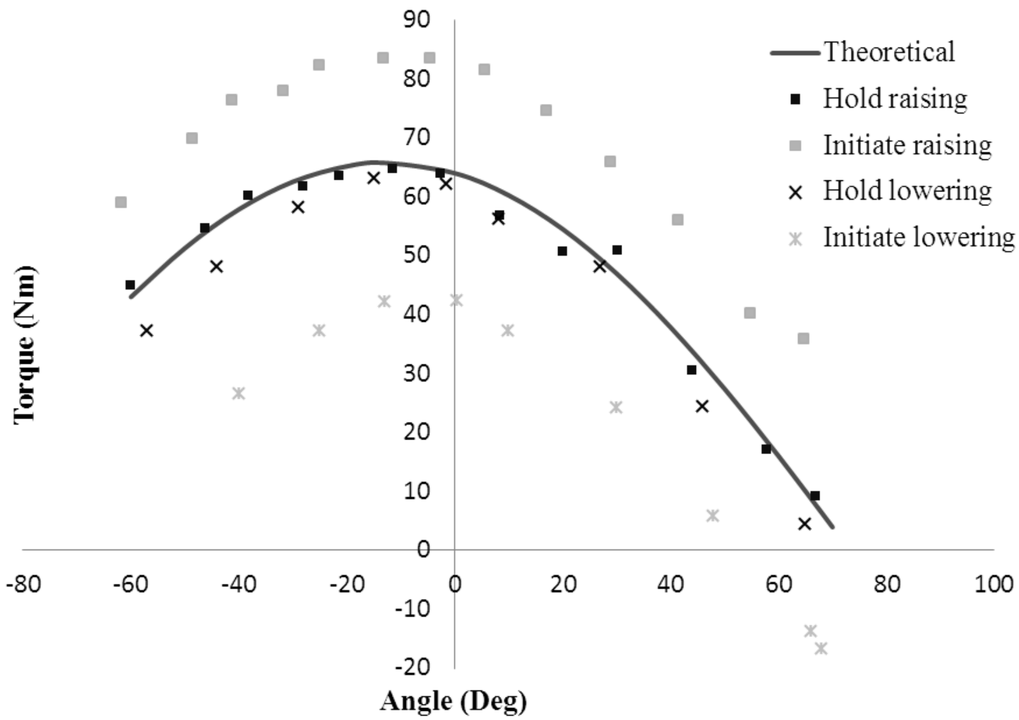

Figure 3.7. The static holding and static transient torques for raising and lowering the Deere FROPS.

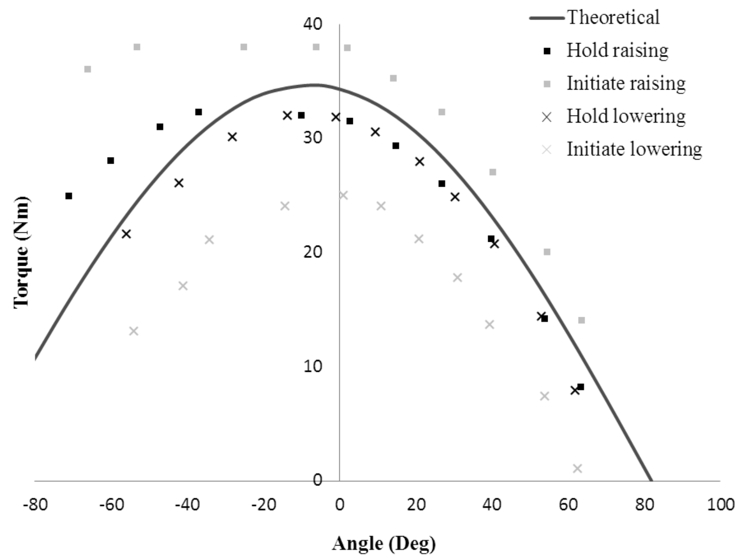

Figure 3.8. The static holding and static transient torques for raising and lowering the FEMCO FROPS.

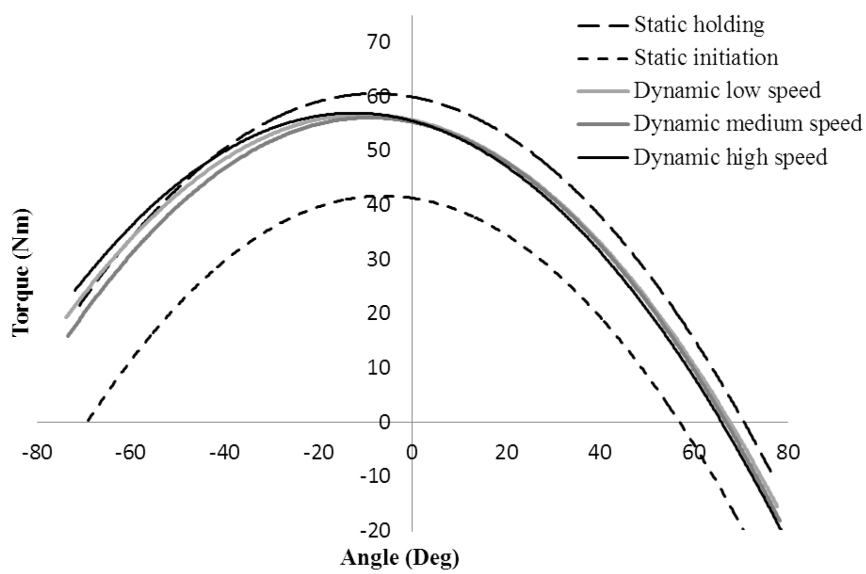

Figure 3.9. The regression lines of lowering Deere FROPS.

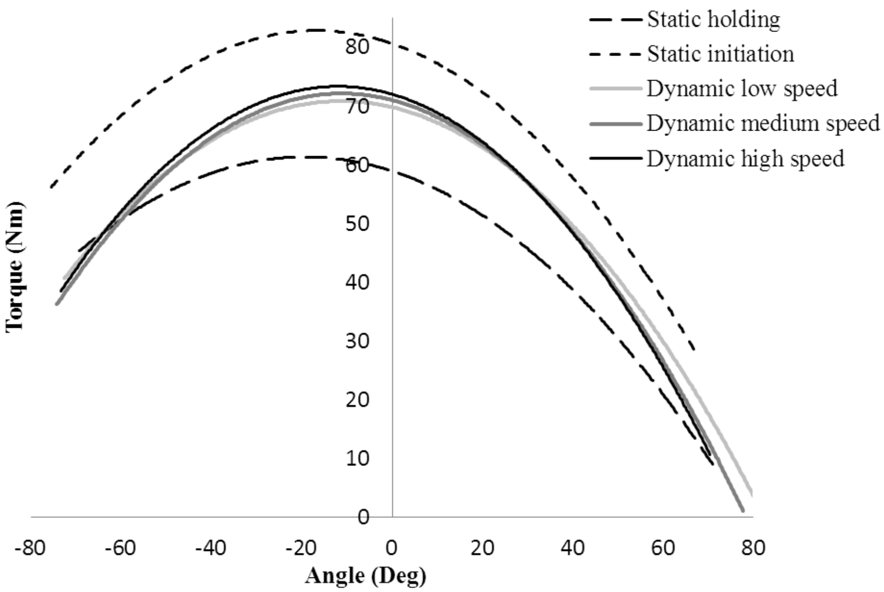

Figure 3.10. The regression lines of raising Deere FROPS.

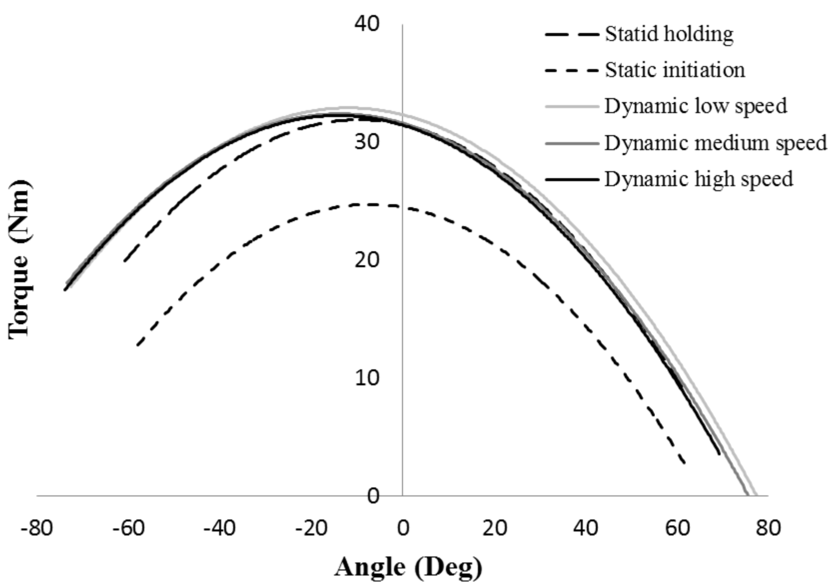

Figure 3.11.The regression lines of lowering FEMCO FROPS.

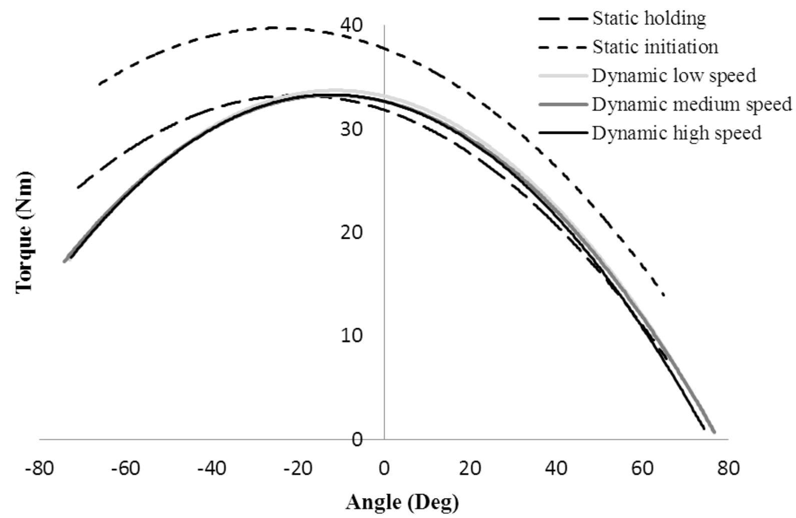

Figure 3.12. The regression lines of raising FEMCO FROPS.

Table 3.3. The regression lines equations for lowering the Deere FROPS.

Treatments	Regression lines equations	R^2
Static holding	$T = -0.0098\theta^2 - 0.1547\theta + 59.95$	0.96
Static initiation	$T = -0.0105\theta^2 - 0.1290\theta + 41.33$	0.98
Dynamic low speed	$T = -0.0093\theta^2 - 0.1928\theta + 55.69$	0.98
Dynamic medium speed	$T = -0.0097\theta^2 - 0.1768\theta + 55.33$	0.97
Dynamic high speed	$T = -0.0093\theta^2 - 0.2317\theta + 55.54$	0.98

Table 3.4. The regression lines equations for raising the Deere FROPS.

Treatments	Regression lines equations	R^2
Static holding	$T = -0.0079\ \theta^2 - 0.240\ \theta + 61.565$	0.98
Static initiation	$T = -0.0077\theta^2 - 0.2614\theta + 80.574$	0.95
Dynamic low speed	$T = -0.0081\theta^2 - 0.1826\theta + 69.743$	0.96
Dynamic medium speed	$T = -0.0090\theta^2 - 0.2007\theta + 70.954$	0.93
Dynamic high speed	$T = -0.0092\theta^2 - 0.2217\theta + 71.949$	0.95

Table 3.5. The regression lines equations for lowering FEMCO FROPS.

Treatments	Regression lines equations	R^2
Static holding	$T = -0.0045\theta^2 - 0.0862\theta + 31.51$	0.99
Static initiation	$T = -0.0046\theta^2 - 0.0663\theta + 24.51$	0.96
Dynamic low speed	$T = -0.0041\theta^2 - 0.0979\theta + 32.34$	0.99
Dynamic medium speed	$T = -0.0040\theta^2 - 0.1120\theta + 31.64$	0.95
Dynamic high speed	$T = -0.0041\theta^2 - 0.1157\theta + 31.46$	0.93

Table 3.6. The regression lines equations for raising FEMCO FROPS.

Treatments	Regression lines equations	R^2
Static holding	$T = -0.0035\theta^2 - 0.1397\theta + 31.80$	0.99
Static initiation	$T = -0.0032\theta^2 - 0.1584\theta + 37.74$	0.97
Dynamic low speed	$T = -0.0043\theta^2 - 0.0959\theta + 33.14$	0.99
Dynamic medium speed	$T = -0.0041\theta^2 - 0.0987\theta + 32.63$	0.98
Dynamic high speed	$T = -0.0043\theta^2 - 0.1053\theta + 32.63$	0.96

3.5 CONCLUSIONS

A measurement setup was developed to measure the actuation torque and the turning angle of the upper part of the FROPS. The influence of rotational speed on the actuation torque for FROPS was investigated. Actuation torques were measured for three dynamic levels and two static levels for two different FROPS. The static levels included the initiation and holding static torques. Experimental test results showed that the dynamic actuation torque for raising the FROPS was greater than when lowering if frictional resistance exists. The mathematical model was developed based on the FROPS upper part dimensions, shape, and material density. The developed model can predict the dynamic actuation torque for FROPS with little friction. With friction, the theoretical torque at a given angle is between the measured raising and lowering torques. The static initiation actuation torque for raising was higher than when lowering the FROPS. The initiation torque values for raising the FROPS at the peak points were 30 and 19% lower than the holding values for the Deere and FEMCO FROPS respectively. The lowering initiation torques values decreased by 33 and 25% for Deere and FEMCO FROPS, respectively.

Indicator variable regression analysis showed significant differences ($P>0.05$) between quadratic regression lines parameters of five-speed levels. The torque angle relationships were modeled using non-linear regression lines. Although the results showed that the speed has a significant effect on actuation torque, the differences between the three regression lines of dynamic actuation torques were relatively small. The static levels and dynamic levels are apparently different. The static initiation actuation torques include the inertial force and were distinctly different than all other speed levels.

3.6 THE EFFECT OF FRICTION ON THE FROPS ACTUATION FORCE

The main objective of this study is to evaluate the influence of friction on actuation torque. The actuation torque to raise and lower ten FROPS were measured. The specific objectives are to measure and compare:

1. The actuation torque with and without greasing.
2. The dynamic and static actuation torques.
3. The actuation torque for several models of the FROPS.
4. The actuation torque of several FROPS of the same model.

3.6.1 MATERIALS AND METHODS

The test includes raising and lowering ten FROPS with two levels of speed (dynamic and static) with multiple replications. The dynamic tests includes two levels (with and without greasing) and the static tests include two levels (holding and initiation). The greasing oil was Loctite (Lb 8529, Lithium grease). The static tests were done before greasing. A new setup for raising and lowering the ROPS was used which included a new motor (Groschopp, Model, PM 8014-PL 731000) with a constant speed equal to 3.3 rpm (20 deg s^{-1}). This new setup did not include the speed controller (fig. 3.13).

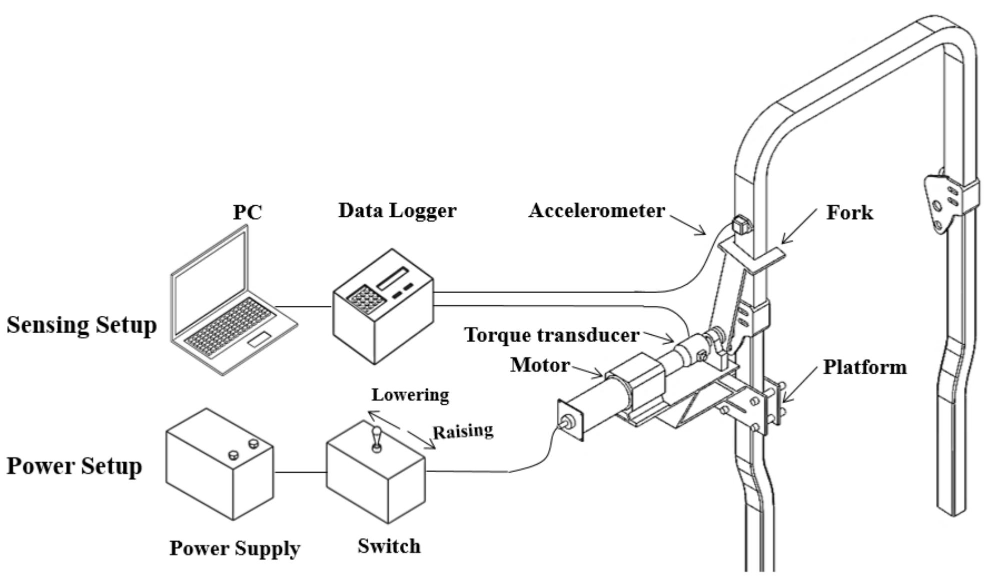

Figure 3.13. Actuation torque measurement with constant speed.

Ten FROPS were selected from 5 different FROPS models, including Snapper Pro, Pro Master, Kubota, Exmark Lazer Z (7 FROPS),and Exmark ultra cut (Table 3.7). These models were selected as variety of these used FROPS are available in the University of Tennessee (UT) landscaping service.

Static hold torque was measured while the upper part of the FROPS was held at certain angles for at least 3 s, both for raising and lowering. As the FROPS started its transition from static to dynamic movement, a sharp change in the torque values around the measured initiation torque value was initially apparent. The initial value of the torque in the transient step was recorded as the initiation torque as the upper part of the ROPS was raised or lowered from a static position to 3.3 rpm. For greasing, oil was sprayed between the pivot point plates which were the only contacting surfaces in FROPS, therefore the only source of friction.

Table 3.7 shows the information about the FROPS and vehicle model, and some dimensions of FROPS. The measured dimensions includes, the pinned position. The pinned positions include the angles of the lower part and the upper part. The angle of the upper part in raised locking position is called up locking and the angle of the upper part in the lower locking position is called down locking point. The up locking point is around +90 and the down locking point is a negative value.

3.6.2 RESULTS AND DISCUSSION

The measured actuation torques for raising and lowering are shown in figures A.1 to A.29 in appendix. Each test included at least three replications and in some cases the measurements were replicated five times. The test included five models of ROPS including, Snapper Pro, Pro master, Kubota, Exmark Lazer Z, and Exmark Ultra Cut. The actuation torques for raising and lowering seven FROPS, model Exmark (both Lazer Z and Ultra Cut) were measured. Each ROPS shows different results, which may be due to the difference in manufacturing (the small inconsistency in assembling process and part size) also the differences in maintenance and working condition, friction, and the age of both the vehicle and FROPS.

Table 3.7. Test, vehicle, and FROPS information.

Vehicle Manufacturer	Vehicle Model	Series	ROPS label	ROPS standard	Pinned positions (Deg)		
					Lower part	Up locking	Down locking
Snapper Pro	S200	S series	NA	OSHA 1928-51	92.0	90.0	-31.0
Pro master	PM-320 Pm 3084	Weight 737 kg	FEMCO model 301113835	N/A	89.6	89.6	-87.9
Exmark (1)	Lazer Z	LZ740KC 604	Exmark Co. MFG co INC	OSHA 1928.51	88.8	77.0	-40.8
Kubota	Kubota	B7510	SFB-F24	OSHA 1928.51	NA	NA	NA
Exmark (2)	Lazer Z	S- Series	Exmark Co. MFG co INC	OSHA 1928.51	85.0	82.4	-34.1
Exmark (3)	Lazer Z	S- Series	Exmark Co. MFG co INC	OSHA 1928.51	87.3	77.7	NA
Exmark (4)	Lazer Z	S- Series	Exmark Co. MFG co INC	OSHA 1928.51	89.5	88.1	-52.2
Exmark (5)	Lazer Z	S- Series	Exmark Co. MFG co INC	OSHA 1928.51	89.4	80.3	-38.4
Exmark (6)	Ultra-Cut 60	Lazer Z above 510000 And laser Xp/Xs mid mount zero turn movers	Exmark Co.	OSHA 1928.51	105.0	73.9	-55.2
Exmark (7)	Lazer Z	Lazer Z mid mount above 790000	Exmark Co.	OSHA 1928.51	98.3	79.8	NA
N/A	N/A	model 301013466	FEMCO	OSHA 29CFR Part 1928.51	86.0	82.0	-95.0
Deere & Company ROP	N/A	model Se1 0095	Deere & Company ROPS	SAE J2194, OSHA 29CFR Part 1928.51	97.0	78.0	-71.0

For several FROPS, there are some large differences between torques to raise and lower the FROPS which occurred due to the effect of friction. For the FROPS with high friction, the difference between the raising and lowering torque is high up to 190%. The graphs (A.1-A.29) also include theoretical models that developed based on the FROPS dimension, weight, and shape. The theoretical model did not consider the effect of friction and inertial forces. Friction caused the differences between the theoretical model and the experimental test results. The vertical components of the friction force and weight were in the same direction and toward the ground during the raising process. However, the vertical components of the friction force and weight were in opposite directions during the lowering process. Thus, the actuation torques for raising the FROPS were greater than the measured resistive torques when lowering the FROPS. Roughly, the theoretical torque plus the torque due to friction was equal to the raising torque. Conversely, the theoretical torque minus the torque due to friction produced the lowering torque.

For example for Snapper Pro (fig. A.1), Kubota (fig. A.19) Exmark 5 (fig. A.21). Exmark 6 (fig. A.24) Exmark 7 (fig. A.27) the friction forces were high. For Pro master ROPS (fig. A.4), Exmark 2 (fig. A.12) the friction was low, and there is very small difference between the raising, lowering and the theoretical curves. Some cases had small friction at beginning and high friction at the end, such as Exmark 1 (fig. A.7) which has a small friction form 80 to -10 and a high friction from -10 to -40 and Exmark 3 (fig. A.15) which has a small friction between +80 to 0 and high friction between 0 to -40 and Exmark 4 (fig. A.18) has a small friction from +75 to 45 and a very high friction between 45 to -25.

The static actuation torque for raising and lowering the FROPS are shown in figure (A.2, A.5, A.8, A.10, A.13, A.16, A.19, A.22, A.15, and A.28). The static initiation raising and lowering has the highest and lowest values, respectively, compared to the other treatments. The static initiation torque comprised of the weight, dynamic friction, and inertial force effects. The inertial force, dynamic friction, and weight vectors were in the same direction for transient raising. The inertial and frictional force vectors were in the opposite direction of weight for transient lowering.

The static holding torque includes the moment of static friction and the weight of the upper part around the pivot point. The holding torques had a good agreement with the theoretical curves, considering the effect of friction. For FROPS with high friction the difference between the static initiation raising and lowering is high (figs. A.2, A.10, A.19, A.22, A.25, A.28) and for FROPS with low friction it is low (fig. A.5, A.8, A.13, A.16).

The measured actuation torque for raising and lowering the FROPS after greasing are shown in figures (A.3, A.6, A.11, A.14, A.17, A.20, A.23, A.26, and A.29). The results in table (A.1, A. 2, A.3, and A.4) showed that the friction force could decreased by greasing the FROPS, but decreasing the friction increase the lowering actuation forces and decrease raising forces of FROPS with high friction. The amount of (friction %) in tables (A. 1- A. 4) is the percentage of the difference between the theoretical values and the average of the measured value indicating the influence of friction. Results for raising and lowering the FROPS, before and after greasing, at a representative point for different replications are presented in figures (A.30-A.33).

The clockwise actuation torques are positive torque as shown in figure 3.14. The actuation torques for raising the all of the ROPS are positive. But for lowering the ROPS, for low friction, the actuation torques are positive, which means that the actuation force hold the ROPS from falling. And for FROPS with very high friction the actuation torque is negative. Which means that the motor pushes the upper part of the ROPS downward.

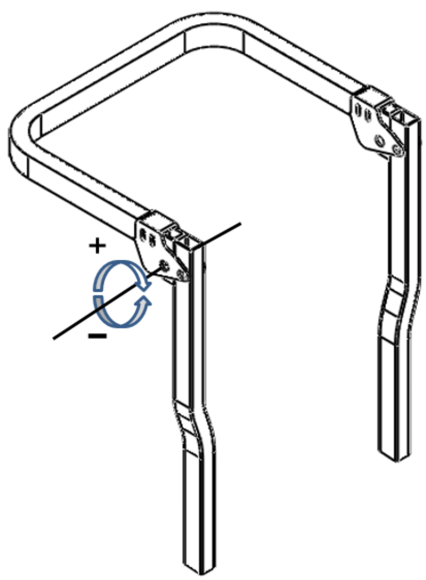

Figure 3.14. The actuation torque directions.

It means that the moment of the friction force is much higher than the moment of weight of the upper part of the ROPS, for example, Snapper Pro (fig. A.15 and A.17) and Exmark 6 Ultra cut (fig. A.38 and A.40). This very high friction also occurred for some FROPS before breaking point, for example Kubota (fig. A.23) around 50°, Exmark 2 (fig. A.29) around 75°and Exmark 5 (fig. A.35) around 55°.

Figures (A.1-A.29) represents the torque-angle raw data. Each figure includes several data sets and each data set represents a replication. For some figures, it is difficult to follow the data set for each replication. Therefore figures (A.34- A.44) were developed to solve the issue. These figures (A.34- A.44) include maximum, minimum, and average lines that present the highest and lowest, and average torque-angle values for raising the FROPS for several replications, before greasing. These figures (A.34- A.44) demonstrate the spread of the data sets. For each 10 degrees increment, the maximum, average, and minimum values were determined and plotted.

3.6.3 CONCLUSION

The actuation torque for raising and lowering the FROPS include the moment due to friction, weight, and inertial forces. For raising and lowering the ROPS the effect of inertial force is significant at the beginning and the end of each rotation, as the final speed and consequently the acceleration is low. Generally, by greasing the FROPS the friction will be decreased. The moment due to friction is in positive direction for lowering and it is in negative direction for raising, considering that the friction is all the time in the reverse direction of the movement direction (fig. 3.14). Therefore for raising the FROPS, by decreasing the friction the actuation torque decreases. For lowering the FROPS with high friction, the actuation torque and the friction are in the reverse directions and therefore by decreasing the friction the actuation torque decreases. For lowering the FROPS with low friction the restriction torque and the friction are in the same directions and therefore by decreasing the friction, the restriction torque increases.

3.7 REFERENCES

Ayers, P. D., Dickson, M., & Warner, S. (1994). Model to evaluate exposure criteria during roll-over protective structures (ROPS) testing. *Trans. ASAE, 37*(6), 1763-1768. http://dx.doi.org/10.13031/2013.28265

Hoy, R. M. (2009). Farm tractor rollover protection: Why simply getting rollover protective structures installed on all tractors is not sufficient. *J. Agric. Saf. Health, 15*(1), 3-4. http://dx.doi.org/10.13031/2013.25418

NIOSH. (2013). Science blog: Preventing death and injury in tractor over-turns with roll-over protective structures. Washington, DC: NIOSH. Retrieved from http://blogs.cdc.gov/niosh-science-blog/2009/01/05/rops/

NIOSH. (2014). Science blog: Agricultural safety. Washington, DC: NIOSH. Retrieved from http://www.cdc.gov/niosh/topics/aginjury/

NIOSH. (2015). Fatality assessment and control evaluation (FACE) program. Washington, DC: NIOSH. Retrieved from http://wwwn.cdc.gov/NIOSH-FACE/Default.cshtml?state=ALL&Incident_Year=ALL&Category2=0001&Submit=Submit

OECD. (2014). Standard codes for the official testing of agriculture and forestry tractors, sub-working group on rear foldable ROPS. TAD/CA/T/WD (2104)8/REV1. Paris, France: Organization for Economic Co-operation and Development.

Pessina, D., Facchinetti, D., & Giordano, D. M. (2015). Narrow-track agricultural tractors: A survey on the load of hand-operated foldable roll-bar. In *Proc. Intl. Conf. on Rural Health and Ragusa SHWA: Safety Health Welfare in Agriculture Agro-food and Forestry Systems.* Catania, Italy: University of Catania.

Spielholz, P., Sjostrom, T., Clark, R. E., & Adams, D. A. (2006). A survey of tractors and rollover protective structures in Washington State. *J. Agric. Saf. Health, 12*(4), 325-333. http://dx.doi.org/10.13031/2013.22012

Thelin, A. (1998). Rollover fatalities: Nordic perspectives. *J. Agric. Saf. Health, 4*(3), 157-160. http://dx.doi.org/10.13031/2013.15353

CHAPTER Ⅳ
MODELING THE EFFECT OF LIQUID MOVEMENT ON THE CENTER OF GRAVITY LOCATION OF OFF-ROAD VEHICLES

This chapter is a reformatted version of a paper, by the same name, submitted to the Journal of Thera mechanics by Farzaneh Khorsandi, Paul. D. Ayers, Robert. S. Freeland, Xang. Wang.

4.1 ABSTRACT

Off-road vehicles may be prone to rollover whenever operated on steep slopes or while maneuvering sharp turns. Being susceptible to overturning is often due to a vehicle having a high terrain clearance. A high static center-of-gravity (CG) location makes the vehicle more vulnerable to overturns. As a vehicle tilts, its liquid payloads, fuel, liquid ballast, hydraulic liquid, and lubricants not entirely contained will shift in position and form. Although many authorities acknowledge that this liquid movement will reposition the static CG location, no studies have investigated the extent of this effect. A mathematical model was developed to predict the effect of liquid movement on the CG location of a tilted vehicle using the lifting axle method of ISO 16231-2:2015. This project modeled the effect of liquid mass and volume, container dimensions, and tilt angle. The model was first validated using a prototype, which was a small four-wheel cart that carried a partially filled water tank. The model was also validated using an agricultural utility tractor.

The experimental test results showed that by increasing the tilting angle the CG height of a vehicle decreased due to liquid movement. The developed model predicted the measured CG height with less than 5% error. The effect of liquid shift on CG height measurement for a vehicle with 16% liquid mass was 19.5% and for the tractor with 2% of liquid mass was 0.35%. Results showed that depending on the desired accuracy the effect of liquid shift can be considered or neglected in the CG height calculation. Although this effect is so small for full size agricultural tractor.

4.2 INTRODUCTION

The center of gravity (CG) is the location of a theoretical point representing the total mass of a body. Dynamic and static free-body calculations routinely use CG, such as for studying vehicle stability (Demšar et al., 2012; Spencer, 1978), vehicle dynamics (Hyun & Langari, 2003), and vehicle continuous rolling (Fabbri & Molari, 2004). Since off-road vehicles often possess many irregular shapes, it is practically impossible to find the CG location using analytical methods. Various techniques can physically determine the CG of vehicles. These methods are vertical hang (ISO, 1982), pendulum (Fabbri & Molari, 2004; ISO, 2011), lifting axle (ISO, 2014; Liljedahl, Turnquist, Smith, & Hoki, 1996; OECD, 2002; Wang et al., 2016), and tilt table. The lifting axle method (LAM) is a popular method for determining the CG height of a vehicle (ISO, 2011).

In the LAM, the lateral and longitudinal CG dimension can be measured when the vehicle is in a horizontal position. The lateral and longitudinal CG measurements are straightforward; however, the CG height measurement is a complicated procedure. When measuring the CG height of a vehicle, one axle is lifted, be it either the front or rear. Measured parameters in the LAM are load distribution on all tires when the vehicle is in a horizontal position, the load on the raised axle in the lifted vehicle, and some structural geometries of the vehicle. Several factors affect CG height measurement in the LAM, such as, scale accuracy, lifting height, liquid shift, tire deflection, loose mechanical component movement, and vehicle structure deflection.

Wang et al. (2016) used a test method to measure the effect of loose mechanical parts (e.g., springs, elastic cells) and fluids (e.g., fuel, hydraulic, and lubricant oils) on the CG height of a zero turning radius (ZTR) mower. Their test method followed ISO 16231-2. ISO 16231-2 is a standard method for stability assessment of self-propelled farm machinery (ISO, 2015). The first section of ISO 16231-2 describes measuring the CG location of non-laden, self-propelled, agricultural machinery. This standard employs the LAM. Wang et al. (2016) found that liquid shift within a tilting vehicle affects its CG height calculation. However, ISO 16231-2 recommends to take into account the effect of movement liquids on the CG height calculation, but no method was provided to quantify the effect of liquid shift on CG height calculation.

Measurement standards call for tilting the vehicle in determining the CG height. As a vehicle tilts, any unrestrained liquids inside the vehicle shift in both their position and shape (fig. 4.1). Several researchers suggest that liquid shift affects the CG height calculation in the LAM (ISO, 2011; Wang et al., 2016) and pendulum method (Fabbri & Molari, 2004). Liquids commonly found in off-road vehicles are fuel, coolants, hydraulic oils, lubricants, battery electrolyte, and liquid tire ballast.

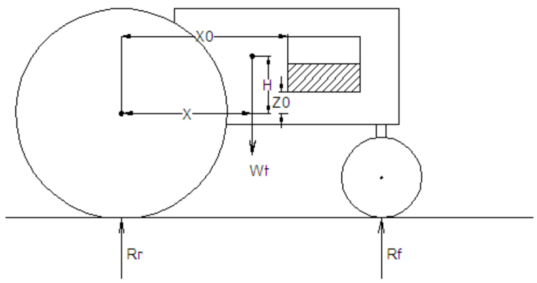

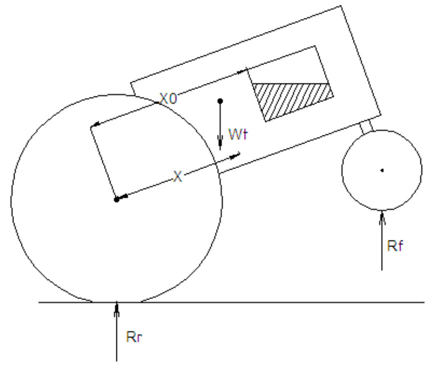

(a) **(b)**

Figure 4.1. Liquid fuel shifts in position and shape within a partially filled fuel tank: (a) level (b) tilted.

Several standards provide suggestions to decrease the impact of uncontained liquid movement and tire deflection on CG measurements. Following ISO 789/6 (ISO, 1982), which is a standard for measuring CG height of an agricultural tractor, evaluators fill the radiator, hydraulic, and other reservoirs to a particular working level.

The fuel tank is full, empty, or at a specified quantity that the manufacturer and the testing authority agrees upon (ISO, 1982). ISO 10392 (ISO, 2011**)** is a standard method for determining the CG of road vehicles. Based on ISO 10392, the fuel tank is full. Furthermore, this standard requires evaluators to note any effects of other liquids that may move.

4.3 GOALS AND OBJECTIVES

Although many experts acknowledge that liquid shift in a tilted vehicle affects the measurement of its CG, few studies have investigated the extent of the effect. Currently, there is no recommendation to adjust the CG height calculation due to liquid movement.

Therefore, the overall goals of our research are 1) to develop, demonstrate, and validate a theoretical model to predict the effect of liquid repositioning on the CG location, and 2) validate the model using a prototype and an agricultural utility tractor.

4.4 MATERIAL AND METHODS

The procedure is divided into two parts based on the specific objectives. The first part includes generating an analytical model to quantify the liquid shift and predict the effect of liquid shift on CG height calculation. The second part includes the model validation using a wagon that carries a liquid tank and a full-size agricultural tractor. The results of experimental tests were used to validate the developed model.

4.4.1 DEVELOPING ANALYTICAL MODEL

An analytical model was developed to predict the effect of the liquid shift on CG height calculation in the LAM. CG height calculation depends on the load on the rear and the front axles. By tilting the vehicle, the load distribution on the rear and the front axles changes which is called weight movement. The weight movement means weight movement from the raised axle to the fixed axle, due to the change in the horizontal distance between the axles center lines and the CG point. The CG is positioned more over the fixed axle as the tractor is tilted (fig. 4.1). By tilting a vehicle, two types of weight movement occur, natural weight movement and liquid weight movement. The effects of liquid amount, the liquid container dimension, and location of on liquid weight movement were investigated.

4.4.1.1 LIQUID AMOUNT

Liquid amount includes both liquid weight and liquid volume, which is the relative volume of the liquid to the liquid container. The weight of a known volume of a special liquid can be calculated by knowing liquid density. The common liquids in the off-road vehicles are fuel, coolant liquid, hydraulic oil, lubricant oil, electrolyte liquid in the electrical battery, and the liquid in the tire that is used for vehicle ballast. The density of hydraulic oil, lubricant oil, and fuel are in ranges 950-1030, 750-950, and 750-835 kg m^{-3}, respectively.

4.4.1.2 LIQUID VOLUME AND TANK VOLUME

Liquid containers of the off-road vehicles have different shapes, rectangular, chamfered rectangle, cylindrical, and irregular. In this study, the container was assumed to be rectangular. Therefore, the cross section of the liquid in the partially filled liquid reservoir in the horizontal position will be a rectangle. There are four possible shapes for cross section of the liquid in planes parallel to median longitudinal plane. Factors that affect the shape of cross section of liquid in the rectangular tank are width (b), height (a'), depth of liquid in the tank (a), and tilting angle (θ) (fig. 4.2). By tilting the liquid reservoir, the shape of the cross section of liquid inside the tank will change the height and lateral position of CG of liquid in a tilted tank. This is defined by equation (4.1-4.5). Where X_L and Z_L represent the CG location of liquid.

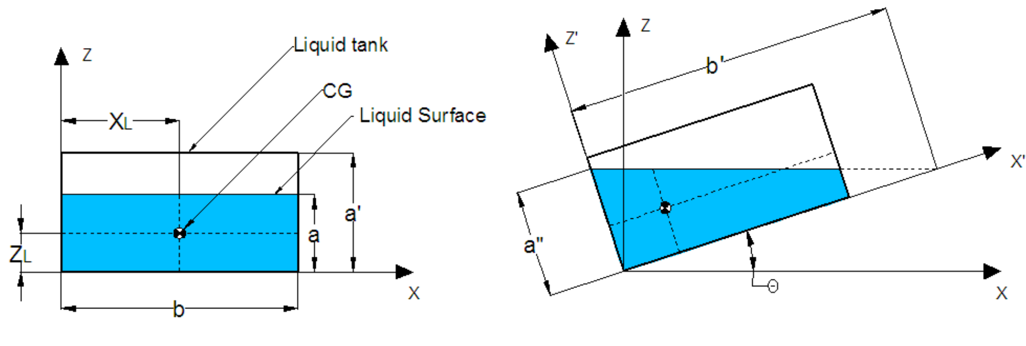

(a) (b)

Figure 4.2. Cross section shape in median longitudinal.

$$(a):\ X_L = 0.5\text{b} \qquad Z_L = 0.5\text{a} \qquad a'' = \text{a},\ b' = \text{b} \tag{4.1}$$

$$(b):\ X_L = \frac{6ab - b^2\tan\theta}{12a} \qquad Z_L = \frac{12a^2 + b^2\tan^2\theta}{24a} \qquad a'' \le \acute{a},\ b' \ge \text{b} \tag{4.2}$$

$$(c): X_L = \frac{b''}{3} = \frac{1}{3}\sqrt{\frac{2ba}{\tan\theta}} \qquad Z_L = \frac{a''}{3} = \frac{1}{3}\sqrt{2ba\tan\theta} \qquad a'' \le \acute{a},\ b' \le b \tag{4.3}$$

$$(d): X_L = b - \frac{b\acute{a}}{2\,a} - \frac{(\acute{a} - a)}{3\text{a}}\sqrt{\frac{2b(\acute{a} - a)}{\tan\theta}} \qquad Z_L = \acute{a} - \frac{\acute{a}^2}{2a} + \frac{(\acute{a} - a)}{3\text{a}}\sqrt{2b(\acute{a} - a)\tan\theta} \qquad a'' \ge \acute{a},\ b' \ge \text{b} \tag{4.4}$$

$$(e): X_L = \frac{12B^2 + a^2\,cot^2\theta}{24B} \qquad Z_L = \frac{6aB - a^2\,cot\,\theta}{12B} \qquad a'' \ge \acute{a},\ b' \le b \tag{5.5}$$

$$Where;\ B = \frac{ab}{\acute{a}}.$$

4.4.1.3 THE LIQUID TANK LOCATION

Liquid tanks can be locate in different places within the body of the vehicle. The real CG location of a vehicle that carry a liquid tank in a known location can be calculated by equation 4.6 and 4.7:

$$Z_2 = \frac{W_L(Z_L + Z_0) + W_S Z_S}{W_T} \tag{4.6}$$

$$X_2 = \frac{W_L(X_L + X_0) + W_S X_S}{W_T} \tag{4.7}$$

Where, X_2 and Z_2 are the real horizontal and vertical position of the vehicle CG point, X_0 and Z_0 are the horizontal and vertical distance between the origin of the liquid tank and the vehicle origin (4.1), W_L is the liquid weight, W_S is the weight of the vehicle with no liquid, and W_T is the total weight of the vehicle.

4.4.1.4 ERROR CALCULATION

The aim of this study is to find the actual CG location by considering the effect of liquid shift. By tilting the liquid tank, the liquid moves and changes the CG location both horizontally and vertically. Changing the location of the CG horizontally and vertically affects the actual CG height calculation. Three different CG locations were defined and simulated based on the CG movement. These three CG location are defined for a rectangular liquid container which the container weight is zero (fig. 4.2).

In the first case, the CG of the liquid was calculated by the assuming that the liquid inside the tank replaced with a solid body. It is assumed that the physical properties of the solid body are the same as physical properties of the liquid (fig. 4.3), but the only difference is that the solid part does not flow under shearing stresses due to gravity. The calculated CG height (Z_1) in the first scenario is not affected by the liquid shift, and the only weight movement is natural weight movement.

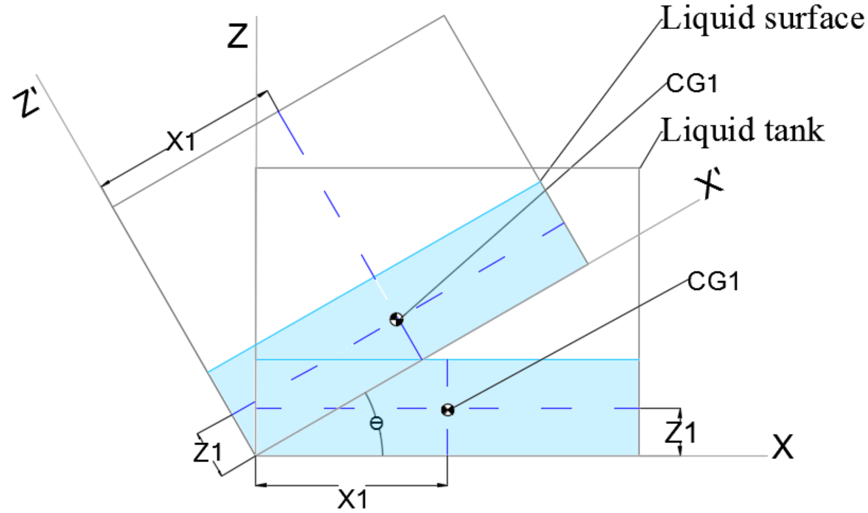

Figure 4.3. Replacing the liquid in a liquid container with a solid part.

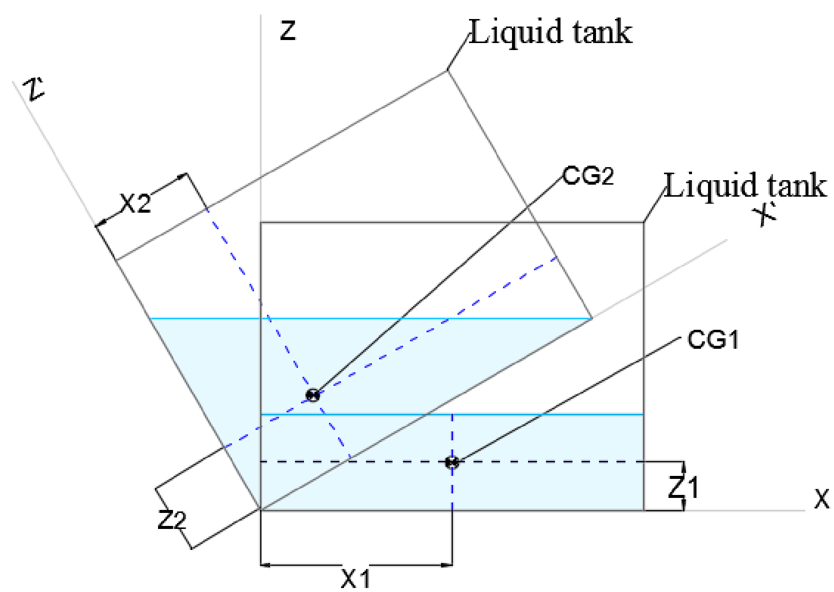

Figure 4.4. Liquid shift and ACG calculation.

In the second scenario, the liquid container is tilted, and the CG locations (X_2 and Z_2) at each tilting angles is different. In this case, both vertical and horizontal liquid movement was considered in the CG height calculation (fig. 4.4). These CG heights are called Z_2.

In second scenario, the CG point moves both horizontally and vertically and goes closer to the pivot point (o). The weight movement in the second scenario is higher than the first scenario (fig. 4.5). The weight shift due to the liquid shift is higher than the natural weight movement. Due to the liquid shift, the CG point moves both horizontally and vertically. The liquid weight movement is calculated by equations (4.8, 4.9, and 4.10).

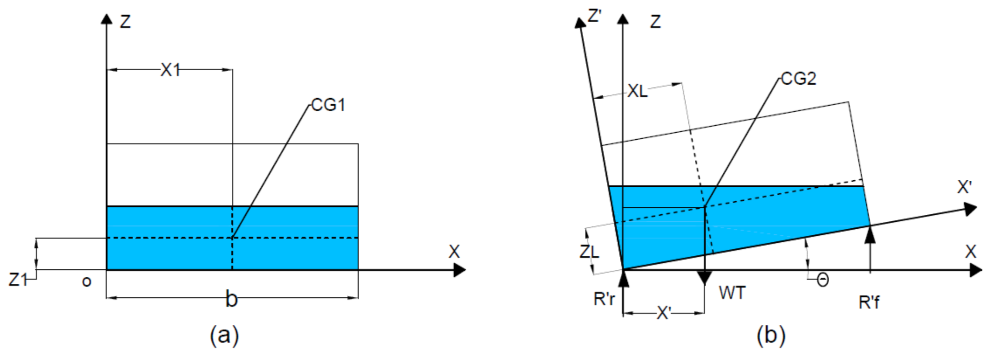

Figure 4.5. Liquid cross section. a) In horizontal position and b) tilted tank.

$$X' = X_L \cos\theta - Z_L \sin\theta \quad (4.6)$$

$$X' = \frac{\acute{R}_f \, \acute{b} \, \cos\theta}{W_t} \quad (4.7)$$

$$\acute{R}_f = \frac{(X_L \cos\theta - Z_L \sin\theta) \, W_t}{\acute{b} \cos\theta} \quad (4.8)$$

Where, R'_f is the weight on front axle and R'_r is the weight on rear axle, X' is the horizontal distance from the CG point to pivot point.

Tilting the liquid tank, the CG point of the liquid moves horizontally from X_1 to X_2 which means that the horizontal distance from the CG point to the pivot point (O) decreases (fig. 4.6). The projection horizontal movement (m) of the CG point is equal to m'. By decreasing the horizontal distance from the CG point to the pivot point, the weight on the pivot point increases. By tilting the liquid tank, the liquid also moves vertically from CG_1 to CG_2, (n) which also decrease the horizontal distance from the CG point to the pivot point. The vertical movement of the CG point is equal to *n*. The projection of the vertical movement from CG_1 to CG_2 is equal to n'.

In the third scenario, the weight movement due to the horizontal and vertical movement of the CG_1 to CG_2 is assumed and calculated to be just due to a movement in the vertical direction. So, in the second scenario, due to the liquid shift the CG location moves from CG_1 to CG_2, but in the third scenario it is assumed that the CG_1 moves to CG_3 (fig. 4.6). The vertical movement of the CG point in this scenario is equal to q (fig. 4.6). The q value can be calculated by equation 4.13. The calculated CG height based on the third scenario is called Z_3. The calculated CG height based on ISO 16231-2 does not consider the CG movement of liquid. This Z_3 height was calculated using ISO 16231-2 equations is higher than Z_1 and Z_2 (Equ. 4.11-4.14).

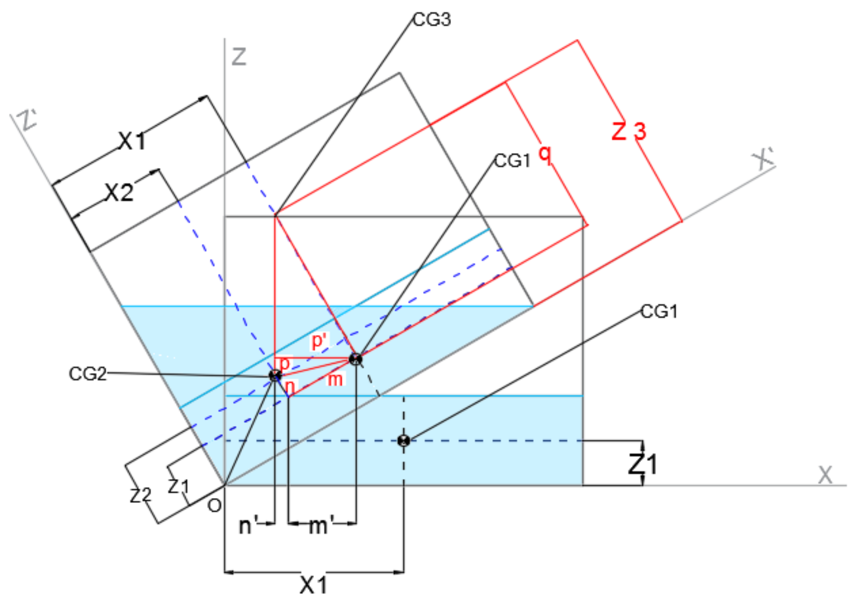

Figure 4.6. Z3 in tilting angle smaller than the stability angle.

$$\acute{m} = \left(\acute{X}_s - X_l\right)\cos\theta \qquad (4.11)$$

$$\acute{n} = \left(Z_l - \acute{Z}_s\right)\sin\theta \qquad (4.12)$$

$$q = (\acute{m} + \acute{n})\ /\sin\theta \qquad (4.13)$$

$$Z_3 = q + Z_1 = (X_1 - X_2)\cot\theta + Z_2 \qquad (4.14)$$

Two concepts were defined based on these CG height values, the model error and the effect of liquid shift on CG height calculation. The model error was defined based on the difference between the calculated and the theoretical Z3 values.

$$Error\% = \frac{(Z_{3E} - Z_{3T})}{Z_{3E}} \times 100 \tag{4.15}$$

Where Z_{3E} is the experimental and Z_{3T} is the calculated Z_3 based on the theoretical model. The effect of liquid shift (LS) is defined as the difference of the real CG height in horizontal position with the calculated CG height (Z3) based on ISO 16231-2. The LS was calculated by equation (4.16).

$$LS\% = \frac{(Z_3 - Z_1)}{Z_1} \times 100 \tag{4.16}$$

4.4.2 EXPERIMENTAL MODEL VALIDATION

The developed model was validated using two vehicles, a wagon that carries a liquid tank and a full-size agricultural tractor. The experimental CG height was measured based on ISO 16231-2 standard method. The procedure includes three steps, discharge most of the liquids of the vehicle, and measure the CG location of the solid body. The next step was to fill the liquid tank to special levels and measure the CG height (experimental Z_3). Each test was replicated several times. The final stage was to measure the required dimensions of the solid body and liquid tank to calculate the CG height Z_1, Z_2, and Z_3 theoretical by using the developed theoretical models.

Standards usually provide some remarks to decrease the error caused by unexpected factors such as tire deflection. ISO 16231-2 provides several statements to improve the test procedure. Since the CG height measurement was mainly based on the ISO 16231-2, these remarks were considered during the test. The suspension system was locked during the test. The plane of the scale was kept horizontal and parallel to the ground plane. The test occurred on a flat surface. The wheels on the scale were free to rotate and in the position for towing the vehicle. Therefore, the parking brakes were not applied and the transmission system was in the position for towing the vehicle. The axle with the smaller wheel diameter should be lifted. Therefore, the front axle of the tractor was lifted. The diameter of four tires of the wagon were the same, and the front axle was raised. The weight on the scale was read after complete rest of the lifted axle on the scale (ISO, 2015). Before the test, the tires were inflated to the maximum permissible pressure specified by the tire manufacturer .The tire of the wagon was inflated to 59 kPa, the front (6.5 0-16) and rear (16.9-28 6 ply) tires of full-size agricultural tractor inflated to pressure 248 kPa and 124 kPa, respectively. The tires deflections in the horizontal and the tilted positions were measured. As the change in the tires radii during the test were less than the 1.5% of the tire radius, the effect of tire deflection in CG height measurement was neglected.

4.4.2.1 WAGON AND LIQUID TANK

The model was validated by using wagon that carried liquid tanks. In the first step of the model validation, the CG location of the solid body (X_s, Z_s) without liquid was determined based on ISO 16231-2. In the second step the liquid tank was filled to half of the liquid tank (fig. 4.7), and the CG height (Z_3) for each angle was measured. Knowing CG height of the solid body and liquid tank dimensions, the developed model was used to calculate Z_1, Z_2, and Z_3. The vehicles were tilted to about 20° in several steps. Each test replicated two times. One set of scale (*Intercomp, model SW650*) was used for these tests.

Figure 4.7. Model validation with a wagon that carries a liquid tank.

4.4.2.2 FULL SIZE AGRICULTURAL TRACTOR

The model was validated by CG height measurement of a full size agricultural tractor, Massey Ferguson 265. The wheel base, the location of the liquid tank, and dimensions of the fuel tank were measured once before the test. The amount of liquid that was added to the liquid tank was measured before each test. Tire radius, raising height, tilting height, weight on front and rear axles were measured for each step and replication. The accuracy of the LAM depends on the height of the wheel stand as a proportion of the wheel base and the accuracy of the scale.

Several instruments such as a fork lift (*Clark, Model C500YS-60 type G*), a platform, two scales sets, a tire pressure gauge, measurement tapes, measurement stands, were used for tractor CG height measurement. The fork lift capacity was 2700 kg and the lifting height was 314 cm. The scales sets included two scales for front axle (*Intercomp, model SW650*) and two scales for rear axle (*DigiWeigh 5000Lb/1Lb Floor Scale DWP-5500R*). The accuracy of the two scales were 0.03 (*Intercomp scale*), 0.45 Kg (*DigiWeight scale*), and the vehicle dimensions were measured within 5 mm resolution.

A platform was designed to raise the front axle of the tractor by means of the fork lift. The platform was made of mild steel. Two Intercomp scales were placed on the platform to measure the weight on the raised axle which was the front axle. The other set of scales were placed below the rear tires. Measurement stands were used to measure the raising height and also the tire radius (fig. 4.8). In the first step, most of the tractor liquids include the transmission, hydraulic, engine oil, the coolant liquids in the radiator, and fuel in the fuel tank were discharged. The electrolyte remained in the battery. In the second step, the fuel tank was filed to (1/4, 2/4, 3/4, and full) and finally the test was run with all of the liquids in the tractor and full fuel tank. For each liquid level, the test were replicated three times, each test included eight measurement. The tractor front axle was raised to 85 cm which was equivalent to 22°. The front and rear weight was measured every 10 cm or 3°.

Figure 4.8. Tractor CG height measurement by using a fork lift.

4.5 RESULTS AND DISCUSSION

Results of the theoretical model and the experimental tests of wagon and a full size tractor are presented in this section. Results include the measured Z_3, the theoretical Z_1, Z_2, and Z_3. The effect of liquid shift on CG height was explored based on the presented results and by using equation 4.16. Also the performance of the developed model was evaluated by comparing Z_{3E} and Z_{3T} (equation 4.15).

The theoretical Z_1, Z_2, and Z_3 were calculated in several steps. In the first step, the CG location of the solid body (X_S, Z_S) was measured. Knowing the dimension of the liquid tank and also the amount of the liquid, by applying equation 4.1-4.5, the CG location of liquid (X_L, Z_L) were calculated. The applied equations for each test are presented in table 4.1. Knowing the location of the liquid tank, CG location of liquid, and CG location of the solid body, the true CG location of the vehicle (X_2, Z_2) in each angle was calculated by applying equations 4.6 and 4.7. The X_1 and Z_1 were equal to the X_2 and Z_2 values at zero degree, respectively. Therefore X_1 and Z_1 were constant values. The Z_2 increases by increasing the tilting angle (figs. 4.9- 4.14). The Z_3 values were calculated by applying equation 4.11-4.15 and decrease by increasing the tilting angle (figs. 4.9-4.14). In the second test, the CG location of the wagon was measured. About 16% of the vehicle weight composed of water weight in a half-full liquid tank. There were small differences between Z_1 and Z_2 values which increased by increasing tilting angle. There was a notable difference between the Z_3 and Z_2, since a significant portion of the vehicle weight was the liquid weight. This difference caused by weight shift of liquid. There was a significant difference between the Z_1 and Z_3 values. Since the liquid weight was a big portion of the vehicle weight. The theoretical Z_3 predicted the experimental Z_3 with a good agreement.

The experimental and theoretical test results for the tractor are shown in graph 4.11-4.14. The percentage of liquid weight, for all five tests changes from 0.65% to 3.9% of the total tractor weight. The Z_1 and Z_2 values showed negligible difference (figs. 4.11-4.14). By increasing the stand height and the tilting angle the difference between Z_3 and Z_1 decreases. The Z_3 and Z_1 are not equal even at the maximum tilting angle which based on the ISO 789/6 standard should be tilted between 20° and 25°. Wang et al. (2016) reported similar results. They identified the influence of liquid shift on CG height measurement, but was not quantified. They correctly measured and reported Z_3 as the CG height, but Z_3 cannot be accepted as actual CG height (Z_2), as Z_3 was higher than the Z_2 at the maximum tilting angle.

Table 4.1. The applied equations to calculate the CG location of liquid (X_L, Z_L) for each test (The maximum tilting angle was 22°).

Required Equation	Wagon (1/2 FT)	Tractor (1/4 FT)	Tractor (1/2 FT)	Tractor (3/4FT)	Tractor (Full)
Equation 4.1 (a)	Θ =0	Θ =0	Θ =0	Θ =0	0-22
Equation 4.2 (b)	0≤Θ≤ 13.15	0≤Θ≤ 14.56	0≤Θ≤ 22	0≤Θ≤ 7.4	-
Equation 4.3 (c)	13.15≤Θ≤20	14.50≤Θ≤22	-	-	-
Equation 4.4 (d)	-	-	-	7.4≤Θ≤ 22	-
Equation 4.5 (e)	-	-	-	-	-

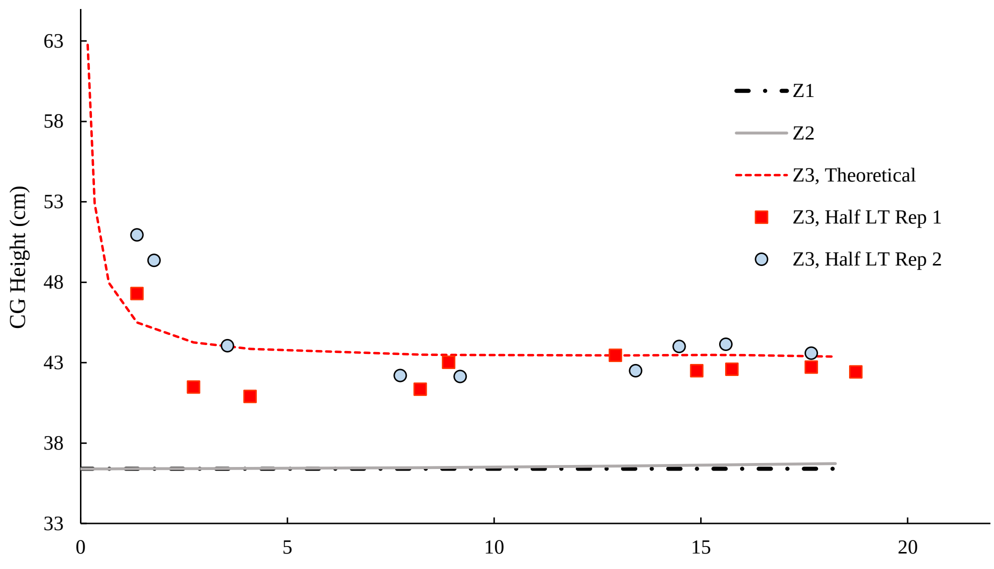

Figure 4.9. The calculated Z_1, Z_2, Z_3 and the experimental Z_3 for the heavy wagon with a half full liquid tank.

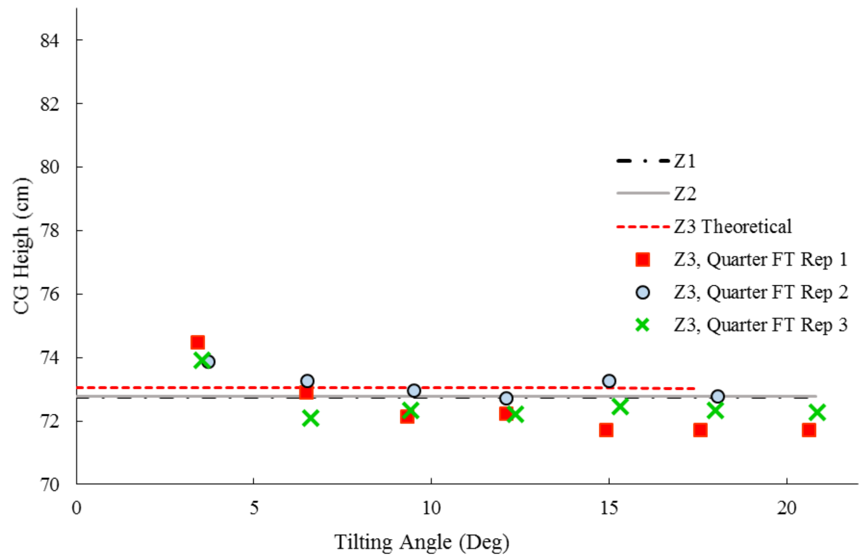

Figure 4.10. The calculated Z1, Z2, Z3 and the experimental Z3 for the full size agricultural tractor with a quarter full liquid tank.

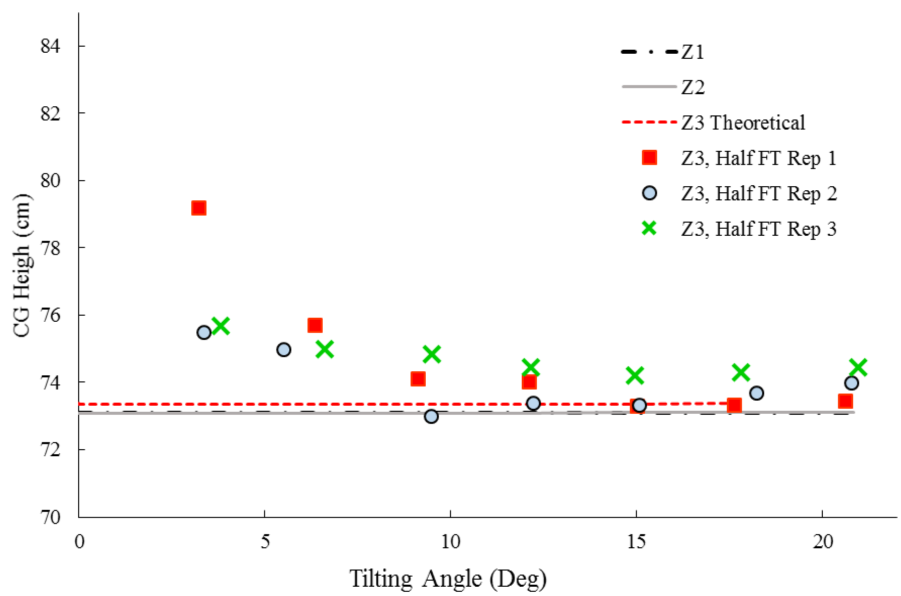

Figure 4.11. The calculated Z1, Z2, Z3 and the experimental Z3 for the full size agricultural tractor with a half full liquid tank.

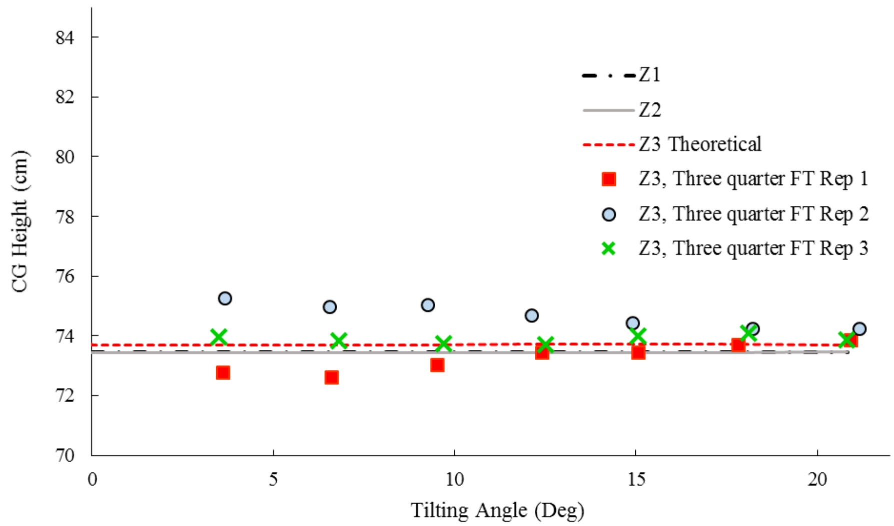

Figure 4.12. The calculated Z1, Z2, Z3 and the experimental Z3 for the full size agricultural tractor with a three quarter full liquid tank.

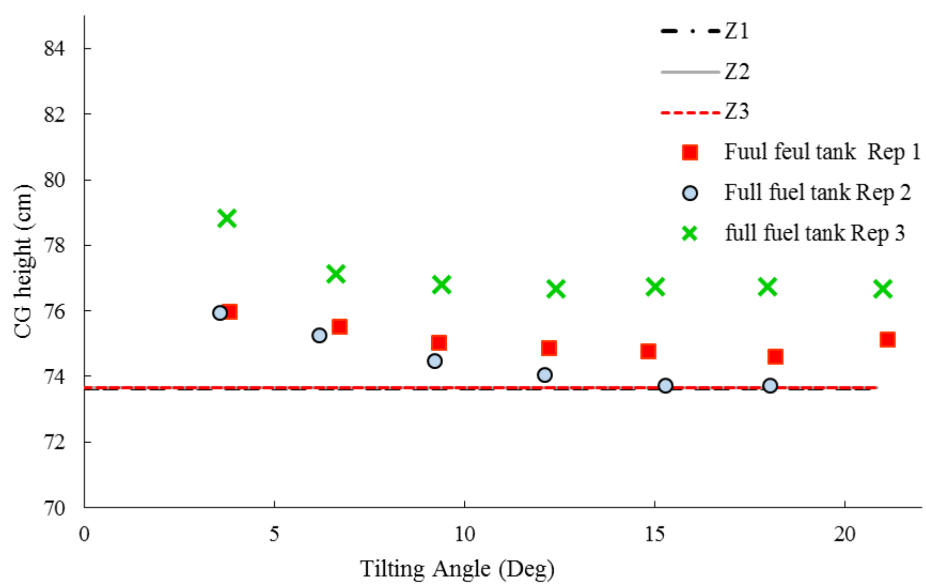

Figure 4.13. The calculated Z1, Z2, Z3 and the experimental Z3 for the full size agricultural tractor with a full liquid tank.

The presented results in table 4.2 was used to discuss about three different concepts. The first one was the effect of liquid on CG height which are shown as Z_1 in table 4.2. The second one, was the effect of liquid shift on CG height which presented as LS%. The third one was the performance of the developed model (Error %).

Table 4.2. Z_1, Z_{3T}, Z_{3E}, LS%, and Error %.

Vehicle	Liquid %	Z_1	Z_{3T}	Z_{3E}	LS%	Error%
Wagon Heavy	16.0%	38.5	46.4	44.5	19.5%	4.3%
Tractor Solid	0.0%	72.5	NA	72.5	0.0%	NA
Tractor ¼ FT	0.6%	72.8	73.0	72.3	0.33%	1.0%
Tractor ½ FT	1.2%	73.1	73.4	74.0	0.36%	0.8%
Tractor ¾ FT	1. 8%	73.3	73.7	74.0	0.35%	0.4%
Tractor full FT	2.1%	73.5	73.9	75.2	0.0%	2.1%

Table 4.2 shows the CG height values for wagon and the tractor with a fuel tank filled to different levels with fuel. For the tractor, by increasing the amount of liquid in the fuel tank, the CG height (Z_1) increased. In the final step, all of the liquids were added to the tractor and the CG height increase as the CG point of liquid tanks located higher than the CG point of the tractor solid body. The total change in CG height due to adding fuel was about1% and by adding all of the liquids was about 2%.

The other point was the effect of liquid shift on CG height measurement. The bigger LS% means the higher effect of liquid shift. LS% was bigger in low tilting angle, the presented LS% in table 4.2 was calculated at 20°. By increasing the tilting angle the difference between the Z_3 and Z_1 decreases. But there was a constant difference between Z_1 and Z_3 which this never disappears in tilting angle between 0 and 20. The LS% depends both on percentage of liquid and also the amount of liquid in liquid tank. Comparing the results of wagon and the tractor, by increasing the percentage of liquid the LS% increased significantly. But comparing different levels of liquid in tractor fuel tank, the LS% increases from 0.33 to 0.36 % by adding fuel to the liquid tank from 1/4 to 1/2 FT. The LS% decrease from 0.36% to 0.35% by adding fuel to the liquid tank from 1/2 to 3/4 FT. The LS% drop, after half full fuel tank occurs due to decrease in amount of liquid that moves by tilting the vehicle. In a 3/4 full fuel tank, there was no enough empty space for liquid to moves inside the liquid tank. For one quarter full fuel tank there was enough space for liquid to move, but the amount of liquid was low. The half full liquid tank has the best combination of liquid amount and free space, therefore the liquid shift (LS%) was the highest amount for half full fuel tank.

The performance of the developed model was evaluated by error calculation (equation 3.16). The Z_3 values decrease by increasing the tilting angle. The decrease in theoretical Z_3 values for tractor were so small. The developed model can predict the Z_3 values by error less than 5% at 20° lift angle.

4.6 CONCLUSION

The aim of this study was to determine the effect of liquid and liquid shift on CG height measurements and calculations. A mathematical model was developed to quantify and predict the liquids effects on CG height. The developed model was validated by testing a wagon and a full-size agricultural tractor. The percentage of liquid weight was 16% for the wagon and this percentage varies between 0.65 to 3.5% for different levels of liquid in the tractor.

Results showed that the liquid shift affect the CG height based on the liquid amount and the liquid container dimension. The liquid container location does not change the effect of liquid shift on CG point movement. A model was developed based on the liquid amount and dimension of liquid container. Results showed that the model can predict the experimental test results with error less than 5%. The effect of liquid shift on CG height calculation related to amount of liquid and the available free space for liquid to move. For the wagon the effect of liquid shift on CG height was significant, but for the tractor, it was a small value which can be neglected. There was a difference between the real CG height locations and the calculated based on ISO 16231-2 standard. The difference was more notable for the wagon compared to the tractor. The developed model predicted the measured CG height with less than 5% error. The effect of liquid shift on CG height measurement for a vehicle with 16% liquid was 19.5% and for the tractor with 2% of liquid was 0.35%.

4.7 REFERENCES

Demšar, I., Bernik, R., Duhovnik, J., 2012. A Mathematical Model and Numerical Simulation of the Static Stability of a Tractor. Agriculturae Conspectus Scientificus (ACS), 77(3), 143-150.

Fabbri, A., Molari, G., 2004. Static measurement of the centre of gravity height on narrow-track agricultural tractors. Biosystems engineering, 87(3), 299-304.

Hyun, D., Langari, R., 2003. Modeling to predict rollover threat of tractor-semitrailers. Vehicle System Dynamics, 39(6), 401-414.

ISO, 1982. ISO 789/6: Agricultural Tractors-Test procedures- Part 6: Centre of gravity. Geneva: International Standard Organization.

ISO, 2011. ISO 10392:2011: Road vehicles: Determination of center of gravity. Geneva: International Standard: Organization.

ISO, 2015. ISO /DIS 16231-2:Self-propelled agricultural machinery-Assessment of stability-Part 2: Determination of static stability and test procedures. Geneva, Switzerland: International Standard Organization.

Khorsandi, F., P. D. Ayers. 2015. Study on the effect of liquid movement on the static overturning angle (SOA) measurement of off road vehicles. Paper No. 2015043. ISTVS. Rome, Italy.

Liljedahl, J., Turnquist, P., Smith, D., Hoki, M., 1996. Tractors and Their Power Units, ASAE, St. Joseph, MI.

OECD, 2002. Standard code for the official testing of agricultural and forestry tractor performance. Paris: Organization for Economic Co-operation and Development.

Spencer, H., 1978. Stability and control of two-wheel drive tractors and machinery on sloping ground. Journal of Agricultural Engineering Research, 23(2), 169-188.

Wang, X., Gao, L., Ayers, P. D., Su, S., Yuan, C., 2016. The Influence of the Lift Angle on the Center of Gravity: Measurements for Zero Turning Radius Mowers. Applied Engineering in Agriculture, 32(2), 189-199.

CHAPTER V
CONCLUSIONS

5.1 DEVELOPING AND EVALUATING A FINITE ELEMENT MODEL FOR PREDICTING THE ROLLOVER PROTECTIVE STRUCTURE NONLINEAR BEHAVIOR UNDER SAE J2194 STATIC TEST

In the first project a finite element (FE) model was developed to predict the ROPS behavior under SAE J2194 standard test. For two types of ROPS (Allis Chalmers 5040 and Long 460), 24 FE models for rear and side load tests with variation in element type and size as well as material properties were developed. The developed FE models were validated by comparing virtual test results with the experimental test results.

Results showed that the developed FE models can predict the rear test results more accurately than the side load test results. In most of the side tests the FE models were stiffer than the experimental tests, as the developed geometries were a single part and did not consider the adjustments at holes, rotations, and movements between parts. The FE model results could be improved by using an assembled structure which may predict the movement and rotations between parts. The developed FE model by applying experimentally measured material properties, resulted in the most accurate ROPS performance Deflection (RPD) prediction in 75% of the tests (three out of four tests). The meshed ROPS with fine quadratic mesh (C3D10M node, 0.01), resulted in the more accurate FE model compared to the linear coarse mesh (C3D4 node, 0.08). The developed FE model (C3D10M node, 0.01) based on ASTM material properties had an average error about 9%.

Two ROPS passed all of the virtual tests as the experimental tests based on calculated RPD. Therefore all of the finite element results appears to be acceptable. But for a ROPS with close RPD value to ROPS allowable Deflection (RAD) value, the less conservative FE models may not result (pass or fail) as the experimental test. The other criterion that should be considered for evaluating the FE tests reliability is the similarity of force-deflection curves of the virtual tests with the experimental tests.

The developed FE models using the ASTM material properties and meshed ROPS with C3D10M elements with global size 0.01 are recommended for future test FE models. As these FE models appear to be more conservative, and the predicted force-deflection curve matched the experimental force-deflection curves. Since the model results for two model of ROPS designed by CRDP are accurate, it can be used for other two-post ROPS designed by CRDP. The recommended FE model may be used to evaluate the effect of the small structural modification on ROPS behavior under SAE J2194 standard test without retesting the ROPS.

5.2 THE EFFECT OF SPEED ON FOLDABLE ROPS ACTUATION FORCES

A measurement setup was developed to measure the actuation torque and the turning angle of the upper part of the Foldable ROPS (FROPS). The influence of rotational speed on the actuation torque for FROPS was investigated. Actuation torques were measured for three dynamic levels and two static levels for two different FROPS. The static levels included the initiation and holding static torques. Experimental test results showed that the dynamic actuation torque for raising the FROPS was greater than when lowering if frictional resistance exists. The mathematical model was developed based on the FROPS upper part dimensions, shape, and material density. The developed model can predict the dynamic actuation torque for FROPS with little friction. With friction, the theoretical torque at a given angle is between the measured raising and lowering torques. The static initiation actuation torque for raising was higher than when lowering the FROPS. The initiation torque values for raising the FROPS at the peak points were 30 and 19% lower than the holding values for the Deere and FEMCO FROPS respectively. The lowering initiation torques values decreased by 33 and 25% for Deere and FEMCO FROPS, respectively.

Indicator variable regression analysis showed significant differences ($P>0.05$) between quadratic regression lines parameters of five-speed levels. The torque angle relationships were modeled using non-linear regression lines. Although the results showed that the speed has a significant effect on actuation torque, the differences between the three regression lines of dynamic actuation torques were relatively small. The static levels and dynamic levels are substantially different. The static initiation actuation torques include the inertial force and were substantially different than all other speed levels.

5.3 THE EFFECT OF FRICTION ON FOLDABLE ROPS ACTUATION FORCES

The actuation torque for raising and lowering the FROPS include the moment due to friction, weight, and inertial forces. For raising and lowering the ROPS the effect of inertial force is significant at the beginning and the end of each rotation, as the final speed and consequently the acceleration is low. Generally, by greasing the FROPS the friction will be decreased. The moment due to friction is in positive direction for lowering and it is in negative direction for raising, considering that the friction is all the time in the reverse direction of the movement direction (fig. 3.14). Therefore for raising the FROPS, by decreasing the friction the actuation torque decreases. For lowering the FROPS with high friction, the actuation torque and the friction are in the reverse directions and therefore by decreasing the friction the actuation torque decreases. For lowering the FROPS with low friction the restriction torque and the friction are in the same directions and therefore by decreasing the friction, the restriction torque increases.

5.4 MODELING THE EFFECT OF LIQUID MOVEMENT ON THE CENTER OF GRAVITY (CG) LOCATION OF OFF-ROAD VEHICLES

The aim of this study is to determine the effect of liquid and liquid shift on CG height measurements and calculations. A mathematical model was developed to quantify and predict the liquids effects on CG height. The developed model was validated by testing a wagon and a full-size agricultural tractor. The percentage of liquid weight is 16% for the wagon and this percentage varies between 0.65 to 3.5% for different levels of liquid in the tractor.

Results showed that the model can predict the experimental test results with error less than 5%. The effect of liquid shift on CG height calculation related to amount of liquid and the available free space for liquid to move. For the wagon the effect of liquid shift on CG height is significant, but for the tractor, it is a small value which can be neglected. There is a difference between the real CG height locations and the calculated based on ISO 16231-2 standard. The difference is more notable for the wagon compared to the tractor. The developed model predicted the measured CG height with less than 5% error. The effect of liquid shift on CG height measurement for a vehicle with 16% liquid is 19.5% and for the tractor with 2% of liquid is 0.35%.

APPENDIX

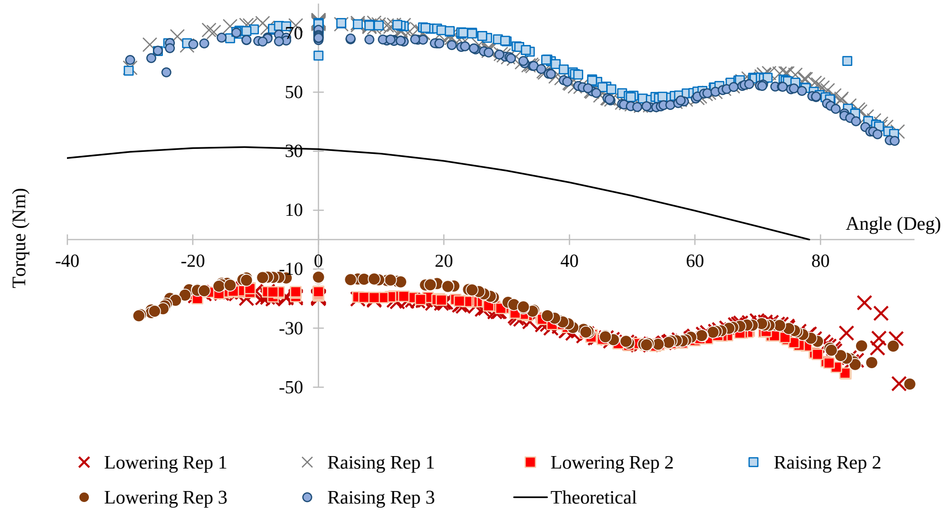

Figure A.1. Actuation torques for raising and lowering for three replications for Snapper Pro ROPS and theoretical torque.

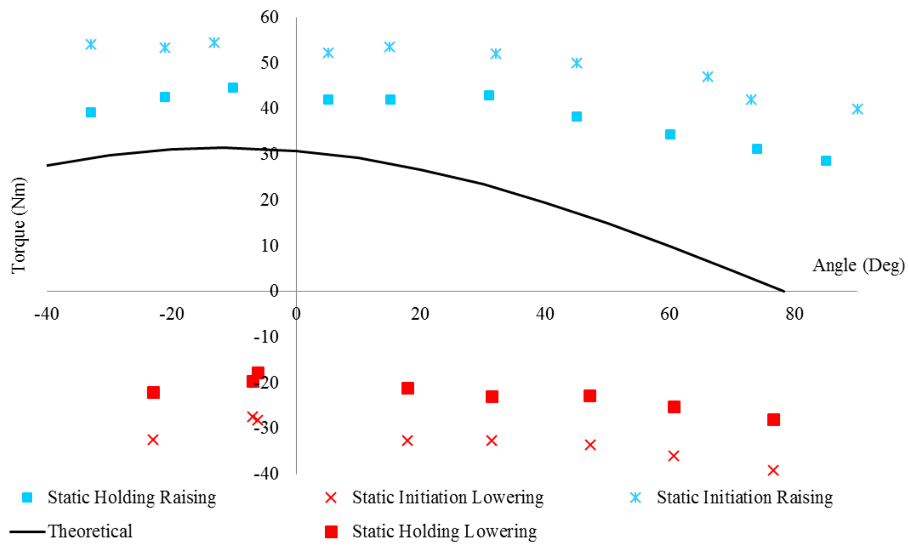

Figure A.2. The static holding and static transient torques for raising and lowering the Snapper Pro ROPS.

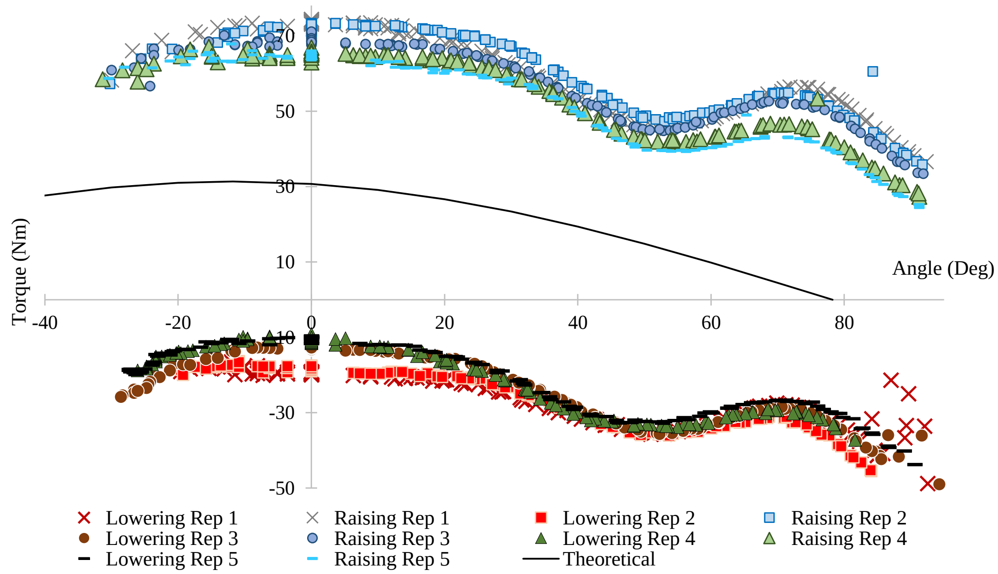

Figure A.3. Actuation torques for raising and lowering for five replications for Snapper Pro ROPS after greasing and theoretical torque.

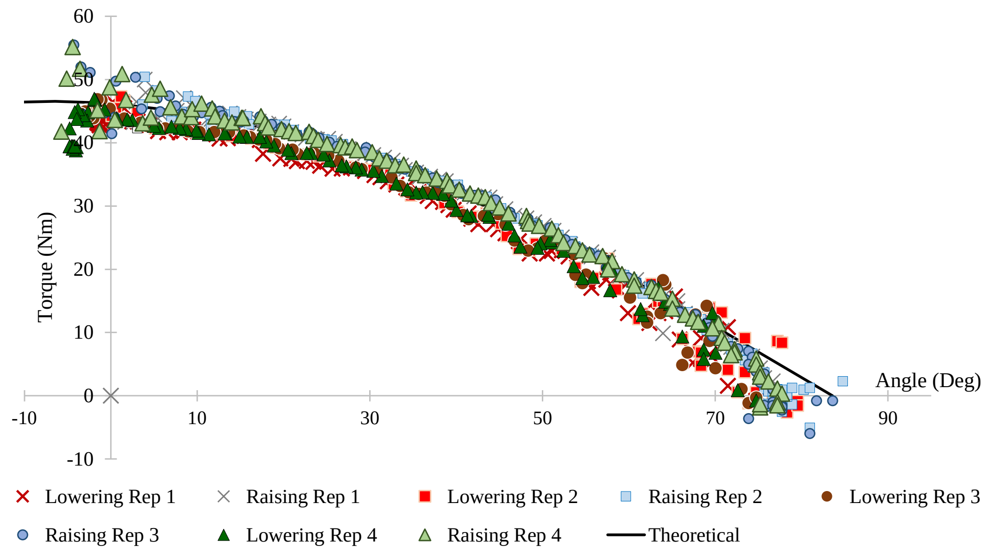

Figure A.4. Actuation torques for raising and lowering for four replications for Pro master, FEMCO model 301113835 ROPS and theoretical torque.

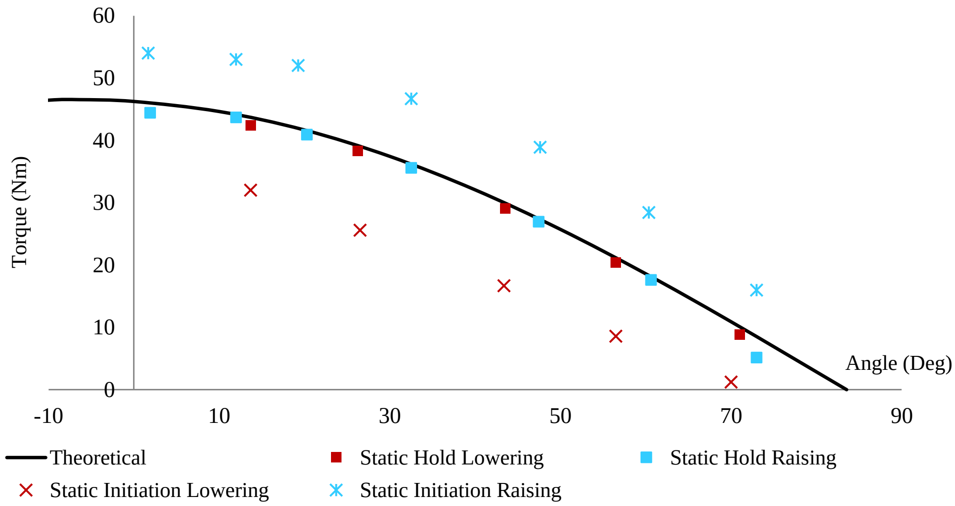

Figure A.5. The static holding and static transient torques for raising and lowering the Pro master, FEMCO model 301113835 ROPS.

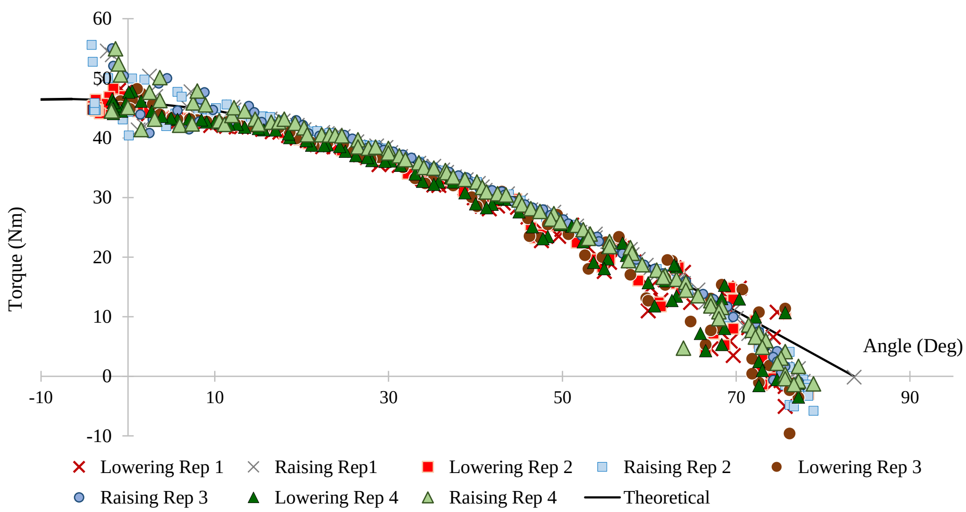

Figure A.6. Actuation torques for raising and lowering for four replications for Pro master, FEMCO model 301113835 after greasing and theoretical torque.

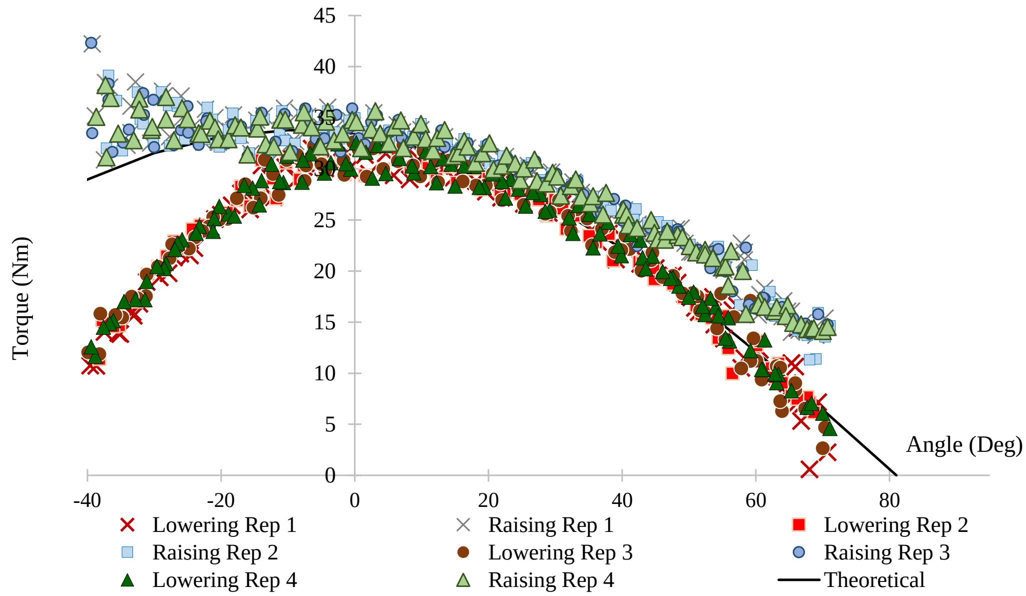

Figure A.7. Actuation torques for raising and lowering for four replications for Exmark (1) ROPS and theoretical torque.

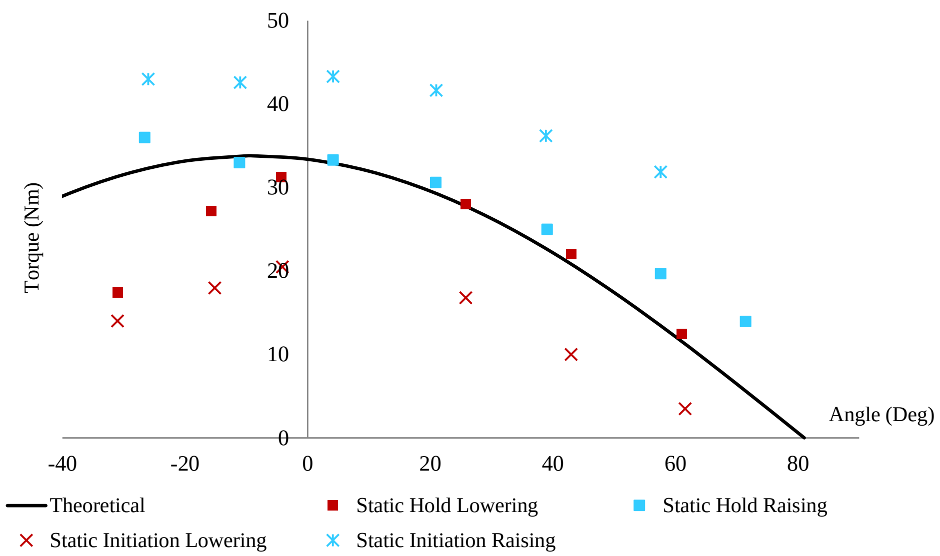

Figure A.8. The static holding and static transient torques for raising and lowering the Exmark (1) ROPS.

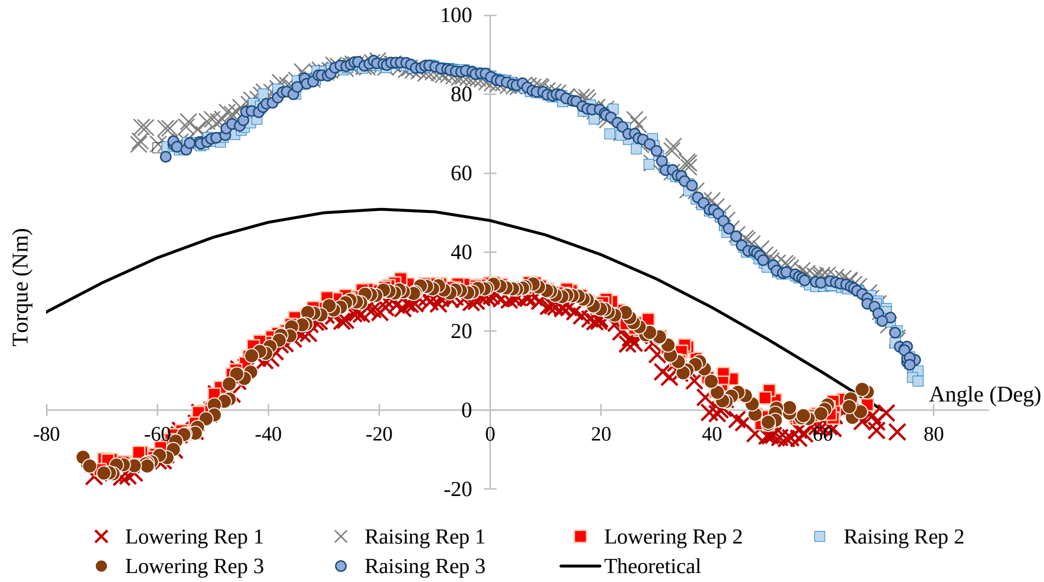

Figure A.9. Actuation torques for raising and lowering for three replications of Kubota ROPS and theoretical torque.

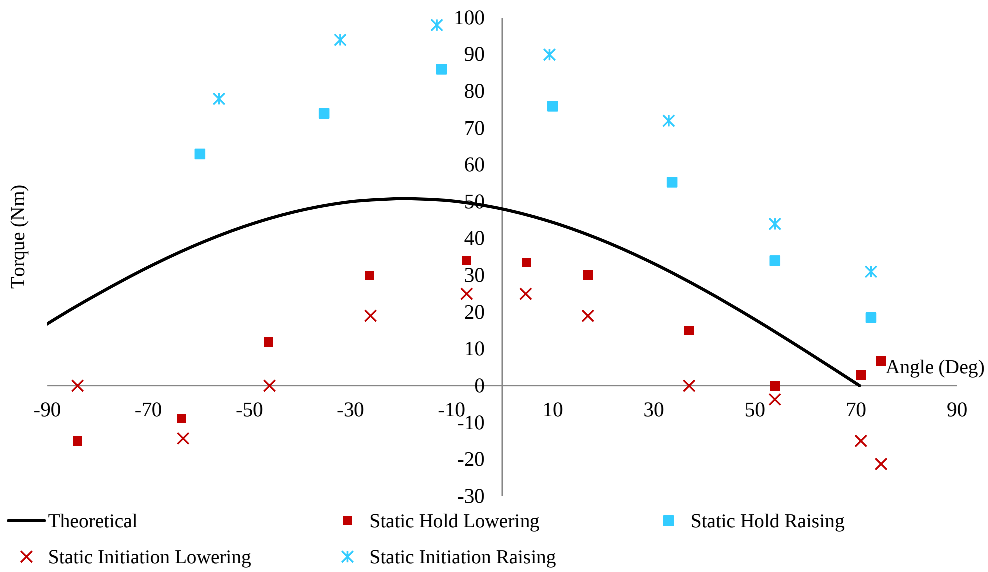

Figure A.10. The static holding and static transient torques for raising and lowering the Kubota ROPS.

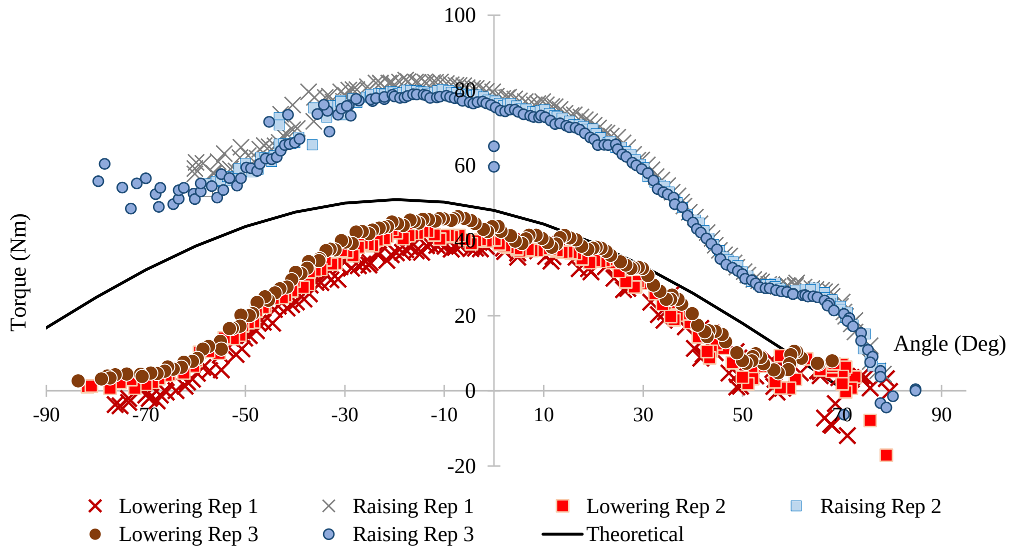

Figure A.11. Actuation torques for raising and lowering for three replications for Kubota after greasing and theoretical torque.

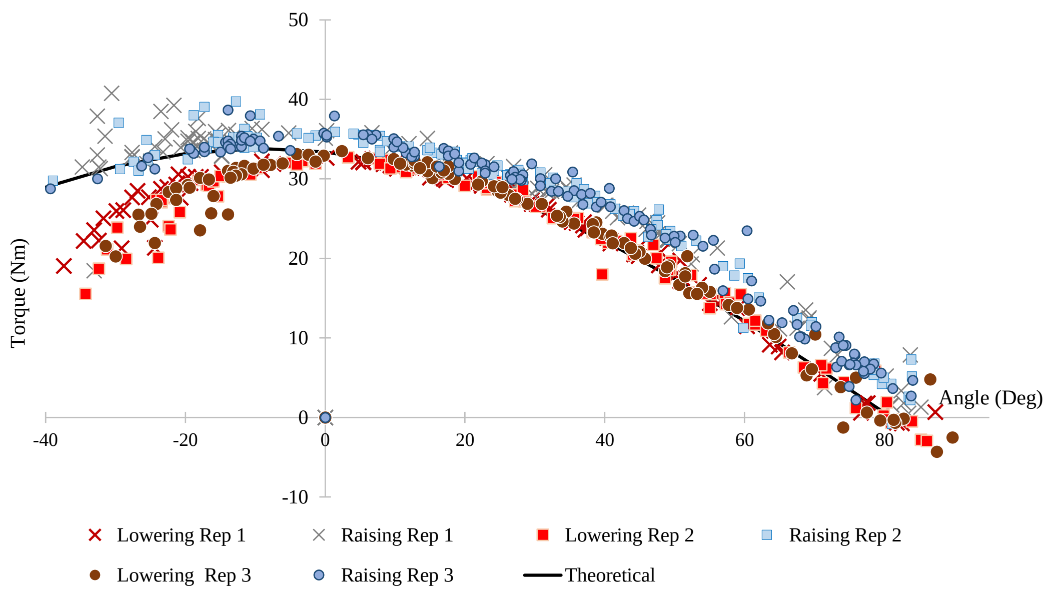

Figure A.12. Actuation torques for raising and lowering for three replications for Exmark (2) Lazer Z and theoretical torque.

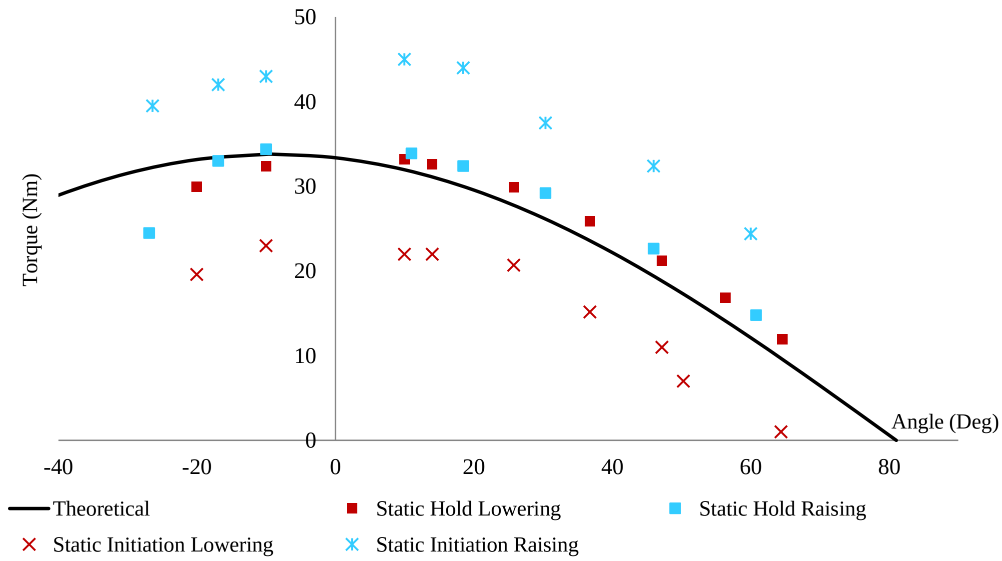

Figure A.13. The static holding and static transient torques for raising and lowering the Exmark (2) Lazer Z ROPS.

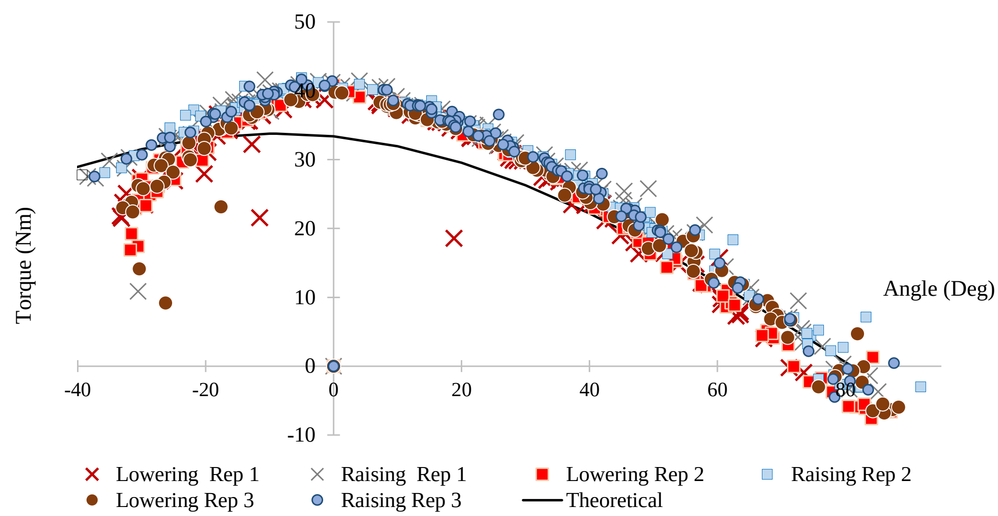

Figure A.14. Actuation torques for raising and lowering for three replications for Exmark (2) Lazer Z ROPS after greasing and theoretical torque.

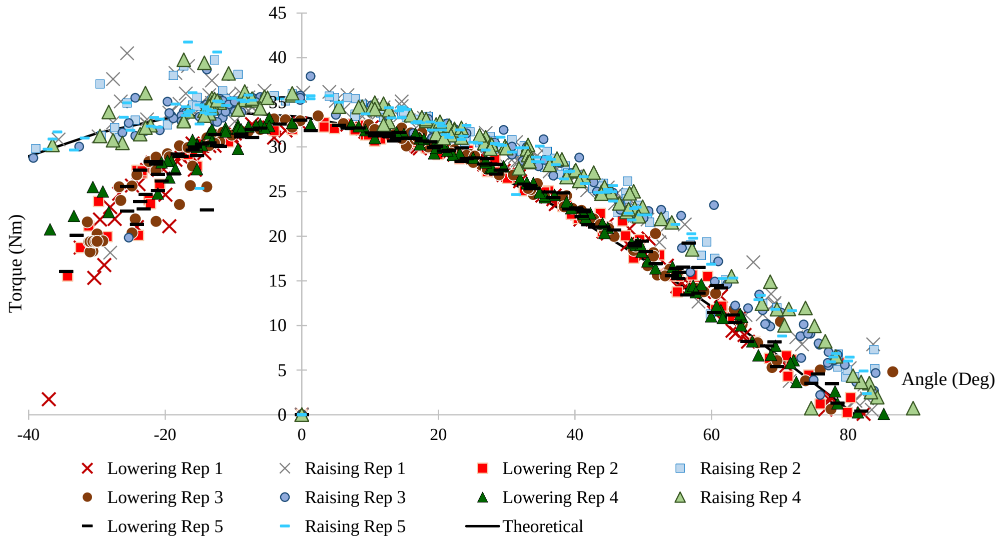

Figure A.15. Actuation torques for raising and lowering for five replications for Exmark (3) Lazer Z and theoretical torque.

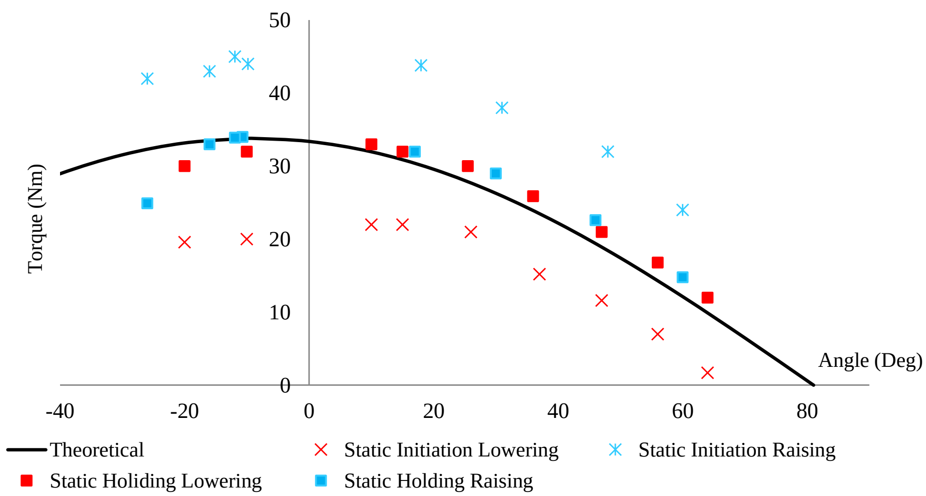

Figure A.16. The static holding and static transient torques for raising and lowering the Exmark (3) Lazer Z ROPS.

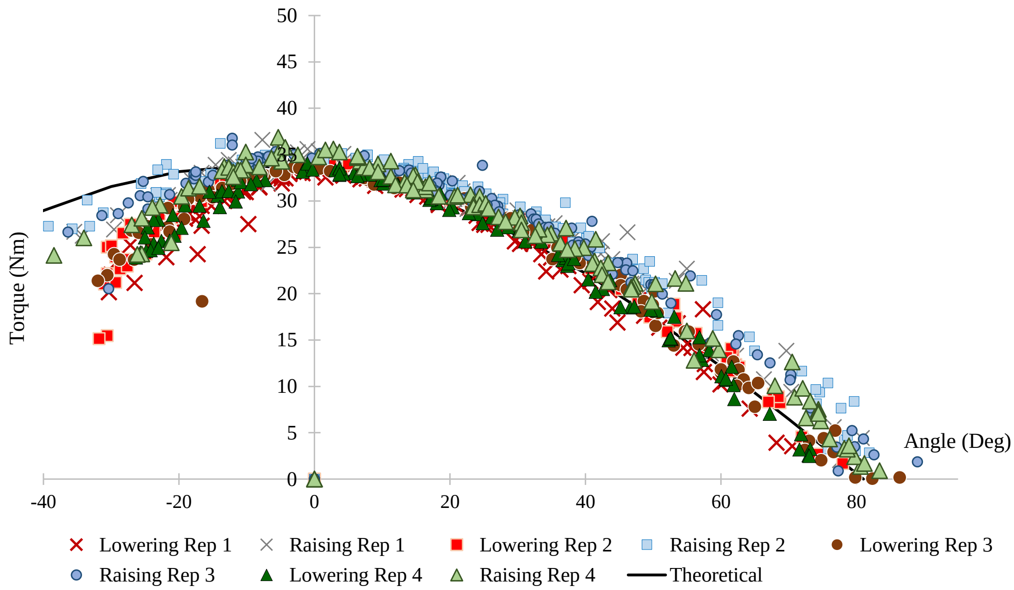

Figure A.17. Actuation torques for raising and lowering for four replications for Exmark (3) Lazer Z ROPS after greasing and theoretical torque.

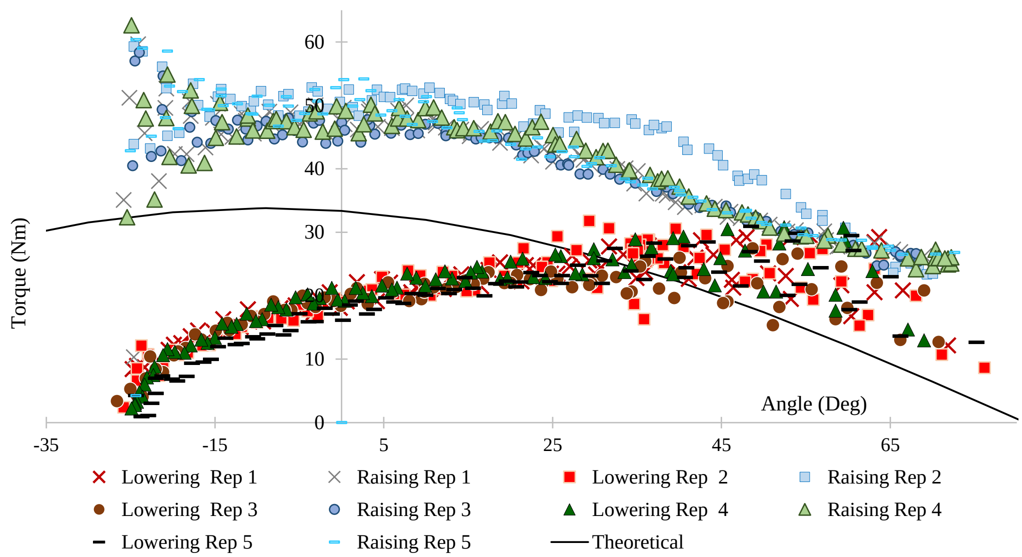

Figure A.18. Actuation torques for raising and lowering for five replications for Exmark (4) Lazer Z and theoretical torque.

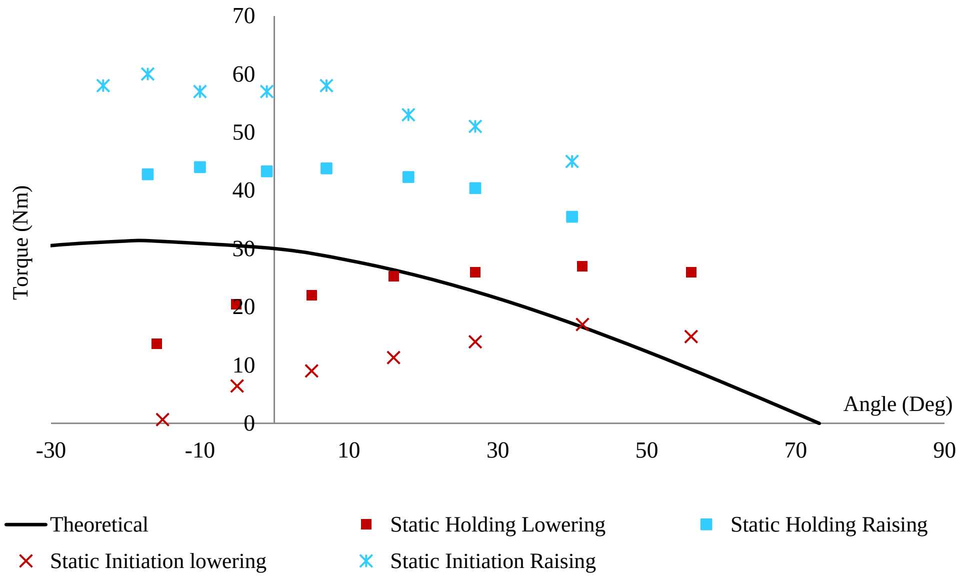

Figure A.19. The static holding and static transient torques for raising and lowering the Exmark (4) Lazer Z ROPS.

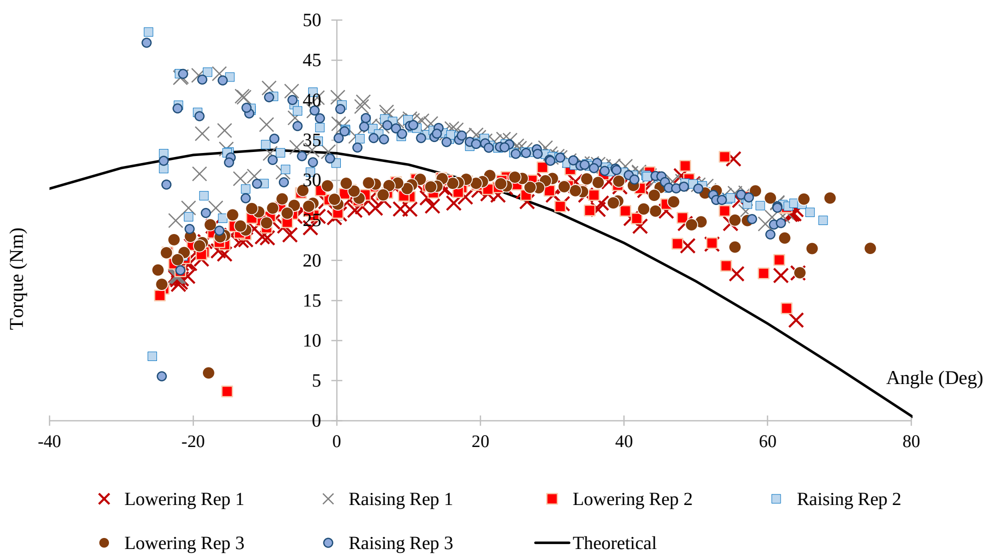

Figure A.20. Actuation torques for raising and lowering for three replications for Exmark (4) Lazer Z ROPS after greasing and theoretical torque.

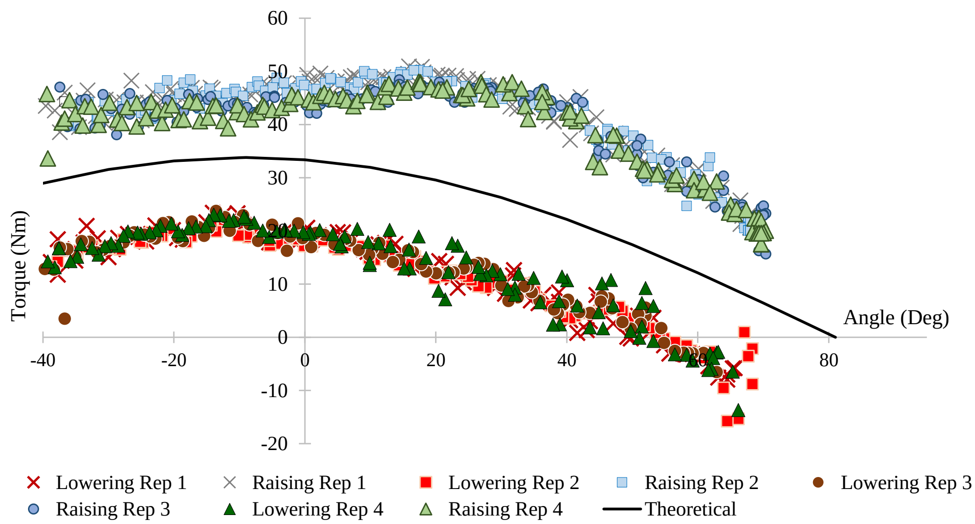

Figure A.21. Actuation torques for raising and lowering for four replications for Exmark (5) Lazer Z and theoretical torque.

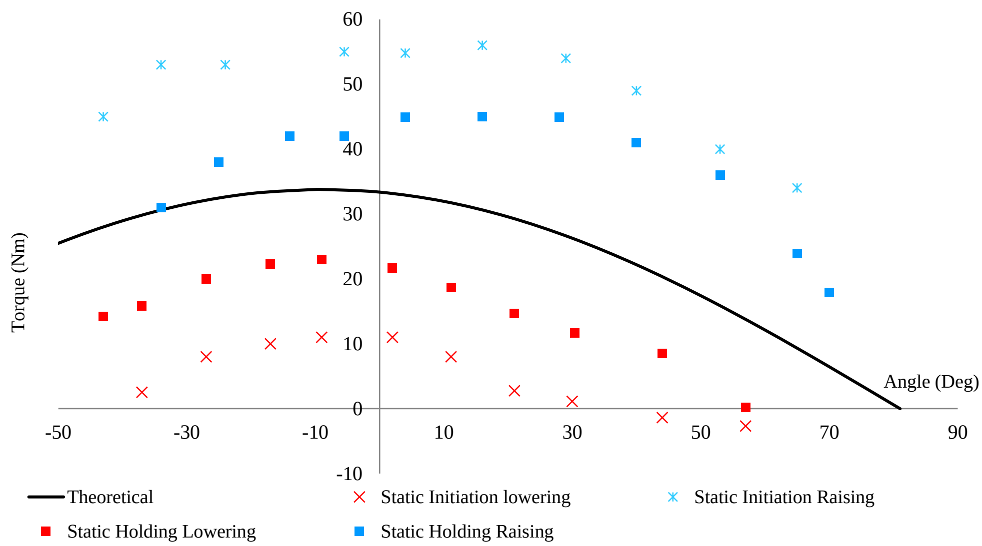

Figure A.22. The static holding and static transient torques for raising and lowering the Exmark (5) Lazer Z ROPS.

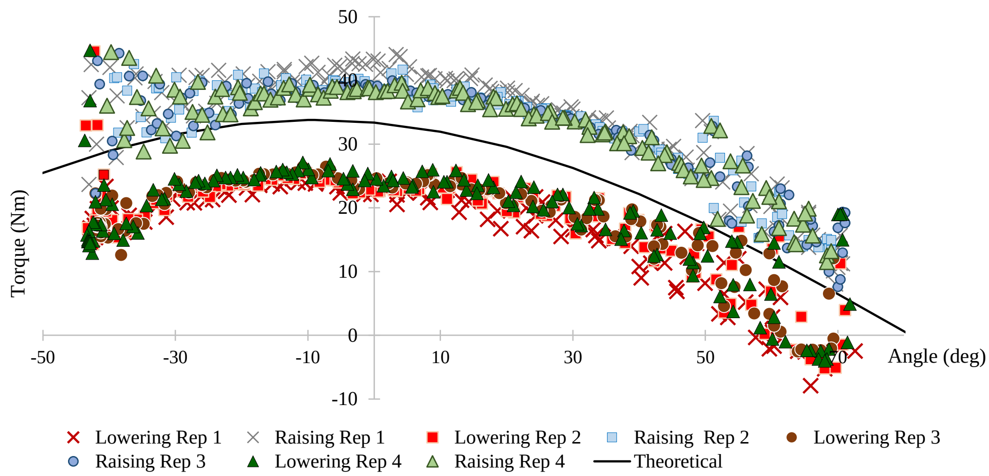

Figure A.23. Actuation torques for raising and lowering for four replications for Exmark (5) Lazer Z ROPS after greasing and theoretical torque.

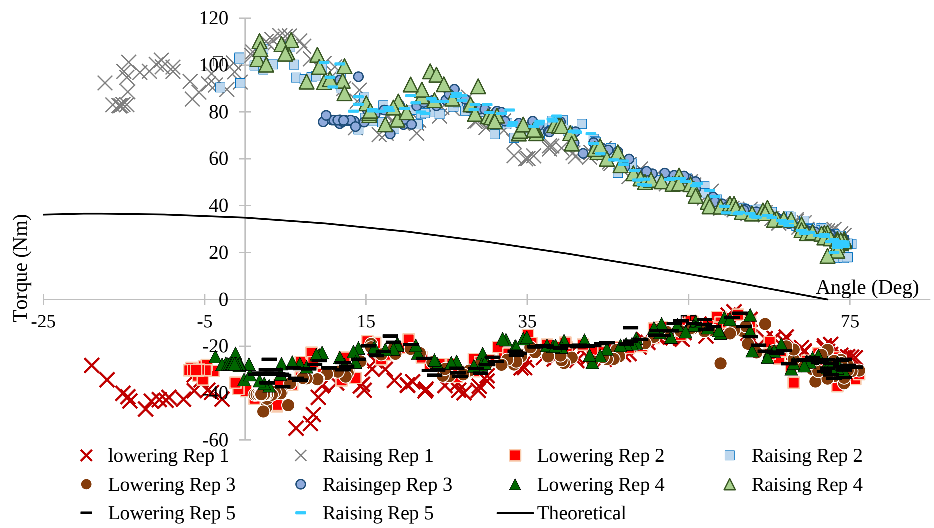

Figure A.24. Actuation torques for raising and lowering for four replications for Exmark (6) Ultra cut and theoretical torque.

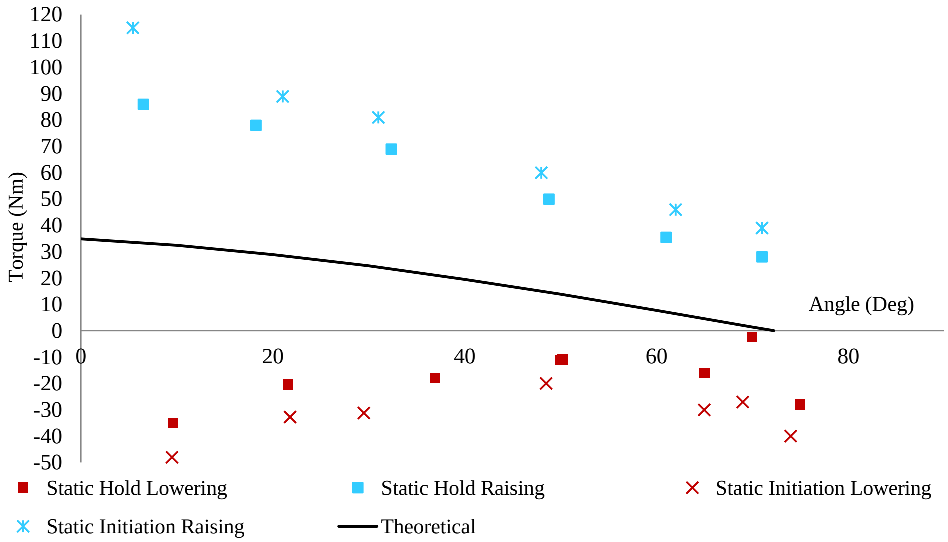

Figure A.25. The static holding and static transient torques for raising and lowering the Exmark (6) Ultra cut ROPS.

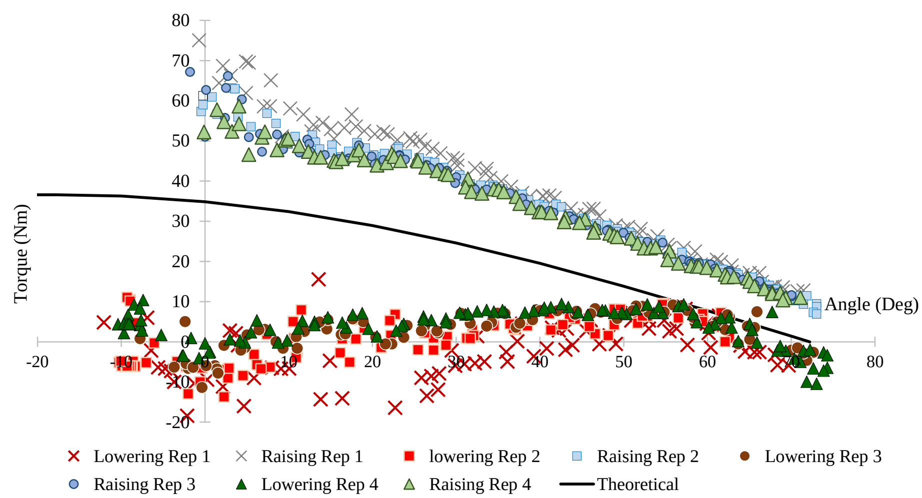

Figure A.26. Actuation torques for raising and lowering for four replications for Exmark (6) Ultra Cut ROPS after greasing and theoretical torque.

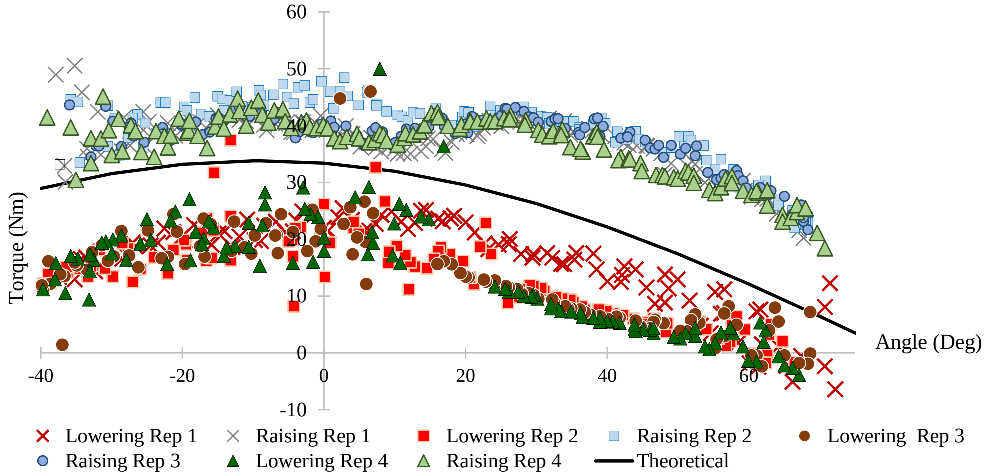

Figure A.27. Actuation torques for raising and lowering for four replications for Exmark (7) Lazer Z and theoretical torque.

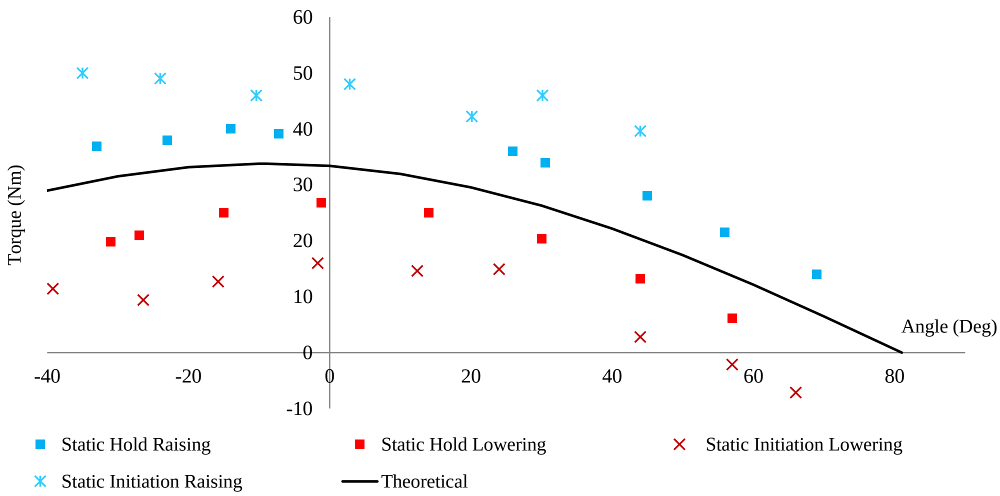

Figure A.28. The static holding and static transient torques for raising and lowering the Exmark (7) Lazer Z ROPS.

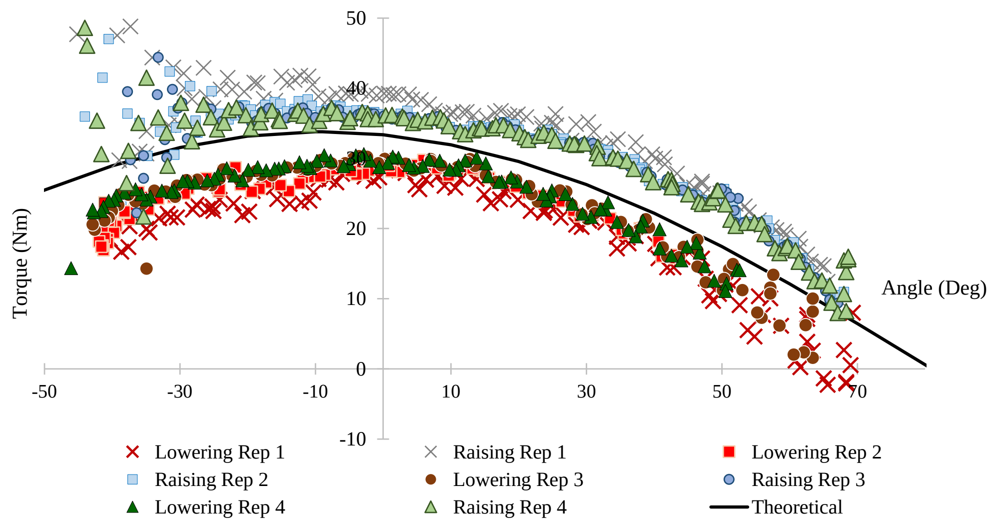

Figure A.29. Actuation torques for raising and lowering for four replications for Exmark (7) Lazer Z ROPS after greasing and theoretical torque.

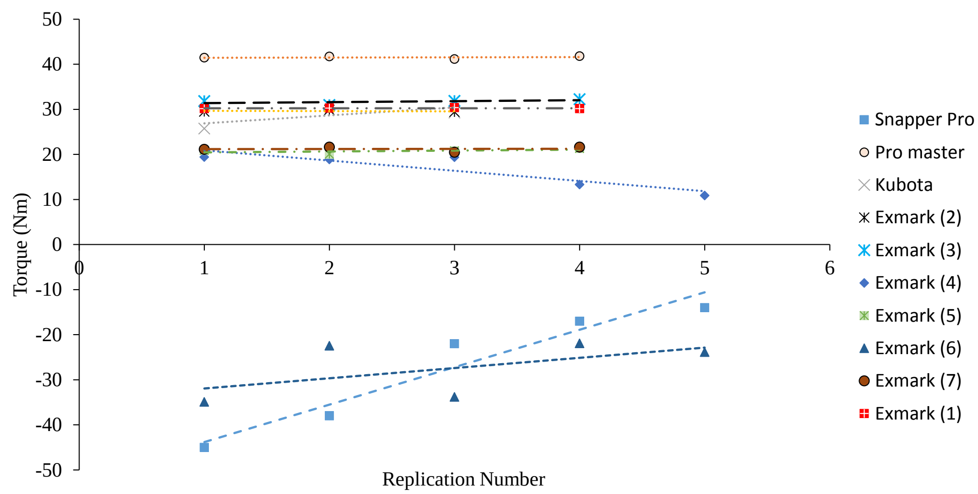

Figure A.30. Representative actuation torque in different replication for lowering 10 ROPS.

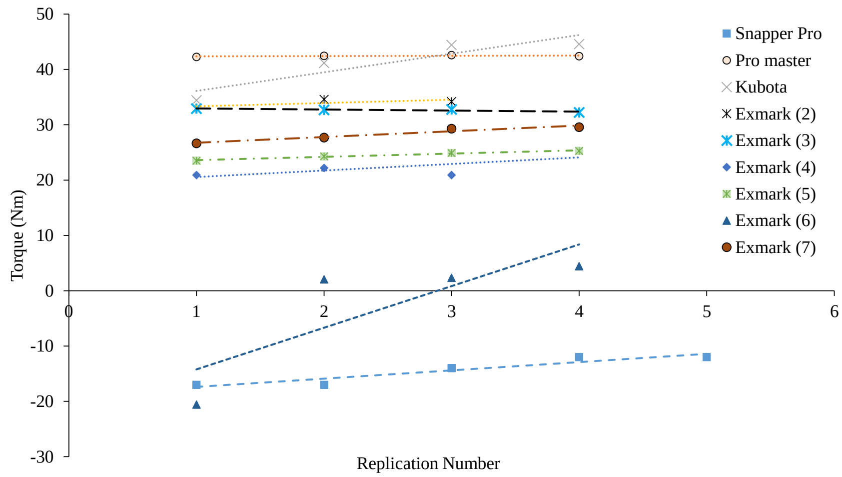

Figure A.31. Representative actuation torque in different replication for lowering 9 ROPS after greasing.

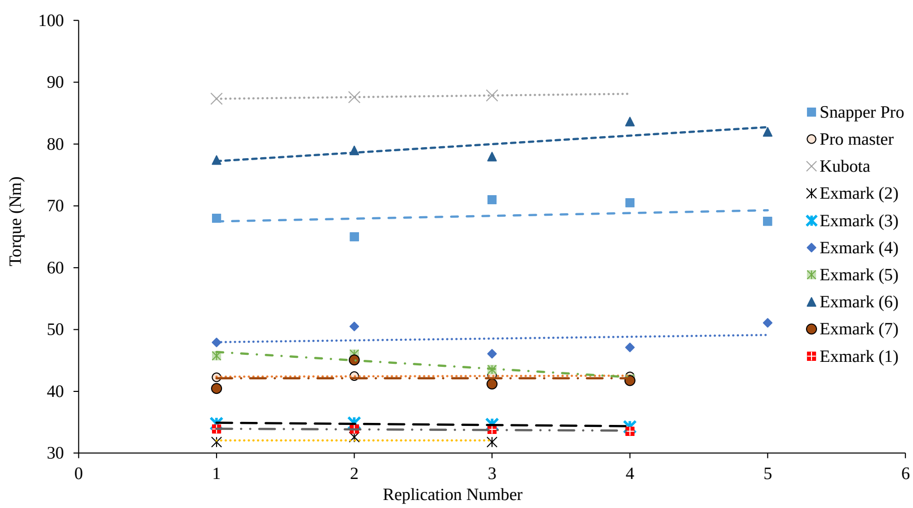

Figure A.32. Representative actuation torque in different replication for Raising 10 ROPS.

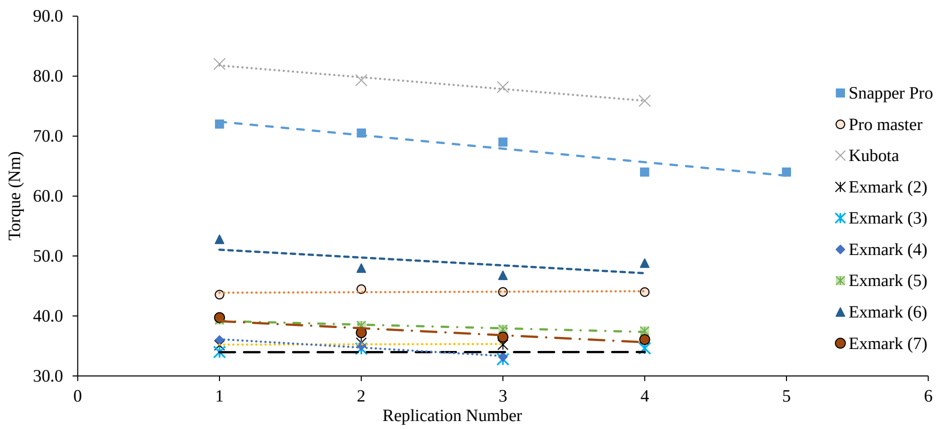

Figure A.33. Representative actuation torque in different replication for Raising 9 ROPS after Greasing.

Table A.1. The actuation torque for lowering FROPS in multiple replications.

	Representative torque (Nm), Experimental							Representative point, Theoretical	
ROPS	Rep 1	Rep 2	Rep 3	Rep 4	Rep 5	Mean	Friction %	Angle (Deg)	Torque (Nm)
Snapper	-45.0	-38.0	-22.0	-17.0	-14.0	-27.2	-187%	-11.8	31.4
Pro master	41.5	41.7	41.2	41.8	NA	41.5	-7%	10.0	44.6
Exmark (1)	30.2	30.3	30.4	30.1	NA	30.2	-11%	-9.0	33.8
Kubota	25.7	31.0	29.3	NA	NA	28.7	-44%	-19.3	50.9
Exmark (2)	29.5	29.9	29.4	NA	NA	29.6	-20%	20.0	37.0
Exmark (3)	31.8	30.9	31.9	32.2	NA	31.7	-25%	-7.0	42.3
Exmark (4)	19.4	18.9	19.4	13.3	10.9	16.4	-48%	-16.8	31.3
Exmark (5)	20.9	20.1	20.8	21.3	NA	20.8	-34%	-16.8	31.3
Exmark (6)	-34.9	-22.5	-33.8	-21.9	-23.9	-27.4	-175%	-7.8	36.6
Exmark (7)	21.1	21.6	20.5	21.6	NA	21.2	-50%	-7.8	42.0

Table A.2. The actuation torque for lowering FROPS in multiple replications after greasing.

	Representative torque with Greasing(Nm), Experimental							Representative point, Theoretical	
ROPS	Rep 1	Rep 2	Rep 3	Rep 4	Rep 5	Mean	Friction %	Angle (Deg)	Torque (Nm)
Snapper	-17.0	-17.0	-14.0	-12.0	-12.0	-14.4	-146%	-11.8	31.4
Pro master	42.3	42.5	42.6	42.4	NA	42.4	-5%	10.0	44.6
Exmark (1)	NA	NA	NA	NA	NA	NA	NA	-9.0	33.8
Kubota	34.4	41.2	44.4	44.6	NA	41.2	-19%	-19.3	50.9
Exmark (2)	33.0	34.6	34.2	NA	NA	33.9	-8%	20.0	37.0
Exmark (3)	32.9	32.7	32.8	32.2	NA	32.7	-23%	-7.0	42.3
Exmark (4)	20.9	22.2	20.9	25.3	NA	22.3	-29%	-16.8	31.3
Exmark (5)	23.5	24.3	24.9	25.3	NA	24.5	-22%	-16.8	31.3
Exmark (6)	20.6	2.1	2.4	4.5	NA	-2.9	-108%	-7.8	36.6
Exmark (7)	26.7	27.7	29.3	29.6	NA	28.3	-33%	-7.8	42.0

Table A.3. The actuation torque for raising FROPS in multiple replications.

ROPS	Representative torque (Nm), Experimental							Representative point, Theoretical	
	Rep 1	Rep 2	Rep 3	Rep 4	Rep 5	Mean	Error%	Angle (Deg)	Torque (Nm)
Snapper	68.0	65.0	71.0	70.5	67.5	68.4	118%	-11.8	31.4
Pro master	42.3	42.5	42.6	42.4	NA	42.4	-5%	10.0	44.6
Exmark (1)	33.9	33.9	33.9	33.5	NA	33.8	0%	-9.0	33.8
Kubota	87.3	87.6	87.9	NA	NA	87.6	72%	-19.3	50.9
Exmark (2)	31.8	32.6	31.8	NA	NA	32.1	NA	20.0	37.4
Exmark (3)	34.8	34.9	34.6	34.3	NA	34.6	-18%	-7.0	42.3
Exmark (4)	47.9	50.5	46.1	47.1	51.1	48.5	55%	-16.8	31.3
Exmark (5)	45.7	46.0	43.5	42.0	NA	44.3	42%	-16.8	31.3
Exmark (6)	77.4	79.0	78.0	83.6	82.0	80.0	119%	-7.8	36.6
Exmark (7)	40.5	45.1	41.2	41.8	NA	42.1	0%	-7.8	42.1

Table A.4. The actuation torque for raising FROPS in multiple replications after greasing.

ROPS	Representative torque with Greasing(Nm), Experimental							Representative point, Theoretical	
	Rep 1	Rep 2	Rep 3	Rep 4	Rep 5	Mean	Error %	Angle (Deg)	Torque (Nm)
Snapper	72.0	70.5	69.0	64.0	64.0	67.9	116%	-11.8	31.4
Pro master	43.5	44.5	44.0	44.0	NA	44.0	-1%	10.0	44.6
Exmark (1)	NA	NA	NA	NA	NA	NA	NA	-9.0	33.8
Kubota	82.0	79.3	78.2	75.9	NA	78.8	55%	-19.3	50.9
Exmark (2)	35.1	35.5	35.2	NA	NA	35.3	-6%	20.0	37.4
Exmark (3)	34.0	34.6	32.8	34.6	NA	34.0	-20%	-7.0	42.3
Exmark (4)	36.0	35.0	33.2	NA	NA	34.7	11%	-16.8	31.3
Exmark (5)	39.3	38.4	37.8	37.5	NA	38.2	22%	-16.8	31.3
Exmark (6)	52.8	48.0	46.8	48.8	NA	49.1	34%	-7.8	36.6
Exmark (7)	39.7	37.2	36.5	36.1	NA	37.4	-11%	-7.8	42.0

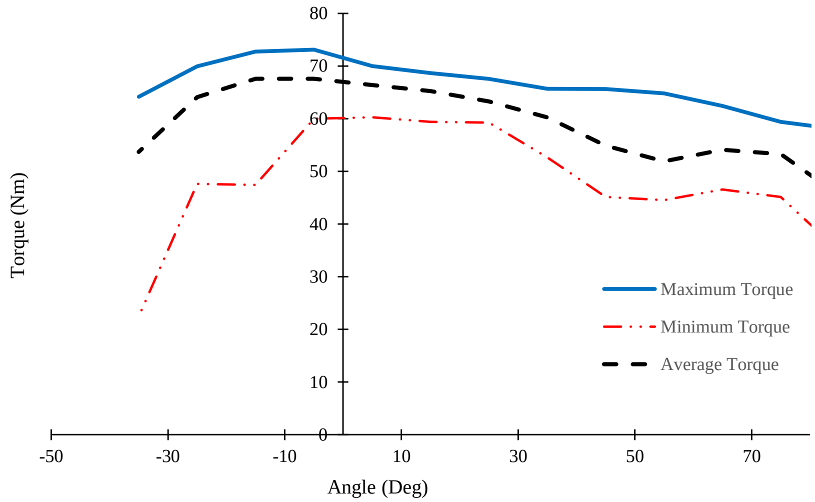

Figure A.34. The maximum, minimum, and average values of actuation torques for raising Snapper Pro.

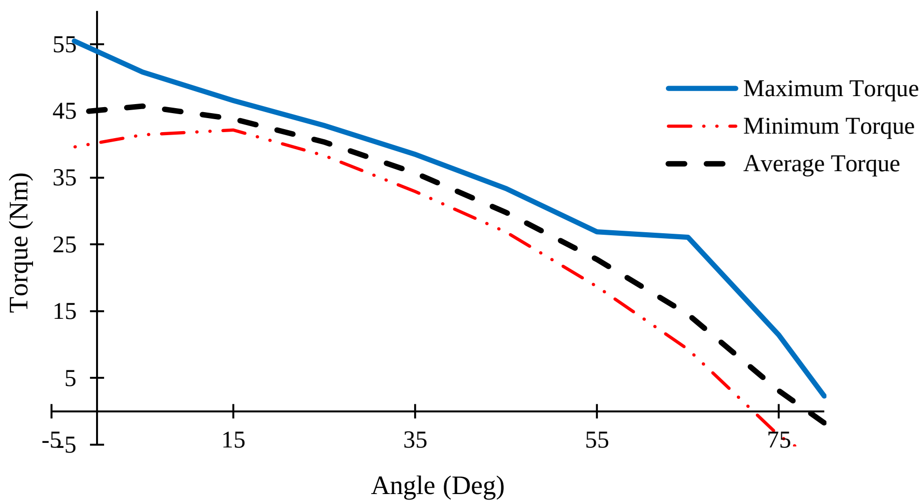

Figure A.35. The maximum, minimum, and average values of actuation torques for raising Pro Master.

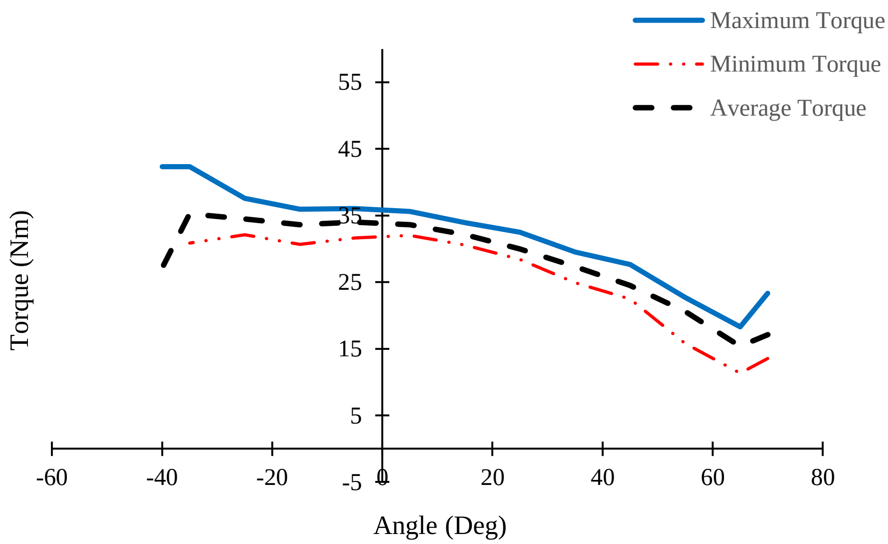

Figure A.36. The maximum, minimum, and average values of actuation torques for raising Exmark (1).

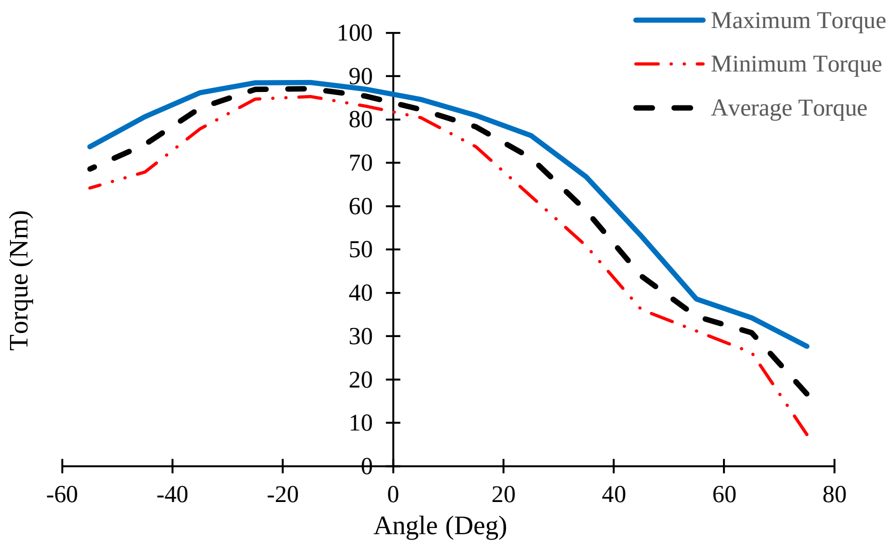

Figure A.37. The maximum, minimum, and average values of actuation torques for raising Kubota.

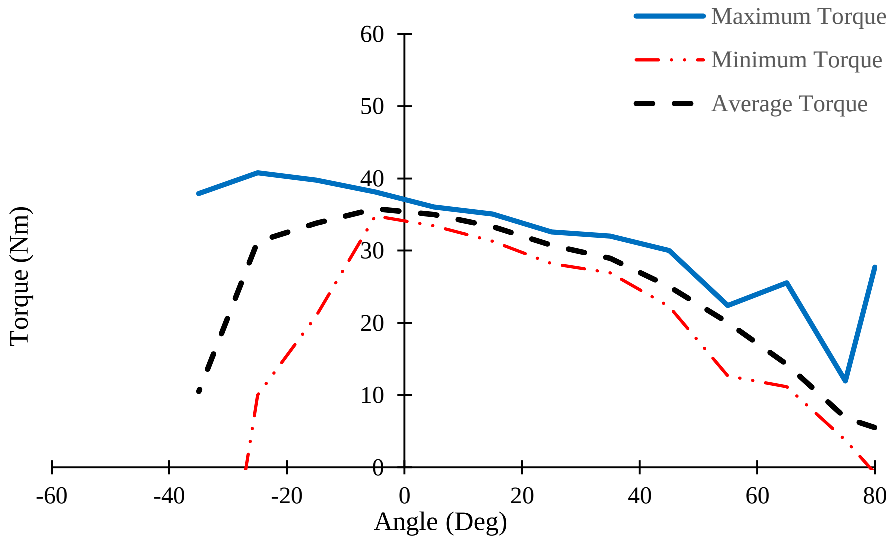

Figure A.38. The maximum, minimum, and average values of actuation torques for raising Exmark (2).

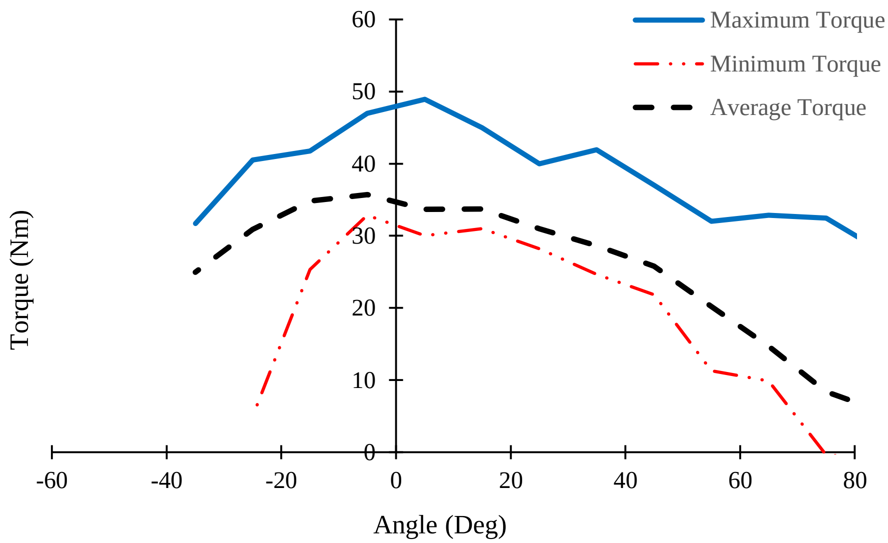

Figure A.39. The maximum, minimum, and average values of actuation torques for raising Exmark (3)

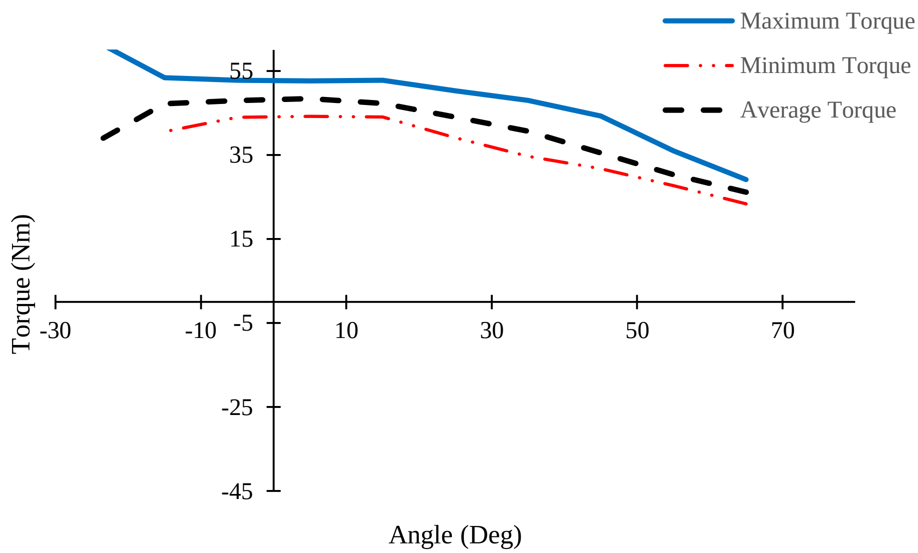

Figure A.40. The maximum, minimum, and average values of actuation torques for raising Exmark (4).

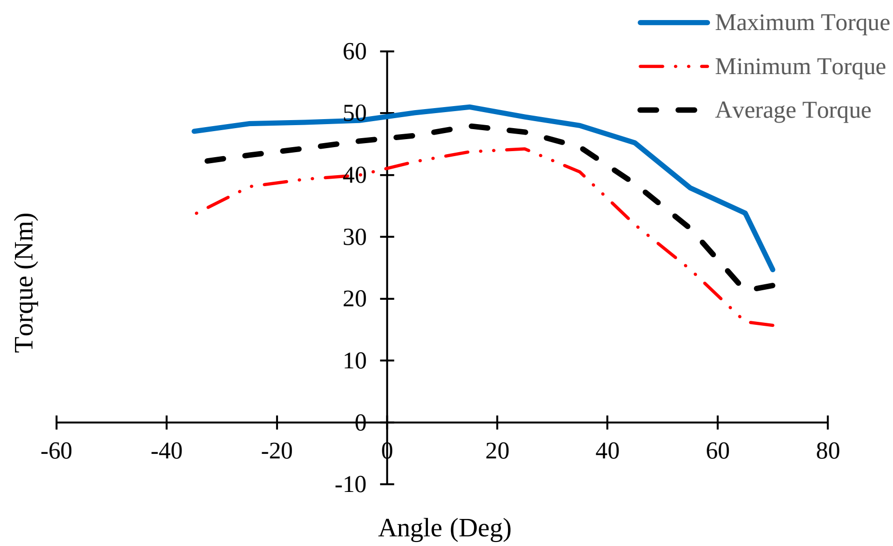

Figure A.41. The maximum, minimum, and average values of actuation torques for raising Exmark (5).

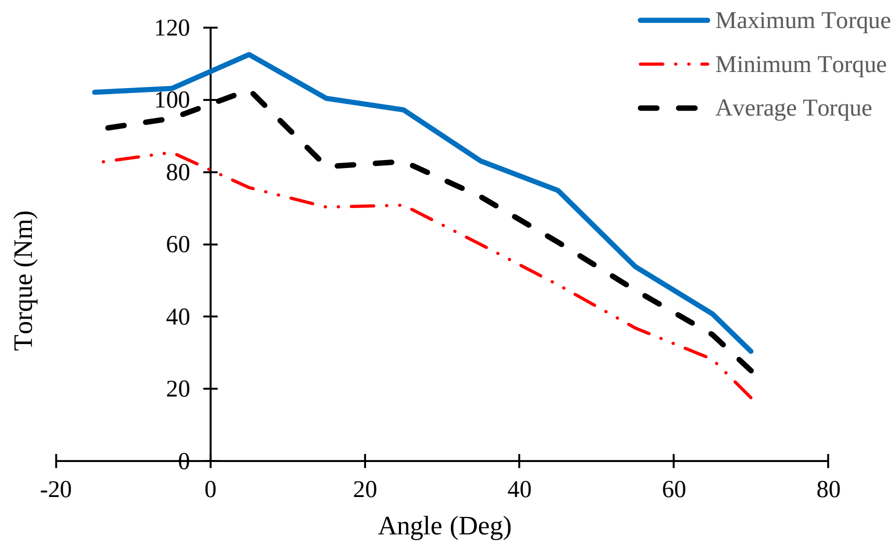

Figure A.42. The maximum, minimum, and average values of actuation torques for raising Exmark (6).

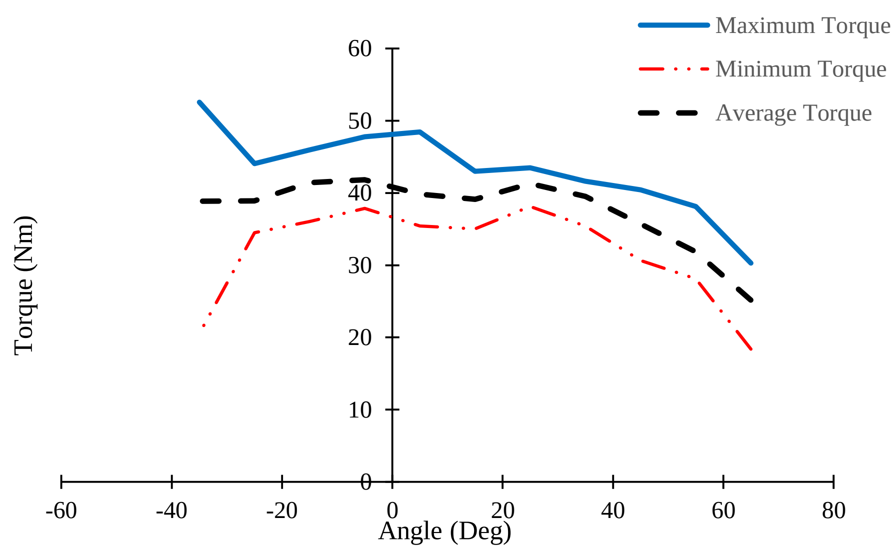

Figure A.43. The maximum, minimum, and average values of actuation torques for raising Exmark (7).

VITA

Farzaneh Khorsandi is from Esfahan, Iran. She has a Bachelor's degree in Mechanics of Agricultural Machinery Engineering, from Shahrekord University and a Master's degree in Mechanics of Agricultural Machinery Engineering from Shiraz University. During her education at the Shiraz University and University of Tennessee, she received a number of awards such as outstanding graduate student of Department of Mechanics of Agricultural Machinery Engineering (2010) and graduate student with professional promise in Biosystems Engineering (2016). She has presented her research at annual meetings of the American Society of Agricultural and Biological Engineering, International Society for Terrain-Vehicle Systems, Proceeding of the International Conference on Rural Health. Her research results were presented as journal publications.